

**The Tectonic Evolution of the Central Himalaya,  
Marsyandi Valley, Nepal**

by

**Margaret E. Coleman**

M.Sc. Geology  
Carleton University (Ottawa), 1990

B.A., Geology  
Middlebury College, 1987


Submitted to the Department of Earth, Atmospheric, and Planetary Sciences in Partial  
Fulfillment of the Requirements for the Degree of

Doctor of Philosophy  
at the  
Massachusetts Institute of Technology

**August, 1996**

© Massachusetts Institute of Technology, 1994. All rights reserved.


Signature of Author

  
\_\_\_\_\_  
Department of Earth, Atmospheric, and Planetary Sciences  
August, 1996

Certified by

  
\_\_\_\_\_  
Kip V. Hodges  
Thesis Advisor

Accepted by

  
\_\_\_\_\_  
Thomas H. Jordan  
Department Head

MASSACHUSETTS INSTITUTE  
OF TECHNOLOGY

AUG 19 1996

LIBRARIES

LIBRARIES



# The Tectonic Evolution of the Central Himalaya, Marsyandi Valley, Nepal

by

Margaret E. Coleman

Submitted to the Department of Earth, Atmospheric, and Planetary Sciences at the Massachusetts Institute of Technology on August 5, 1996, in Partial Fulfillment of the Requirements for the Degree of Doctor of Philosophy in Geology

## ABSTRACT

The metamorphic core of the central Himalaya, the Greater Himalayan sequence, is exposed in a 15 km thick section of amphibolite facies gneisses in the Marsyandi Valley of central Nepal. The sequence is bound by the Miocene north-dipping Main Central Thrust (MCT) at the base, and roofed by coeval north-dipping normal faults of the South Tibetan detachment system. Structurally above the Greater Himalayan sequence are lower-grade rocks of the Tibetan sedimentary sequence, and below are greenschist facies rocks of the Lesser Himalayan sequence. All of these rocks are Indian crust that was deformed and metamorphosed during intercontinental collision between India and Eurasia. Collision initiated in the Eocene and continues today. This study combines structural analysis with U-Pb and  $^{40}\text{Ar}/^{39}\text{Ar}$  geochronology and metamorphic petrology to determine the structural and thermal history of the central Himalayas. The results are threefold and include 1) significant crustal thickening within the Indian plate, north of the MCT, by the mid-Oligocene; 2) Early Miocene orogen parallel extensional deformation within the upper half of the Greater Himalayan sequence during peak metamorphism; 3) a transition from north-south to east-west extension within the middle and upper crust of the northern Himalaya and southern Tibetan plateau during the Miocene.

A minimum Oligocene age for crustal thickening within the Tibetan sedimentary sequence is constrained by ~30 Ma  $^{40}\text{Ar}/^{39}\text{Ar}$  cooling ages from phlogopite that is synkinematic with south verging folds. The Oligocene syn-metamorphic deformation is preserved within the hanging wall of the South Tibetan detachment. The South Tibetan detachment in the Marsyandi valley dips to the NW and footwall mylonites indicate top-to-the-west displacement (orogen-parallel) at sillimanite through greenschist-grade conditions. Uranium-lead geochronology of migmatite from the base and the top of the Greater Himalayan sequence and from undeformed leucogranite at the top indicate syn-metamorphic displacement on the South Tibetan detachment and the MCT between 18 and 22 Ma. Thermobarometric results indicate that the metamorphic core was at a minimum of 900K throughout by 22 Ma. A minimum age of 14 Ma for east-west extension of the southern Tibetan plateau was determined by  $^{40}\text{Ar}/^{39}\text{Ar}$  dating of muscovite-filled extensional fractures.

Thesis advisor: Kip V. Hodges, Professor of Geology





## Acknowledgments

The following section provides an opportunity to thank those who have helped with this project. A few simple twists of fate lead me to embark on a Ph.D. in tectonics at MIT, and I owe those largely to Sharon Carr and Allison Macfarlane. Sharon Carr did not have time to accompany Allison to do field work in Nepal, but she was kind enough to inform Allison that I did. In November of 1990, somewhere up the Langtang Valley, Allison convinced me (over lunch and a particularly nice view), that pursuing a Ph.D. in tectonics at MIT was a good idea. I am grateful to Allison as well as my friends and mentors from Carleton University, in particular Randy Parrish, Dick Brown, Sharon Carr and Lisel Currie, for convincing me to follow this path.

The essential advice, scientific interaction, editorial prowess, and friendship of my thesis advisor Kip Hodges are thankfully acknowledged. Kip's approach to Himalayan tectonics and tectonics in general will always be an inspiration. I would also like to thank my committee members Clark Burchfiel, Tim Byrne, Maureen Raymo, and Kip Hodges, for their time and complete reviews of this dissertation, and for actually making the defense a pleasant experience.

I am particularly indebted to those individuals who helped me carry out the field work. First I must thank Allison Macfarlane for thoroughly teaching me how to manage the logistics of doing field research in Nepal, including introducing me to all the right people in Kathmandu, showing me how to get research permission, how to get rocks out of the country, introducing me to the geology, etc., and also for being a great friend. The other person who I cannot thank enough is Kate Bull, my dear friend and most excellent field partner (she definitely does not qualify as assistant!). Kate spent both entire field seasons with me and contributed a great deal to the success of the field mapping component of this project. Kate is one of the finest geologists/mountaineers/ EMT/Black belt/ Didis I have the pleasure of knowing and I hope we have more opportunities for mountain adventures together. Thanks for everything Kate! Several Nepalese also helped us carry out the field work, in particular Mangale Sherpa and D.R. Thulung; they were fantastic guides and cooks during the field season and their hard work and good cheer will never be forgotten. There is also a long list of Nepalese who helped us carry our gear and rocks around the Marsyandi region and they are sincerely thanked for their hard labor. I

am grateful to Dr. B.N. Upreti and Surrendra Shresthra for helping me obtain research permission, and to the Nepali Government for granting research permission.

U-Pb geochronology was carried out at the Geological Survey of Canada under the supervision of Randy Parrish. I would like to thank Randy for his help with the U-Pb work as well as the rest of the GSC geochronology lab in particular V. McNicoll, P. Hunt, K. Santowski, J. Crowley, and M. Villeneuve. During my visit to Ottawa I enjoyed the hospitality of the Hodges family, who generously offered me a home for an entire month during their sabbatical. Many thanks to Larky, Kip and Rachel for all their hospitality over the past five years.

Bill Oszewski has been an excellent source of information and provided essential assistance in the CLAIR facility. Mike Jerconovic and Neel Chatterjee provided patient and thorough technical support in the microprobe lab. Pat Walsh took care of all the administrative details (and then some) and always provided a healthy perspective on life here. Nancy Dallaire was also a great source of administrative information (happy retirement!).

Many graduate students and former graduate students have been influential during the course of this study and these include, Allison Macfarlane, Martha House, David Applegate, Audrey Huerta, Anke Friedrich, C.J. Northrup, and David Hawkings. C. J. Northrup, Drew Coleman, and Anke Friedrich are thanked for providing helpful comments on earlier drafts of various chapters. Beverly Saylor, Mousumi Roy, Jim Van Orman, Eric Kirby, Shane Pelechaty, Dave Dinter, Dawn Sumner, Jen Carlson, Nancy Harris, Ellen Dotson, Yu Jin, Peter Kaufman, Mark Simons, Kirstin Nicolaysen, and Mark Schmitz make up most of the other graduate students that I have enjoyed interacting with and learning from over the course of the past five years. Special thanks to Audrey Huerta for providing me with a safe haven over the past couple of months. The past year would not have been nearly as fun nor sane were it not for the almost daily visits to the pool with Beverly Saylor. Thank you Beverly, finishing at the same time made it much more enjoyable!

Outside of MIT there are several people who provided me with a tremendous amount of encouragement and support. They include my immediate family, and good friends Hanna Steffian, Heather Sivert, and Buck deWolf. Special thanks to Hanna for sharing her house over the past two years and making it a real home for me, and Heather

for many memorable meals! Weekend and holiday retreats to my parents home in New Hampshire and Maine sustained me at many different stages of graduate school and is greatly appreciated along with their unconditional love and support. A good portion of this thesis was written at Yale and I thank Philip Bogden and the GFD group for their hospitality. I credit much of my happiness over the past three year to Philip Bogden, who has been a wonderful distraction as well as a source of support and encouragement; and in addition an excellent incentive to finish (yes Kip, you provided me with plenty of reasons too!).



*To William and Mildred Coleman*



## TABLE OF CONTENTS

Title Page .....	1
Abstract .....	3
Acknowledgements .....	5
Dedication .....	9
Table of Contents.....	11
<b>Chapter 1:</b> Introduction.....	13
<b>Chapter 2:</b> Orogen-parallel and orogen-perpendicular extension in the central Nepalese Himalaya.....	17
<b>Chapter 3:</b> U-Pb Constraints on Oligocene - Miocene deformation and Anatexis, Marsyandi valley, central Nepalese Himalaya.....	69
<b>Chapter 4:</b> Insights into the Oligocene thermal history of the central Himalaya from $^{40}\text{Ar}/^{39}\text{Ar}$ thermochronology, Marsyandi valley, central Nepal.....	117
<b>Chapter 5:</b> P-T constraints on metamorphism of the central Greater Himalayan sequence: data from the Marsyandi valley, central Nepal.....	169
<b>Chapter 6:</b> Evidence for Tibetan plateau uplift before 14 Myr ago from a new minimum age for east-west extension.....	205
<b>Chapter 7:</b> Tectonic synthesis.....	209





## Chapter 1

### Introduction

The Himalayan orogen hosts the highest mountains in the world, and is one of the most impressive results of intercontinental collision. Following the closing of the Tethys Ocean, the Indian and Eurasian plates started to collide about 50 million years ago (Gansser, 1964; Patriat and Achache, 1984), and the convergence continues today at a rate of about 5 cm/yr (Molnar and Tapponnier, 1975). The mountain range extends from Pakistan eastwards beyond Bhutan, and reaches elevations of over 8000 m. Most of the Himalayan range is made up of Indian crust that was imbricated during northward subduction of the Indian plate beneath Tibet. In general, the high part of the range consists of a continuous belt of metamorphosed Indian crust, the Greater Himalayan sequence. These rocks were buried down to 40 km and reached temperatures in excess of 700K before being unroofed and uplifted (Hodges et al., 1988). The tectonothermal evolution of the Greater Himalayan sequence is enigmatic in many respects, and understanding this evolution is the focus of this thesis.

One important discovery about orogenic processes in recent years has been the identification of extensional faults that unroof mid-crustal rocks during convergence. The Himalaya provide excellent examples of extensional faulting within a convergent setting (Burchfiel and Royden, 1985). Along the length of the orogen, the contact between the metamorphic core and its suprastructure is a set of north-dipping normal faults and shear zones referred to as the South Tibetan detachment system (Burchfiel et al., 1992, and references therein). One of the principal goals of this study was to evaluate the role of extensional faulting at the top of the Greater Himalayan sequence in the Marsyandi valley of central Nepal. The Marsyandi region was chosen for the following reasons:

- The basic structure and geology is well-constrained by nearly three decades of research by field geologists (e.g. Hagen, 1969; Bordet et al., 1971; LeFort, 1975; Pecher, 1977, 1989; Colchen et al., 1986).
- Previous work had indicated the existence of normal faults at the top of the Greater Himalayan sequence, although they were thought to be minor (Caby et al., 1983).
- Access to the Marsyandi region is relatively easy by Himalayan standards, and provided the opportunity to make detailed maps and also study along strike variation of the South Tibetan detachment system.

The study involved detailed geologic mapping, structural analysis of deformational fabrics, U-Pb and  $^{40}\text{Ar}/^{39}\text{Ar}$  thermochronology, and metamorphic petrology. It was designed to integrate these various tools in order to constrain the geometry and timing of extensional and compressional deformation of the Greater Himalaya, and to evaluate the effects of deformation on the thermal history of the metamorphic core.

The thesis is divided into seven chapters. The second chapter contains a detailed structural analysis of extensional deformation within the upper Greater Himalayan sequence and overlying Tibetan Sedimentary sequence in the Marsyandi and Dudh Khola valleys (Figure 1, Chapter 2). Three generations of orogen-parallel extensional faults were distinguished in the Marsyandi valley, and a single north-dipping extensional fault was identified in the Dudh Khola valley. Chapter 3 presents U-Pb age constraints on deformation and anatexis within the lower and upper Greater Himalayan sequence. These data provide limits on the age of extensional faulting on the South Tibetan detachment and on the age of thrust faulting at the base of the sequence. Chapter 4 presents  $^{40}\text{Ar}/^{39}\text{Ar}$  thermochronologic results from the hanging wall and footwall of the South Tibetan detachment system. The thermochronologic data provide supporting evidence for large displacement on the South Tibetan detachment in this region, and give new insights into the

early stages of Himalayan metamorphism and deformation within the Indian plate.

Chapter 5 discusses the metamorphic petrology of the Greater Himalayan sequence and the timing of metamorphism and deformation. Temperatures and pressures throughout the sequence were calculated by quantitative thermobarometric analysis. Chapter 6 presents  $^{40}\text{Ar}/^{39}\text{Ar}$  constraints on the minimum age of east-west extension within the northern Himalaya and southern Tibetan plateau, and discusses implications for timing of the uplift of the Tibetan plateau. Finally, Chapter 7 synthesizes the major contributions of this dissertation.

Chapters 2 through 6 were written as stand alone papers for publication, which requires a certain amount of repetition among the chapters. Chapter 2 is in press in the *Geological Society of America Bulletin*, and Chapter 3 will be submitted for publication in a *Geological Society of America Special Volume* on Himalayan tectonics. Chapters 4 and 5 will be submitted for publication in *Tectonics* and the *Journal of metamorphic Geology*, respectively, both with K.V.Hodges as co-author. Chapter 6 was co-authored by K.V. Hodges and was published as a letter to *Nature* in March of 1995.

### **Acknowledgement of support**

My dissertation research has been supported by National Science Foundation grant EAR-9104291 awarded to Kip Hodges and by a teaching assistantship at the Massachusetts Institute of Technology.

### **References Cited**

Bordet, P., M. Colchen, D. Krummenacher, P. LeFort, R. Mouterde, and J.M. Rémy.  
1971. Recherches géologiques dans l'Himalaya du Népal, région de la Thakkola.  
Paris: Centre Natl. Rech. Sci.

- Burchfiel, B.C., Z. Chen, K.V. Hodges, Y. Liu, L.H. Royden, C. Deng, and J. Xu. 1992. The South Tibetan Detachment System, Himalayan Orogen: Extension Contemporaneous With and Parallel to Shortening in a Collisional Mountain Belt. Geological Society of America Special Paper 269. Boulder, CO: Geological Society of America.
- Burchfiel, B.C., and L.H. Royden. 1985. North-south extension within the convergent Himalayan region. *Geology* **13**, 679-682.
- Caby, R., A. Pêcher, and P. LeFort. 1983. Le M.C.T. himalayen: nouvelles données sur le métamorphisme inverse à la base de la Dalle du Tibet. *Revue Géogr. phys. Géol. dynam.* **24**, 89-100.
- Colchen, M., P. LeFort, and A. Pêcher. 1986. Annapurna - Manaslu - Ganesh Himal. Paris: Centre National de la Recherche Scientifique.
- Gansser, A. 1964. Geology of the Himalayas. London: Wiley Interscience.
- Hagen, T., 1969. Report on the geological survey of Nepal. *Denkschr. Schweiz. naturf. Gesell.*, **86**. 185p.
- Hodges, K.V., Mary S. Hubbard, and D.S. Silverberg. 1988. Metamorphic constraints on the thermal evolution of the central Himalayan Orogen. *Phil. Trans. R. Soc. Lond. A* **326**, 257-280.
- LeFort, P. 1975. Himalayas: the collided range. Present knowledge of the continental arc. *Am. J. Sci.* **275-A**, 1-44.
- Patriat, P., and J. Achache. 1984. India-Eurasia collision chronology and its implications for crustal shortening and driving mechanisms of plates. *Nature* **311**, 615-621.
- Pêcher, A. 1977. Geology of the Nepal Himalaya: Deformation and petrography in the Main Central thrust zone. In *Himalaya: Sciences de la Terre*. C.N.R.S. Paris: 301-318.
- Pêcher, A. 1989. The metamorphism in the central Himalaya. *J. Metamorphic Geol.* **7**, 31-41.

## Chapter 2

### Orogen-parallel and orogen-perpendicular extension in the central Nepalese Himalaya

#### Abstract

North-dipping, gravitationally-driven-extensional structures that unroof the high-grade core of the Himalaya have been recognized in several parts of the orogen. Recent work in west-central Nepal demonstrates that the extensional history at the top of the Greater Himalayan metamorphic sequence in this region is laterally variable. In the upper Marsyandi valley there is evidence for three generations of Early to Middle Miocene west-directed (orogen-parallel) extensional structures. The study area consists of two tectonostratigraphic sequences. The lower consists of a 12 km thick section of high-grade metasedimentary rocks of the Greater Himalayan sequence. The higher one consists of a 4 km-thick section of medium-grade marble of the Tibetan sedimentary sequence; it overlies the Greater Himalayan sequence in the Marsyandi valley along a northwest-dipping ductile shear zone (the Chame detachment). Mylonitic fabrics in footwall rocks show evidence of top-to-the-west displacement at sillimanite-grade through greenschist-grade conditions. A cataclastic zone indicates progressively more brittle deformation at the eastern end of the outcrop trace of the Chame detachment. In the Dudh Khola valley, 15 km east of the Marsyandi valley, the Tibetan sedimentary sequence is juxtaposed with the Greater Himalayan sequence by an Early Miocene north-dipping ductile shear zone (the Dudh Khola detachment) with well-developed, north-trending stretching lineations formed during sillimanite-grade metamorphism. North-directed (orogen perpendicular) extension in the Dudh Khola region is interpreted as coeval with west-directed (orogen-parallel) extension in the Marsyandi region. Along-strike variations in the orientation of extensional strain at the top of the Greater Himalayan sequence may be explained by lateral crustal thickness gradients.

## Introduction

Discussions regarding the role of extensional faulting in the evolution of the Himalaya and Tibet commonly focus on two classes of structures. The oldest are E-W-striking, shallowly N-dipping normal faults of the South Tibetan detachment system (Burchfiel et al., 1992). Presently exposed near the crest of the range, these features are thought to have developed during evolving gravitational instability of the Himalayan topographic front in Early Miocene time (Burchfiel and Royden, 1985). The second class of structures are N-S-striking, E- and W-dipping normal faults that bound extensional basins throughout much of the southern Tibetan Plateau and continue as far south as the outcrop trace of the South Tibetan detachment (Armijo et al., 1986; Molnar and Tapponnier, 1978). These features are commonly regarded as the manifestation of E-W extension of the Tibetan Plateau over the Middle(?) Miocene to Holocene interval (Molnar et al., 1993).

Although there is a tendency by many geologists to emphasize the importance of S-directed thrusting and N-directed extension in the structural history of the Himalaya and view orogen-parallel deformation in this region as a "Tibetan" phenomenon, there is no *a priori* reason to presume that orogen-parallel deformation should be restricted to Tibet. Indeed, both Brun et al. (1985) and Pêcher (1991) identified structures related to a component of strike-slip displacement within the central Himalaya. This paper describes geologic relationships in the upper Marsyandi and Dudh Khola areas of central Nepal (Figure 1) that demonstrate partitioning of strain associated with the South Tibetan detachment system into discrete westward (orogen-parallel) and northward (orogen-perpendicular) displacement components on roughly contemporaneous extensional structures. This observation implies that the kinematics of the South Tibetan detachment system are more complicated than originally thought, at least in this segment of the orogen. Further work is necessary before we can determine whether this orogen-parallel extension represents the effects of local, lateral crustal thickness gradients or testifies to the regional

importance of transtensional processes during the collapse of the Himalayan topographic front.

### **The Himalayan Orogen**

The Himalaya formed as the result of continued convergence of two continents since the Paleogene (Gansser, 1964; Le Fort, 1975). India has moved in a roughly N10°E direction relative to northern Asia since the collision at a rate of about 5cm/yr (Molnar and Tapponnier, 1975). Collision resulted in the vast elevated region of the Tibetan plateau (Asian plate) and the Himalayan range (of Indian plate affinity). The Himalaya *sensu stricto* are typically divided into three tectonic zones that trend roughly WNW-ESE (Gansser, 1964, Figure 1). The high-grade rocks of the metamorphic core of the range are referred to as the Greater Himalayan sequence. These occur between low to medium grade rocks of the Tibetan sedimentary sequence to the north and the Lesser Himalayan sequence to the south. The Greater Himalayan sequence is made up of amphibolite-facies schists and gneisses, migmatites and scattered leucogranite plutons. The Tibetan sedimentary sequence comprises a nearly continuous section of lower Paleozoic to lower Tertiary marine sedimentary rocks of Tethyan affinity (Gansser, 1964; Le Fort, 1975). The Tibetan sedimentary sequence rocks are unmetamorphosed except very near the contact with the Greater Himalayan sequence, where they reach amphibolite grade in a few areas (Schneider and Masch, 1993). To the south, the Lesser Himalayan sequence consists of low to medium grade metasedimentary and metavolcanic rocks of Mesoproterozoic (?) to lower Eocene age (Stocklin, 1980; Parrish and Hodges, 1995).

The tectonic zones described above are juxtaposed primarily by east-west striking, north-dipping structures along which large amounts of shortening and extension were accommodated: the Main Central Thrust zone (MCT) which separates the Greater and Lesser Himalayan zones (Brunel and Kienast, 1986; Gansser, 1964; Le Fort, 1975; Pêcher, 1989) and the South Tibetan detachment system, which places the Tibetan sequence on higher-grade Greater Himalayan metamorphic rocks (Burchfiel and Royden, 1985;

Burchfiel et al., 1992; Burg et al., 1984; Herren, 1987). This paper focuses on the South Tibetan detachment system in the central Himalaya.

North-dipping extensional structures at the top of the Greater Himalayan sequence were first recognized in southern Tibet north of Nepal and Bhutan (Burg et al., 1984). There, a north-directed detachment juxtaposes slightly metamorphosed rocks of the Tibetan Sedimentary sequence against older highly metamorphosed gneisses and Miocene leucogranites of the Greater Himalayan sequence. These observations led to the hypothesis that gravitationally-driven extension, occurring sub-parallel to the transport direction of the dominant compressional faults during convergence, occurred at the same structural level along a significant length of the orogen (Burchfiel and Royden, 1985; Burchfiel et al., 1992). Subsequently, similar structures were identified in the western Himalaya (Herren, 1987; Searle and Fryer, 1986) .

Continued mapping in the eastern Himalaya demonstrated that the same system of normal faults is continuous for at least 700 km along strike, with roughly 10 km of vertical displacement and at least 35 km of northward displacement in the vicinity of Mt. Everest (Burchfiel et al., 1992). Normal-sense movement on the South Tibetan detachment system in the Everest region is constrained to be between 19 and 22 Ma (Hodges et al., 1992), coeval with south-directed thrusting on the MCT at the same longitude (Hubbard and Harrison, 1989). Normal faulting on the South Tibetan detachment system is thought to have had a significant effect on the thermal history of the Greater Himalayan sequence. Metamorphic assemblages in rocks of the Greater Himalayan sequence record pressure-temperature paths, characterized by isothermal decompression, which suggest a minimum of 6 km of unroofing on the South Tibetan detachment system in the eastern Himalaya (Hodges et al., 1992; Hodges et al., 1993). Anatectic melting in the Greater Himalayan sequence and the emplacement of syn- to late-kinematic leucogranites near the South Tibetan detachment system have been attributed to decompression due to tectonic unroofing (Harris and Massey, 1994).



Where it has been mapped in the eastern and western Himalaya, the basal detachment of the South Tibetan detachment system is an obvious structure that marks a clear metamorphic and structural discontinuity. In the Annapurna - Manaslu region, arguably one of the most intensively studied segments of the Himalayan orogen, the basal detachment has proved remarkably difficult to distinguish. There is no obvious metamorphic break between the Greater Himalayan sequence and the Tibetan sedimentary sequence in this area, and the transition zone between the two appears to have had a complex deformational history.

### **Nature of the Greater Himalayan sequence - Tibetan Sedimentary sequence contact in the Annapurna-Manaslu region of Central Nepal**

Because of difficulties related to accessibility, most previous studies of the South Tibetan detachment system in southern Tibet and India focused on narrow, across-strike transects. The drainage pattern of major rivers in the Annapurna-Manaslu region of central Nepal (Figure 1) is unusual in that it provides relatively easy access to the South Tibetan detachment system over a strike length of 150 km. Although this entire length of the system has not yet been mapped in detail, research along various segments of the Greater Himalayan sequence - Tibetan Sedimentary sequence contact indicates a kinematically complex structural history (Bordet et al., 1971; Le Fort, 1975; Colchen et al., 1981; Caby et al., 1983; Pêcher, 1989; 1991; Brown and Nazarchuk, 1993; Guillot et al., 1994; Hodges et al., in press; this study).

In the western part of the Annapurna range the Greater Himalayan sequence comprises a monoclinial sequence of north-dipping high grade gneisses, exposed below Cambrian (?) to Ordovician medium grade marbles and quartzites of the basal part of the Tibetan sedimentary sequence. Rocks of the Tibetan sedimentary sequence are foliated and also folded into large scale north-vergent recumbent folds that refold earlier south-vergent folds (Brown and Nasarchuk, 1993; Colchen et al., 1981). The north-vergent folds are conspicuously absent below the contact with the Greater Himalayan sequence (cross

section in Colchen et al., 1981). Caby et al. (1983) recognized a structural discontinuity at the base of the large-scale north-vergent folds exposed in the north face of Annapurna within the basal Formation of the Tibetan sedimentary sequence, which they attributed to gravitational collapse. In the Kali Gandaki valley (Figure 1) Brown and Nazarchuk (1993) described ductile and brittle fabrics associated with north-directed normal movement at the top of the Greater Himalayan sequence and interpreted the contact as a strand of the South Tibetan detachment system which they refer to as the Annapurna detachment fault.

In the Modi Khola drainage, thirty kilometers east of the Kali Gandaki transect, structural relationships at the same stratigraphic level are quite different. Parrish and Hodges (1993) reported evidence suggesting both south-directed (thrust-sense) and north-directed (extensional) deformation at this contact. Younger north-directed ductile extensional faulting higher in the Tibetan sedimentary sequence coincides with a break in metamorphic grade (Hodges et al., in press).

Eighty kilometers east of the Modi Khola valley, in the Burhi Gandaki valley, the Greater Himalayan-Tibetan sedimentary sequence contact is deformed by Miocene high-temperature north-dipping shear zones which overprint the main metamorphic foliation and indicate normal and dextral strike-slip displacement (Pêcher, 1991). These structures are considered to be late and not necessarily related to juxtaposition of the Tibetan Sedimentary sequence and Greater Himalayan sequence. The late high-temperature shear zones are interpreted to be synchronous with the last phases of Manaslu pluton emplacement while the temperature was still elevated, and intrusion of the pluton is considered to be late-synchronous to post-kinematic with respect to normal movement on an South Tibetan detachment system-related structure (Pêcher, 1991; Guillot et al., 1994). Although it is likely that there was a structure equivalent to the South Tibetan detachment system in the Manaslu region, emplacement of the Early Miocene Manaslu pluton (Vidal et al., 1982; Deniel et al., 1987; Guillot et al., 1994; Harrison et al., 1995) and elevated temperatures coeval with regional dextral shearing (Pêcher, 1991), have essentially erased its trace.

$^{40}\text{Ar}/^{39}\text{Ar}$  cooling ages from the metamorphic aureole of the pluton show rapid cooling from 19 to 16 Ma and have been interpreted to be the result of normal faulting at higher levels in the Tibetan sedimentary sequence after normal movement on the South Tibetan detachment system and emplacement of the Manaslu pluton (Guillot et al., 1994).

Between the Modi Khola and Burhi Gandaki valleys, a transition occurs from a contact with north-south convergent and north-directed extensional deformation during high-temperature metamorphism to a contact partially obscured by the Manaslu pluton and overprinted by high-temperature right lateral shear zones. The principal aim of the present study was to document the nature of the transition between south directed contraction and north directed extension by mapping structures located along the contact between the Greater Himalayan sequence and the Tibetan sedimentary sequence in the Marsyandi area and in the Dudh Khola valley region (Figures 1 and 2). In the upper Marsyandi valley, the main foliation within the Greater Himalayan sequence and overlying Tibetan sedimentary sequence strikes NE-SW and dips moderately to the NW (Colchen et al., 1980). The Greater Himalayan sequence consists of sillimanite-grade schists and gneisses overlain by biotite-grade marble of the Tibetan sedimentary sequence. Similar to the Kali Gandaki region, this area displays open to tight folds within the Tibetan sedimentary sequence which are absent within the homoclinal Greater Himalayan sequence below, indicating the presence of a structural discontinuity at the contact (Schneider and Masch, 1993).

To evaluate the deformational history of the Greater Himalayan and Tibetan sedimentary sequence contact in the Marsyandi and Dudh Khola valleys, mapping was carried out at 1:12,000 scale during the spring of 1993 and 1994. Previous 1:200,000 scale mapping of central Nepal by Colchen et al. (1981) and Fuchs et al. (1988) provided a regional tectonostratigraphic and structural framework.

## **Tectonic Stratigraphy of the Marsyandi region**

### **Greater Himalayan Sequence**

In Central Nepal, the Greater Himalayan sequence is typically divided into three lithologically distinct packages (e.g., Colchen et al., 1981 and 1986), referred to as Formations I (structurally lowest), II, and III (structurally highest). Formations I, II, and III are continuous along strike for hundreds of kilometers. Formation I comprises a section of pelitic schists, gneisses, and migmatites. The upper 5 km of the Greater Himalayan sequence in the Marsyandi region includes a wide variety of sillimanite-grade calcareous and pelitic metamorphic rocks of Formation II and III, intruded by abundant concordant and cross-cutting leucogranites. The rocks included in Formation II in this part of the section consist of the following (in order of decreasing abundance):

1) Green calc-silicate rocks ( $Di + Ep + Cam + Kfs + Pl + Cal + Qtz + Spn \pm Bt \pm Ms \pm Grt$ ) that vary texturally from massive granofels to banded gneisses.

2) Meta-psammities ( $Bt + Pl + Qtz \pm Ms \pm Ksf \pm Grt$ ) that are foliated and fine-grained. The psammite is interbedded with calc-silicates at the scale of centimeters to tens of meters.

3) Coarse grained pure marble layers ( $Cal \pm Phl$ ) up to several meters thick.

4) Schists ( $Bt + Kfs + Pl + Sil + Qtz \pm Grt$ ), gneisses (similar in composition), and felsic migmatites that are interlayered with the other Formations at a variety of scales.

5) Minor amphibolite layers ( $Hbl + Pl$ ).

In the Marsyandi valley Formation III occurs within the upper half of Formation II. A 400 m thick section of calc-silicate and pelitic gneiss of Formation II overlies Formation III and marks the top of the Greater Himalayan sequence. Formation III is a distinctive augen orthogneiss ( $Qtz + Kfs + Pl + Bt + Sil \pm Ms \pm Grt$ ) characterized by large K-feldspar augen up to 4 cm in the long dimension in a finer-grained foliated to mylonitic matrix. In the Chame region, the augen gneiss is about one kilometer thick and has screens within it up to tens of meters thick of psammite and biotite gneiss. The crystallization age of the augen gneiss was previously thought to be Cambrian based on a composite Rb/Sr plot of whole rock ages from samples from different locations (Le Fort et al., 1986).

Recently obtained U/Pb results from the augen gneiss from the Annapurna region include monazite ages of ca. 36 Ma and discordant zircon ages with a large Paleozoic - Precambrian inherited component (Hodges et al., in press). The U/Pb data are consistent with the interpretation that it is either a deformed Oligocene granite or a Cambro-Ordovician igneous rock that experienced a high temperature Oligocene metamorphic event.

#### Tibetan sedimentary sequence

In the upper Marsyandi valley a complete stratigraphic section of the Tibetan Sedimentary sequence from the Cambrian through the Jurassic is exposed (Fuchs et al., 1988). The basal Formation, referred to as the Cambrian(?) Annapurna Yellow Formation (Cal + Qtz + Pl + Phl ± Di ± Kfs ± Tr), is a 5 km-thick section of complexly folded amphibolite- to greenschist-facies marble. Phlogopite-rich layers define a well-developed foliation within the Annapurna Yellow Formation and give it a brownish-gold color. Compositional layering (alternating phlogopite layers and Cal + Qtz + Pl rich layers) may reflect primary bedding, but the marble is too metamorphosed and deformed to display any primary sedimentary features. Above the Annapurna Yellow Formation, the Ordovician Northface Quartzite (Fuchs et al., 1988) consists of white quartzite interbedded with minor amounts of limestone. Primary sedimentary features, such as cross bedding, can be recognized in outcrop.

#### Intrusive rocks

Tourmaline-bearing leucogranitic dikes that are both concordant and discordant to the foliation intrude the upper part of the Greater Himalayan sequence and the Annapurna Yellow Formation. Cross-cutting leucogranite is much more voluminous in the Dudh Khola region than in the Marsyandi valley, where it comprises 30-50% of the outcrop. Previous U-Pb geochronologic studies from central Nepal have obtained Early Miocene ages of ca. 22 Ma for both cross-cutting and deformed leucogranite at the top of the Greater Himalayan sequence (Nazarchuck, 1993; Harrison et al., 1995). U-Pb monazite and zircon

analyses provide similar direct age constraints for the described leucogranite from the Marsyandi and Dudh Khola valleys (Coleman and Parrish, 1995; Coleman, in prep).

### **Structural History**

The orientation and kinematic interpretation of major structures within the Marsyandi and Dudh Khola valleys (Figure 2 and 3) differ significantly and will be discussed separately. In the Marsyandi region, the Greater Himalayan sequence and the Tibetan sedimentary sequence have undergone a complex deformation history involving at least two penetrative deformational and two metamorphic events. In the following description "D<sub>1</sub>, D<sub>2</sub>, D<sub>3</sub>, ..." notation is used to differentiate the relative ages of deformational structures within specific regions. "D<sub>1</sub>, D<sub>2</sub>, D<sub>3</sub>, ..." structures are not meant to be correlated between different regions or across significant structural sections, where deformation may have been diachronous.

#### Marsyandi transect

##### *Structures within the Greater Himalayan sequence*

Throughout the Greater Himalayan sequence in the Marsyandi valley, compositional layering (S<sub>0</sub>) has been transposed by F<sub>1</sub> isoclinal folds into parallelism with the predominant S<sub>1</sub> foliation. The composite fabrics in the lower half of the Greater Himalayan sequence strike roughly E-W and dip 25°-40° N (Figure 4D). A constantly N-trending L<sub>1</sub> lineation is defined by alignment of micaceous mineral aggregates and quartz and feldspar rods (Figure 4D). S<sub>2</sub> mylonitic fabrics including abundant top-to-the-south S-C mylonitic shear-sense indicators on both macroscopic and microscopic scales and south-verging F<sub>2</sub> folds deform the basal 1 km of the section and indicate that D<sub>2</sub> was an important phase of syn-metamorphic, top to the southwest-directed thrusting (Pêcher, 1977; Pêcher, 1989; Figure 1 and 3, D-D'). L<sub>2</sub> mineral lineation is defined by alignment of kyanite as well as micaceous mineral aggregates in the stretching direction. U-Pb monazite ages from mylonitic kyanite-grade schist indicate an Early Miocene age for D<sub>2</sub> shearing at

the base of the Greater Himalayan sequence during peak metamorphism (Coleman and Parrish, 1995; Coleman, in prep.).

Foliation orientations in the upper half of the Greater Himalayan sequence are not as uniform as in the lower half probably as a consequence of subsequent deformation. The main composite foliation ( $S_2$ ) within the upper 3 km of the Greater Himalayan sequence strikes NE and dips  $25^\circ$ - $45^\circ$  NW (Figure 2 and 4C). A mylonitic  $S_2(?)$  foliation deforms the upper 1000 m of the Greater Himalayan sequence.  $L_2$  lineations range in trend between WSW and WNW.  $D_2$  S-C fabrics indicate top to the west-directed shearing at sillimanite-grade conditions (Figure 5A and 5B). The top to the west-shearing is characterized by penetrative within-sheet deformation that indicates oblique normal sense motion in the upper Marsyandi and it is not limited to deformation at the tectonic contacts shown on the cross sections in Figure 3. There are several generations of lineations within the upper 5 km of the Greater Himalayan sequence. In the pelitic formations, some outcrops clearly exhibit two generations of lineation development, a WNW- to WSW- trending- stretching- lineation ( $L_2$ ) superimposed on an older NE-trending mineral-lineation ( $L_1$ ) (Figure 6). Typically,  $L_1$  is defined by the alignment of micaceous minerals and  $L_2$  is defined by quartz and feldspar rods.  $L_2$  lineations are also formed by the alignment of fibrolitic sillimanite. Within the calc-silicate rocks, it is difficult to distinguish between different generations of lineations. In some places, two generations are weakly preserved, in other locations, the rock is recrystallized and does not preserve a stretching lineation. There is a large scatter in the orientation of lineations measured within the upper half of the Greater Himalayan sequence (Figure 4 C, D). However, the scatter is due (in large part) to the preservation of two generations of lineations, a population of WNW- to WSW- trending  $L_2$  lineations and an older, N- to NE- trending  $D_1$  lineation.

#### *Structures within the Tibetan Sedimentary sequence*

Throughout the Annapurna Yellow Formation, preferred alignment of phlogopite defines an  $S_1$  foliation.  $S_1$  is deformed by open to tight  $F_2$  folds with amplitudes up to 50

meters, that verge primarily (on an individual outcrop scale) to the W to SW. An S<sub>2</sub> foliation is defined by secondary growth of phlogopite, axial planar to F<sub>2</sub> folds. S<sub>2</sub> foliation is variably developed throughout the section but is most intense within the basal 200 meters of the Annapurna Yellow Formation, where it strikes NE-SW and dips moderately to the NW, concordant with the mylonitic foliation of the underlying Greater Himalayan sequence. Within this zone, F<sub>2</sub> folds are sheared out parallel to S<sub>2</sub> foliation planes, so that only the fold hinges or limbs are preserved. Cross-cutting leucogranite dikes that intrude the basal section of the Annapurna Yellow Formation are offset in a normal-sense on shear planes parallel to S<sub>2</sub>.

A shear zone measuring 200-300 meters in thickness occurs three kilometers above the base of the Annapurna Yellow Formation (Figures 2 and 3). This structure is intraformational and does not mark a significant metamorphic break; however, it is a zone of significantly increased strain with well developed D<sub>3</sub>(?) asymmetric structures overprinting older penetrative fabrics. Fold structures within the shear zone range from tight, WSW-verging fold trains to isoclinal recumbent folds with axial planes parallel to S<sub>3</sub> mylonitic foliation. S<sub>3</sub> is defined by layers of recrystallized calcite, quartz and feldspar separated by layers of aligned phlogopite (Figure 7C&D). On mylonitic foliation surfaces, WSW-trending, shallowly-plunging L<sub>3</sub> stretching lineations (Figure 4A) are defined by mineral rods and aligned phlogopite aggregates. Outcrops oriented parallel to the stretching lineation and perpendicular to the foliation exhibit asymmetrically boudinaged pegmatite veins and asymmetric folds that indicate a top to the WSW shear-sense (Figure 7E&F). Petrographic analysis reveals S-C mylonitic fabric also indicative of top to the WSW shearing (Figure 7C&D). All leucogranite bodies within the shear zone are strongly deformed and concordant with the NW-dipping mylonitic foliation (Figure 7A&B). This is in contrast to the section of Annapurna Yellow Formation below the shear zone, which is intruded by both concordant and cross-cutting leucogranite, and is the basis for regarding the higher level shear zone as a D<sub>3</sub> structure. Above the shear zone, a large NW-plunging



F<sub>3</sub> synform, referred to as the Mutsog synform (Colchen et al., 1980), folds the entire remaining Tibetan Sedimentary sequence exposed above this level (Fuchs et al., 1988) (Figures 2 and 3). Fuchs et al. (1988) pair the Mutsog synform with the north-verging anticline in the north face of Annapurna, which has been interpreted as a gravitationally driven drag fold related to along-strike equivalents of the D<sub>2</sub> Chame detachment (see below; Caby et al., 1983; Hodges et al., in press). There are no correlative structures to the Mutsog synform below the D<sub>3</sub> shear zone in the Marsyandi region, and we interpret the fold as related instead to movement on the D<sub>3</sub> shear zone.

#### *Nature of the Chame detachment*

Less than a kilometer west of the village of Chame, marble of the Annapurna Yellow Formation is in direct fault contact with calc-silicate gneiss of the Greater Himalayan sequence. The fault plane, referred to here as the Chame detachment (Figure 2), is concordant with the D<sub>2</sub>-mylonitic foliation of the Greater Himalayan sequence below. Kinematic indicators within pelitic Formations of the footwall on surfaces parallel to L<sub>2</sub>-lineations and perpendicular to S<sub>2</sub>-foliation, include shear bands and S-C fabrics (Platt and Vissers, 1980; White et al., 1980; Berthé et al., 1979; Lister and Snoke, 1984; Pêcher, 1977) that indicate a significant component of top down to the west-directed shearing (oblique normal faulting). Synkinematic growth of minerals suggests that top to the west-south-west shearing occurred at sillimanite grade and lasted through retrograde conditions at greenschist-grade (Figure 5B and 5C). The prevailing sense of displacement across S<sub>2</sub> shear planes within the basal 100-200 meters of the Annapurna Yellow Formation is top to the west, consistent with shear-fabrics in the top 1000 m of the Greater Himalayan sequence.

Along a N-S transect, 2 km east of the confluence of the Naur Khola and Marsyandi rivers (Figure 2), a >20 m thick cataclastic zone juxtaposes marble of the Annapurna Yellow Formation with psammitic schist of Formation II. Petrographic analysis of the cataclasite reveals textures indicative of semi-brittle deformation (Figure 8).

The cataclastic zone dips 45° NW and appears to have cut up section toward the east and exposed a thicker section of Formation II gneisses above the Formation III augen gneiss (Figure 2). The D<sub>2</sub> mylonitic fabrics and L<sub>2</sub> lineations observed in the Chame region are not present in the footwall of the cataclastic zone. The absence of D<sub>2</sub> mylonites indicates either 1) that a shallower level of the Chame detachment is exposed here; or 2) that the fault surface has cut down-section through the mylonitic carapace.

#### *Late structures affecting the upper Marsyandi valley*

The top of the Annapurna Yellow Formation and the overlying Tibetan sedimentary sequence are deformed by multiple high-angle, NNE-striking normal faults (D<sub>4</sub>) (Figures 2, 3, and 9A). These structures truncate the northwest limb of the Mutsog fold (F<sub>3</sub>) (Figure 9C) and deform all foliations within the Tibetan sedimentary sequence, clearly postdating D<sub>2</sub> and D<sub>3</sub> deformation. Extensional fractures and slickenside lineation surfaces within the brittle fault zones consistently indicate normal displacement.

Extensional fractures (Figure 9C&D) are filled with low-T minerals including calcite, quartz and muscovite. <sup>40</sup>Ar/<sup>39</sup>Ar dating of muscovite from the extensional fractures indicates that this phase of brittle extensional deformation is at least 14 Ma (Coleman and Hodges, 1995). The D<sub>4</sub> normal faults are part of a pervasive set of brittle normal faults that deform the region between the upper Marsyandi valley and the Thakkola graben to the west (Colchen et al., 1981)(Figure 1). They are correlated with the oldest NNE-striking extensional faults within the Thakkola graben system (Bordet, 1971; Colchen et al., 1981; Coleman and Hodges, 1995), which predate the Late Miocene opening of the Thakkola graben (Fort et al., 1982) but are indicative of Middle Miocene regional east-west extension (Coleman and Hodges, 1995).

#### Dudh Khola transect

In the Dudh Khola and Surkepek river valleys, adjacent to the main body of the Miocene Manaslu pluton, structural relationships at the contact between the Greater Himalayan sequence and the Tibetan sedimentary sequence are largely obscured by

abundant undeformed leucogranite. However, a north-trending ridge between the Surkepuk and Siklikpuk rivers (Figure 2) exhibits a well exposed section through the contact of the Greater Himalayan sequence and Tibetan sedimentary sequence, with minor interruptions by cross-cutting leucogranite.

#### *Structures within the Greater Himalayan Sequence*

At this location, the top of the Annapurna Yellow Formation is in contact with a 1.5 - 2 km-thick layer of Formation III augen gneiss (Figures 2 and 3, C-C'). The lower part of the augen gneiss has a well-developed  $S_1$  foliation (Figure 10A) that strikes NW-SE and dips moderately to the NE. The augen gneiss does not have a well-developed stretching or mineral lineation indicative of a direction of elongation. In contrast to the lower part, the top 300 m of the gneiss is transposed by a strong  $D_2$ -mylonitic L-tectonite fabric with well-developed  $L_2$  quartz and feldspar rods (Figure 10B). The mylonite zone dips  $40^\circ$  NNE, and the  $L_2$  stretching lineation plunges down dip to the north (Figure 4B). The mylonitized augen gneiss, unfortunately does not display asymmetric fabrics indicative of the shear sense.

#### *Structures within the Tibetan Sedimentary Sequence*

The terrain did not permit close inspection of deformational feature above more than 20 meters of the contact. However, a mylonitic foliation (presumably  $S_2$ ) within marble of the Annapurna Yellow Formation strikes NW-SE, dips  $60^\circ$  NE, and contains NNE trending  $L_2$  lineation. A prominent large-scale (at least 100 m in amplitude) upright synform folds the Annapurna Yellow Formation above the mylonitic-zone and is spectacularly exposed in the cliff faces on the west side of the Siklikpuk Khola (Figure 10C and 10D).

#### *Nature of the contact*

The Annapurna Yellow Formation is in sharp fault contact with Formation III augen gneiss. The contact dips to the northeast and is concordant with  $D_2$  mylonitic fabric of the Greater Himalayan sequence below. Although mylonitic fabric development is well

developed within the fault zone, shear-sense across the zone is ambiguous. The upright orientation of the large-scale synform observed in the hanging wall does not indicate a sense of vergence; however, its geometry is similar to the Mutsog synform and it is most likely a drag fold related to northward displacement on the shear zone at the base of the Tibetan sedimentary sequence. Based on these observations, D<sub>2</sub> deformation at this contact in the Dudh Khola may be compatible with north-directed shearing at the Greater Himalayan - Tibetan sedimentary sequence contact.

### **Timing of deformational Events**

Preliminary U-Pb and <sup>40</sup>Ar/<sup>39</sup>Ar results provide some constraints on the timing of deformation. These results are in preparation and will be available in a complete form in another manuscript. At the top of the Greater Himalayan sequence in the Marsyandi valley, a concordant leucogranite dike from the footwall of the Chame detachment, deformed by west-directed fabrics, yields reversely discordant U-Pb single crystal monazite ages that span 24-34 Ma (Coleman and Parrish, 1995; Coleman, in prep). The spread in ages from a single sample is typical of Miocene Himalayan leucogranites and most likely indicates a ~24 Ma or younger age with an older (~35Ma) inherited component. Muscovite from the same sample that defines the S<sub>2</sub> foliation yields a <sup>40</sup>Ar/<sup>39</sup>Ar cooling age of 17.5 Ma (Coleman and Hodges, 1995). The combined results allow D<sub>2</sub> deformation to be younger than or coeval with ≤ 24 Ma leucogranite intrusion, and require subsequent cooling of the footwall through muscovite closure temperature (~400°C; Robbins, 1972), to have occurred at 17.5 Ma. The higher level, D<sub>4</sub> brittle normal faults in the upper Marsyandi valley are between 14 and 17.5 Ma (Coleman and Hodges, 1995). The 14 Ma age, obtained from secondary muscovite extracted from extensional fractures associated with D<sub>4</sub> normal faults, also places a lower limit on the age of the F<sub>3</sub> Mutsog synform as well as the S<sub>2</sub> foliation that it deforms.

Undeformed leucogranite that intrudes the north-dipping D<sub>2</sub> contact between the Greater Himalayan sequence and the Tibetan Sedimentary sequence in the Dudh Khola

valley yields concordant U-Pb zircon and monazite ages of 18-21 Ma (Coleman and Parrish, 1995; Coleman, in prep). These results indicate that north-directed deformation at this level ceased before ~21 Ma, consistent with previous results in the Manaslu region further east (e.g. Pêcher, 1991; Guillot et al., 1994).

At the base of the Greater Himalayan sequence in the Marsyandi valley, concordant U-Pb monazite analyses from a mylonitic, kyanite-grade gneiss are 18-22 Ma (Coleman, in prep.). This sample is from the D<sub>2</sub> Main Central thrust zone and the results indicate south-directed syn-metamorphic thrusting during monazite growth. Therefore top to the south-directed thrusting is contemporaneous with top to the north-directed extensional faulting and top to the west-directed orogen parallel shearing.

## **Discussion**

### *Lateral strain variation at the top of the Greater Himalayan sequence*

West-directed, orogen-parallel deformation on the Chame detachment was broadly coeval with north-directed normal faulting at the same structural level 15 kilometers to the east. Because of difficult access, the area between the two structures has not been mapped and it is uncertain whether the two fault segments are part of one continuous structure or if they are separated by a cross-structure. West-trending lineations overprint north-trending lineations in the western area, indicating that west-directed shearing was later than north-directed extension in the Marsyandi Valley. Shear fabrics and petrographic analysis indicate that the direction of maximum elongation in the Marsyandi valley changed from north-south to east-west during peak metamorphism while it remained north-south in the Dudh Khola valley.

Simultaneous strain partitioning within thickened sections of penetratively deformed crust is common. However, discussions of this phenomenon usually focus on vertical partitioning of the strain into separate components at different structural levels. Vertical partitioning of strain into incompatible structures can be accommodated by either mechanical decoupling between rheologically contrasting layers (e.g. Burchfiel and

Royden, 1985) or by general noncoaxial flow within a plastically deforming rock mass (Northrup, in press). Both models of deformation are applicable to the Miocene structural development of the Greater Himalayan sequence; however, in central Nepal, the strain pattern not only changes vertically but also laterally over distances on the order of tens of kilometers.

#### *Tectonic denudation at the top of the Greater Himalayan sequence*

The question remains as to whether the South Tibetan detachment system was a through-going structure that accommodated significant tectonic denudation in central Nepal. A prograde increase in metamorphic grade downward through the base of the Tibetan sedimentary sequence was documented by Schneider and Masch (1993) using carbonate solvus thermometry. Maximum temperatures near the base of the sequence were ca. 510-530°C. A strong retrogressive phase of metamorphism at the base of the Tibetan sedimentary sequence, manifested by secondary growth of sphene, clinozoisite, and amphibole, may be attributed to syn to late-syn-metamorphic movement on the Chame detachment (Schneider and Masch, 1993).

#### *Effects of local pressure gradients on flow patterns of plastically deforming rock*

The entire section of the Greater Himalayan sequence throughout the central Himalaya was deforming plastically at temperatures at or above ~500°C during the early to middle Miocene (as reviewed by Hodges et al., 1988; Pêcher, 1989). This temperature is well within the range under which rocks yield by ductile flow at geologic strain rates (Brace and Kohlstedt, 1980). The structural thickness of the Greater Himalayan section increases from 5 km in the Kali Gandaki valley to about 12 km thick in the Marsyandi valley without duplication or truncation of any of the major Formations. The extreme variation in thickness, with relative continuity of Formations, suggests a net flow of material towards the east within the Greater Himalayan sequence. In regions of crustal thickening, lateral pressure gradients caused by differential thinning (or thickening) of the overlying crust will drive lower crustal flow, provided the underlying crust is hot and weak enough (Block and

Royden, 1990). Flow towards the east within the Greater Himalayan sequence could account for west-directed shear between the Greater Himalayan sequence and the relatively rigid overlying Tibetan Sedimentary sequence in the Marsyandi valley. A decrease in the lateral pressure gradient toward the east at the time of deformation could also account for the variation in strain pattern between the two fault segments. Further field analysis is required in order to determine if there is a continuous variation in the strain or "flow" pattern between the two areas that might be reflected in the footwall kinematics.

*Regional orogen parallel strain within the Greater Himalayan sequence*

Orogen-parallel strain at the top of the Greater Himalayan sequence has been described in several locations along the length of the Himalaya. Pêcher (1991) documented top to the east dextral shear east of Manaslu within the Burhi Gandaki transect and, based on the strain pattern there, combined with the pattern of lineation trajectories plotted for the rest of the Himalaya, proposed an orogen scale dextral shear zone. However, the planar fabrics in many transects, associated with orogen-parallel lineations are not asymmetric and may have been produced during a bulk general shearing event with a large component of pure shear strain. In Pêcher's model, the top of the Greater Himalayan sequence provides a mechanical boundary for a relatively rigid Tibetan block extruding eastward. Although this is plausible, the reorientation of the elongation direction within the thermally weakened Greater Himalayan sequence, on the scale of the entire orogen, may also be explained by vertical strain partitioning of the over-thickened wedge.

If dextral shear at the top of the Greater Himalayan sequence was a regional phenomenon, then why is there only evidence of top to the west displacement in the Marsyandi region? From the described field relationships of dextral shearing combined with a kinematic model for emplacement of the Manaslu pluton (Pêcher, 1991; Guillot et al., 1993), it is possible that dextral displacement occurred later than top to the west shear in the Marsyandi valley and it may have been transferred to a higher structural level west of the pluton. Dextral shear east of Manaslu is syn-kinematic with emplacement of the

Manaslu pluton (Pêcher, 1991), whereas west directed-shearing in the Marsyandi valley predates cross-cutting leucogranites of probable Manaslu age. If emplacement of the Manaslu pluton was structurally controlled by a restraining bend in a regional-scale dextral shear zone, as suggested by Guillot et al. (1993), right-lateral shear might have transferred to a higher level of the Tibetan Sedimentary sequence within the Marsyandi valley.

West-directed deformation on the Chame detachment is associated with shallow, obliquely down-dip, lineation trends. On a local scale, these fabrics are extensional. However to the west in the Modi Khola valley, southwest-directed deformation associated with high-temperature metamorphism at a similar structural level results in a transpressional regime accommodated by oblique thrusting across a north-dipping structure (Hodges et al., in press). In both locations, there is a significant component of top to the west-directed orogen parallel deformation, and both fault segments may be part of the same oblique left-lateral shear zone. Although the field relationships in the upper Marsyandi valley all indicate oblique extension, other independent lines of evidence for extension (i.e., as outlined by Wheeler and Butler (1994)), such as the temperature-time history of the footwall and hanging wall, will confirm whether this is a local or regional phenomenon.

Problems of strain compatibility aside, it is clear that orogen-parallel deformation (or at least elongation) at the top of the Greater Himalayan sequence during peak metamorphism was an important element of the Miocene high-temperature deformation. Orogen-parallel deformation during convergence has been documented in other orogens including the Alps (e.g., Mancktelow 1992, Froitzheim et al. 1994, Ratschbacher et al. 1991). In these examples, there is a change from extension normal to the orogenic core zone early in the deformation to extension roughly parallel to the core later in the deformation roughly coeval with peak metamorphic conditions. This consistent pattern suggests a fundamental change in the geometry of the deformation within orogens in general. The fact that the timing of orogen-parallel deformation seems to coincide with



peak metamorphism within the core zone of orogens, suggests a link between the mode of deformation and the strength of the deforming wedge.

#### *Upper crustal, orogen-parallel strain in the Himalaya and Tibet*

Orogen parallel strain is known to be a major component of deformation at the northern margin of the Himalaya and southern Tibetan Plateau (Molnar and Tapponnier, 1978). The active and recent Quaternary tectonics of Tibet and the Himalaya (Molnar and Tapponnier, 1978; Armijo et al., 1986) clearly demonstrate that most of Tibet is undergoing east-west extension during north-south convergence. Numerical experiments show that for this to occur during a constant convergence rate, the plateau must have reached a critically high elevation (England and Houseman, 1989). The most clearly defined structures in the upper Marsyandi region are the youngest brittle normal faults (D4) which strike NNE and deform the metamorphic fabrics associated with west-directed ductile deformation in the region. The orientation of these faults is consistent with the bounding faults of the slightly younger Thakkhola graben, one of the classic examples of recent east-west spreading of the southern Tibetan plateau, and they deform the same physiographic region of the northern Himalaya.

#### **Conclusions**

Results from this study indicate significant along-strike variation in the Miocene deformational history of the South Tibetan detachment system in the Annapurna-Manaslu region. In the Marsyandi region, there are three generations of Early to Middle Miocene top to the west-directed oblique normal faults. The oldest structure, the Chame detachment, accommodated oblique, top to the west-directed shearing during Early Miocene peak metamorphism at the top of the Greater Himalayan sequence and continued to move during retrograde metamorphism. West-trending stretching lineations associated with west-directed displacement on the Chame detachment overprint older north-trending lineations and demonstrate that the orientation of west-directed deformational fabrics was formed by west-directed shearing rather than re-orientation of a previously north-verging

structure. A second zone of obliquely-down-dip, top to the west-directed ductile shear higher in the Tibetan sedimentary sequence is younger than the Chame detachment and is also interpreted to have had a component of normal movement. The youngest deformation in the Marsyandi region is manifested in multiple, moderate- to high- angle brittle normal faults striking to the NNE. To the west of the Marsyandi, in the Dudh Khola region, the top of the Greater Himalayan sequence is deformed by a north-dipping mylonitic zone which is interpreted to be a normal fault. Unlike the Marsyandi region, this area contains north-trending lineations at the top of the high-grade gneisses but no east-west trending lineations. A large scale synform restricted to the hanging wall indicates normal displacement across this zone.

Although the apparently incompatible displacement vectors along the South Tibetan detachment system contact may be diachronous, west-directed extension in the Marsyandi valley on the Chame detachment (orogen-parallel) is roughly coeval with north-directed displacement (orogen-perpendicular) on the South Tibetan detachment system only 15 km away. At present, we can not unequivocally determine how these different fault segments interacted. The footwalls of both structures are thick sections of penetratively deformed crust which was at amphibolite grade during ductile deformation. Extreme lateral thickness gradients in the South Tibetan detachment system footwall, without loss of major Formations, suggests lateral flow of the plastically deforming crust and may account for orogen-parallel deformation at the top of the Greater Himalayan sequence in some locations without requiring large lateral displacement of the upper crustal Formations. Lateral flow could be driven by lateral pressure gradients due to differential thinning of the overlying rock mass during gravitational collapse.

### **Acknowledgments**

The author is grateful to K. Bull for field support, D.R. Thulung and Mangale Sherpa for excellent logistical assistance, and the Nepalese government for research permission. This manuscript benefited from informal reviews by K.V. Hodges, B.C.

Burchfiel, and C.J. Northrup and from discussions with K. Bull and B.N. Upreti. Reviews by H.G. Avé Lallemant, R. D. Law, and an anonymous reviewer also improved the paper. This research has been supported by National Science Foundation Grant No. EAR-9104291 awarded to K.V. Hodges.

## References

- Armijo, R., Tapponnier, P., Mercier, J.L. and Han, T.-L., 1986, Quaternary extension in southern Tibet: field observations and tectonic implications: *Journal of Geophysical Research*, v. 91, p. 803-13,872.
- Berthé, D., Choukroune, P. and Jegouzo, P., 1979, Orthogneiss, mylonite and non coaxial deformation of granites: the example of the South Armorican Shear Zone: *Journal of Structural Geology*, v. 1, p.31-42.
- Block, L. and Royden, L., 1990, Core complex geometries and regional scale flow in the lower crust: *Tectonics*, v. 9, p.557-567.
- Bordet, P., 1971, La tectonique de la Thakkhola, In: *Récherches géologiques dans l'Himalaya du Nepal, région de la Thakkola*, CNRS, Paris, p. 203-232.
- Brace, W.F. and Kohlstedt, D.L., 1980, Limits on lithospheric stress imposed by laboratory experiments: *Journal of Geophysical Research*, v. 85, p. 6248-6252.
- Brown, R.L. and Nasarchuk, J.H., 1993, Annapurna detachment fault in the Greater Himalaya of central Nepal, in P.J. Treloar and M.P. Searle, eds., *Himalayan Tectonics*, The Geological Society, London, Special Publication No. 47, p. 357-374.
- Brun, J.P., Burg, J.P. and Ming, C.G., 1985, Strain trajectories above the Main Central Thrust (Himalaya) in southern Tibet: *Nature*, v. 313, p. 388-390.
- Brunel, M. and Kienast, J.R., 1986, Etude petro-structurale des chevauchements ductiles himalayens sur la transversale de l'Everest-Makalu (Nepal oriental): *Canadian Journal of Earth Science*, v. 23, p. 1117-1137.
- Burchfiel, B.C. and Royden, L., 1985, North-south extension within the convergent Himalayan region: *Geology*, v. 13, p. 679-682.
- Burchfiel, B.C., Zhiliang, C., Hodges, K.V., Yuping, L., Royden, L.H., Changrong, D., Jiene, X., 1992, The South Tibetan Detachment System, Himalayan Orogen: Extension contemporaneous with and parallel to shortening in a Collisional Mountain Belt: *Geological Society of America, Special Paper 269*, 41 p.
- Burg, J.P., Brunel, M., Gapais, D., Chen, G.M. and Liu, G.H., 1984, Deformation of leucogranites of the crystalline Main Central Thrust Sheet in southern Tibet (China): *Journal of Structural Geology*, v.6, p.535-542.
- Caby, R., Pêcher, A. and Le Fort, P., 1983, Le grand chevauchement central himalayen: nouvelles données sur la métamorphisme inverse à la base de la Dalle du Tibet: *Revue de Géologie et de Géographie Physique*, v. 24, p.89-100.
- Colchen, M., Le Fort, P. and Pêcher, A., 1981, Geologic map of Annapurna-Manaslu-Ganesh Himal, Nepal Himalaya, In: *Zagros-Hindu Kush-Himalaya geodynamic*

- evolution, American Geophysical Union, Geodynamic Series, scale 1:200,000, 1 sheet.
- Coleman, M.E. and Hodges, K.V., 1995, Evidence for Tibetan plateau uplift before 14 Myr ago from a new minimum age for east-west extension: *Nature*, v. 374, p. 49-52.
- Coleman, M.E., and Parrish, R.R., Constraints on Miocene high-temperature deformation and anatexis within the Greater Himalaya from U- Pb Geochronology [abs.]: *Eos (Transactions, American Geophysical Union)*, v.76, No. 46, p.F708.
- Deniel, C., Vidal, P.F., A., Le Fort, P. and Peucat, J.-J., 1987, Isotopic study of the Manaslu granite (Himalaya, Nepal): inferences on the age and source of the Himalayan leucogranites: *Contribution to Mineralogy and Petrology*, v. 96, p.78-92.
- England, P., and Houseman, G., 1989, Extension during continental convergence, with application to the Tibetan Plateau: *Journal of Geophysical Research*, v. 94, No. B12, p 17,561-17,579.
- Fort, M., Freytet, P., Colchen, M, 1982, Structural and sedimentological evolution of the Thakkola Mustang Graben (Nepal Himalaya): *Zeitschrift für Geomorphologie N.F.*, Suppl.-Bd 42, p. 75-98.
- Froitzheim, N., Schmid, S.M., and Conti, P., 1994, Repeated change from crustal shortening to orogen-parallel extension in the Austroalpine Formations of Graubünden: *Eclogae geologicae Helvetica*, v. 87, No. 2, p. 559-612.
- Fuchs, G., Widder, R. and Tuladhar, R., 1988, Contribution to the geology of the Manang area (Annapurna Himal, Nepal): *Jahr buch der geologischchen Bundesanstalt, Wien*, v. 131, p.593-607.
- Gansser, A., 1964, *Geology of the Himalaya*, London, England, Interscience Publishers, 289 p.
- Guillot, S., Hodges, K.V., Le Fort, P. and Pêcher, A., 1994, New constraints on the age of the Manaslu leucogranite: evidence for episodic tectonic denudation in the central Himalaya. *Geology*, v. 22, p.559-562.
- Harris, N. and Massey, J., 1994, Decompression and anatexis of Himalayan metapelites: *Tectonics*, v. 13, No. 6, p.1537-1546.
- Harrison, T.M., McKeegan, K.D. and Le Fort, P., 1995, Detection of inherited monazite in the Manaslu leucogranite by  $^{208}\text{Pb}/^{232}\text{Th}$  ion microprobe dating: crystallization age and tectonic implications: *Earth and Planetary Science Letters*, v. 133, p. 271-282.
- Herren, E., 1987, Zaskar shear zone: northeast-southwest extension within the Higher Himalaya (Ladakh, India): *Geology*, v. 15, p.409-413.

- Hodges, K.V., Hubbard, M.S., Silverburg, D.S., 1988, Metamorphic constraints on the thermal evolution of the central Himalayan Orogen: *Philosophical Transactions of the Royal Society of London*, v. A326, p. 257-280.
- Hodges, K.V., Parrish, R.R., Housh, T.B., Lux, D.R., Burchfiel, B.C., Royden, L.H. and Chen, Z., 1992, Simultaneous Miocene extension and shortening in the Himalayan orogen: *Science*, v.258, p.1466-1470.
- Hodges, K.V., Burchfiel, B.C., Royden, L.H., Chen, Z. and Liu, Y., 1993, The metamorphic signature of contemporaneous extension and shortening in the central Himalayan orogen: data from the Nyalam transect, southern Tibet: *Journal of Metamorphic Geology*, v.11, p.721-737.
- Hodges, K.V., Parrish, R.R., Searle, M.P., in press, Tectonic evolution of the Central Annapurna Range, Nepalese Himalaya: *Tectonics*.
- Hubbard, M.S. and Harrison, T.M., 1989,  $^{40}\text{Ar}/^{39}\text{Ar}$  constraints on deformation and metamorphism in the Main Central Thrust zone and Tibetan Slab, eastern Nepal Himalaya: *Tectonics*, v.8, p.865-880.
- Le Fort, P., 1975, Himalaya: the collided range. Present knowledge of the continental arc: *American Journal of Science*, v. 275A, p.1-44.
- Le Fort, P., Debon, F., Pêcher, A., Sonet, J., and Vidal, P., 1986, The 500 Ma magmatic event in Alpine southern Asia, a thermal episode at Gondwana scale, *Sciences de la Terre Mémoire*, v. 47, p. 191-209.
- Lister, G.S. and Snoke, A.W., 1984. S-C Mylonites: *Journal of Structural Geology*, v. 6, p. 617-638.
- Mancktelow, N.S., 1992, Neogene lateral extension during convergence in the Central Alps: Evidence from interrelated faulting and backfolding around the Simplon pass (Switzerland): *Tectonophysics*, v. 215, p. 295-317.
- Molnar, P., England, P. and Martinod, J., 1993. Mantle dynamics, uplift of the Tibetan Plateau, and the Indian monsoon. *Reviews of Geophysics*, v. 31, No. 4, p.357-396.
- Molnar, P. and Tapponnier, P., 1975, Cenozoic tectonics of Asia: effects of a continental collision: *Science*, v.183, p.419-426.
- Molnar, P. and Tapponnier, P., 1978, Active tectonics of Tibet: *Journal of Geophysical Research*, v. 83, p.5361-5375.
- Nazarchuk, J.H., 1993, Structure and geochronology of the Greater Himalaya, Kali Gandaki region, west-central Nepal [Master's thesis]: Ottawa, Carleton University, 157 p.

- Northrup, C.J., in press, General non-coaxial flow at deep levels of a collisional orogen: an example from the northern Scandinavian Caledonides: *Tectonics*.
- Parrish, R.R. and Hodges, K.V., 1993, Miocene (22±1) Ma metamorphism and two stage thrusting in the Greater Himalayan sequence, Annapurna Sanctuary, Nepal: *Geological Society of America Abstracts with Programs*, v. 25, No. 6, p. A-174.
- Parrish, R.R. and Hodges, K.V., in press, Isotopic constraints on the Age and Provenance of the Lesser and Greater Himalayan sequences, *Nepalese Himalaya: Geological Society of America Bulletin*.
- Pêcher, A., 1977, Geology of the Nepal Himalaya: deformation and petrography in the Main Central Thrust zone: in *Ecologie et Geologie de L'Himalaya, Colloques Internationaux du Centre National de la Recherche Scientifique*, Paris, v. 268, p. 301-318.
- Pêcher, A., 1989, The metamorphism in the Central Himalaya: *Journal of Metamorphic Geology*, v.7, p.31-41.
- Pêcher, A., 1991, The contact between the higher Himalaya crystallines and the Tibetan sedimentary series: Miocene large-scale dextral shearing: *Tectonics*, v. 10, p.587-598.
- Platt, J.P. and Vissers, R.L.M., 1980, Extensional structures in anisotropic rocks: *Journal of Structural Geology*, v. 2, No. 4, p. 397-410.
- Ratsschbacher, L., Frisch, W., and Linzer, H.G., 1991, Lateral extrusion in the Eastern Alps, part II; structural analysis: *Tectonics*, v. 10, p. 257-271.
- Robbins, G.A., 1972, Radiogenic argon diffusion in muscovite under hydrothermal conditions [Master's thesis]: Providence, Brown University, 42 p.
- Schneider, C. and Masch, L., 1993, The metamorphism of the Tibetan Series from the Manang area, Marsyandi Valley, Central Nepal, in P.J. Treloar and M.P. Searle, eds., *Himalayan Tectonics*, the Geological Society, London, Special Publication No. 47, p. 357-374.
- Searle, M.P. and Fryer, B.J., 1986, Garnet, tourmaline and muscovite-bearing leucogranites, gneisses and migmatites of the Higher Himalaya from Zaskar, Kulu, Lahoul and Kashmir: In Coward, M.P., and Ries, A.C., eds., *Collision Tectonics*, The Geological Society, London, Special Publication No. 19, p. 185-201.
- Stocklin, J., 1980, Geology of Nepal and its regional framework, *Journal of the Geological Society of London*, v. 137, p.1-34.
- Vidal, P., Cocherie, A., and Le Fort, P., 1982, Geochemical investigations of the origin of the Manaslu leucogranite (Himalaya, Nepal): *Geochimica et Cosmochimica Acta*, v. 46, p. 2279-2292.

Wheeler, J., and Butler, R.W.H., 1994, Criteria for identifying structures related to true crustal extension in orogens: *Journal of Structural Geology*, v. 16, No. 7, p. 1023-1027.

White, S.H., Burrows, S.E., Carreras, J., Shaw, N.D. and Humphreys, F.J., 1980, On mylonites in ductile shear zones: *Journal of Structural Geology*, v. 2, p.175-187.



## Figure captions

Figure 1) Simplified regional tectonic map of central Nepal from Colchen et al. (1980) with minor modifications from this study. The major structures include the Main Central thrust (MCT), the South Tibetan detachment system (STDS), and the Thakkhola graben. There are two normal faults located on the map that are part of the STDS; the basal fault ( $D_2$ ) is decorated with the open half circles and the structurally higher fault ( $D_3$ ) is decorated with filled half circles. The summits of Annapurna I (Ann I), Annapurna II (Ann II), and Manaslu are located by black diamonds. The village of Chame and the city of Pokhara are marked by black squares. The inset map shows the location of the Annapurna-Manaslu region within the Himalaya.

Figure 2) Geological map of the upper Marsyandi and Dudh Khola valley region. Cross section lines A-A', B-B', C-C', and D-D' correspond to Figure 3. A patterned version of the map is used as an inset in Figure 4 and provides a simplified guide to the distribution of the various map units.

Figure 3) Cross sections correspond to section lines marked on the geologic map in Figure 2. Lines A-A' and B-B' show three generations of west-directed deformational structures. The  $D_3$  shear zone marks the upper limit of leucogranite intrusions. Line B-B' shows the Mutsog synform to be limited to the hanging wall of the  $D_3$  shear zone. Line C-C' shows north-ward displacement on a structure which places the Annapurna Yellow Formation in direct contact with the Formation III augen gneiss. Line D-D' includes the lower half of the Greater Himalayan sequence, the south-directed Main Central Thrust zone and the top of the Lesser Himalayan sequence (unpatterned).

Figure 4) Equal area lower hemisphere plots with foliation and lineation data from the Marsyandi and Dudh Khola valleys. The map is simplified from Figure 2.

Figure 5) (a) migmatitic layers in meta-psammite deformed by top to the west-directed S-C fabrics. A vertical leucogranitic dike cross-cuts all fabric. (b) Syn-kinematic fibrolitic sillimanite in top to the west-directed mylonitic S-C foliation planes. (c) Syn-kinematic chlorite in mylonitic shear band foliation indicating top to the west shear-sense at greenschist grade conditions. Photographs a, b, and c, are viewed toward the north. The top to the west shear sense indicates obliquely down dip displacement across the Chame detachment on a local scale, and on a more regional scale indicates orogen-parallel shear.

Figure 6) Photograph of a meta-psammite foliation surface from Chame showing development of two generations of lineation. A west-trending stretching lineation ( $L_{S2}$ ) is defined by quartz and feldspar rods, and a north-trending mineral lineation ( $L_{M1}$ ) is defined by alignment of micaceous aggregates and felsic minerals.  $L_{S2}$  overprints  $L_{M1}$ .

Figure 7) (A) photograph and corresponding line drawing (B) of a 4 km thick section of the Annapurna Yellow Formation. View is towards the north. The horizon of concordant leucogranite (highlighted in the line drawing) coincides with a mylonitic zone with top-to-the-west shear-sense kinematic indicators. (C) photograph and corresponding line drawing (D) of type II S-C mylonite (i.e. Lister and Snoke, 1984) that deforms marble of the Annapurna Yellow formation. The shear sense deduced from S-C mylonites indicates a component of top to the west-directed shear within the Mutsog shear zone. View is towards the north. (E) photograph and corresponding line drawing (F) of west-verging folds and boudinaged pegmatite in the Annapurna Yellow formation also from the Mutsog shear zone. View is towards the north.

Figure 8) Photomicrograph of cataclasite from northwest of the Naur Khola (Figure 2). Clasts of quartz, feldspar and diopside are in a matrix of ductily deformed calcite.

Figure 9) (A) Photograph and corresponding line drawing (B) of the "Mutsog synform", a northwest plunging synform in the hanging wall of the Mutsog shear zone that deforms mylonitic foliation of the Annapurna Yellow formation. The view is towards the southeast across the upper Marsyandi River and the cliff is an exposed dip-slope surface of the folded foliation surface. (C) Photograph (view to the north) of an avalanche gully that follows the trace of a steeply northwest-dipping brittle normal fault that deforms the northeast limb of the Mutsog synform. Also shown are north-striking steeply east-dipping extensional fractures. (D) photograph of vertical north-striking extensional fractures, part of the same fracture system shown in (C). Extensional fractures that deform foliation within the Annapurna Yellow formation filled with secondary muscovite growth.

Figure 10) (A) Photograph of Formation III. Outcrop surface is perpendicular to the foliation and displays the large K-feldspar augen diagnostic of this Formation. (B) L-tectonite from a north-dipping shear zone at the top of Formation III. (C) Photograph and (D) corresponding line drawing of north dipping shear zone separating the Annapurna Yellow Formation from the Formation III orthogneiss at the head waters of the Siklikpuk. A large synform deforms the hanging wall sedimentary Formations.



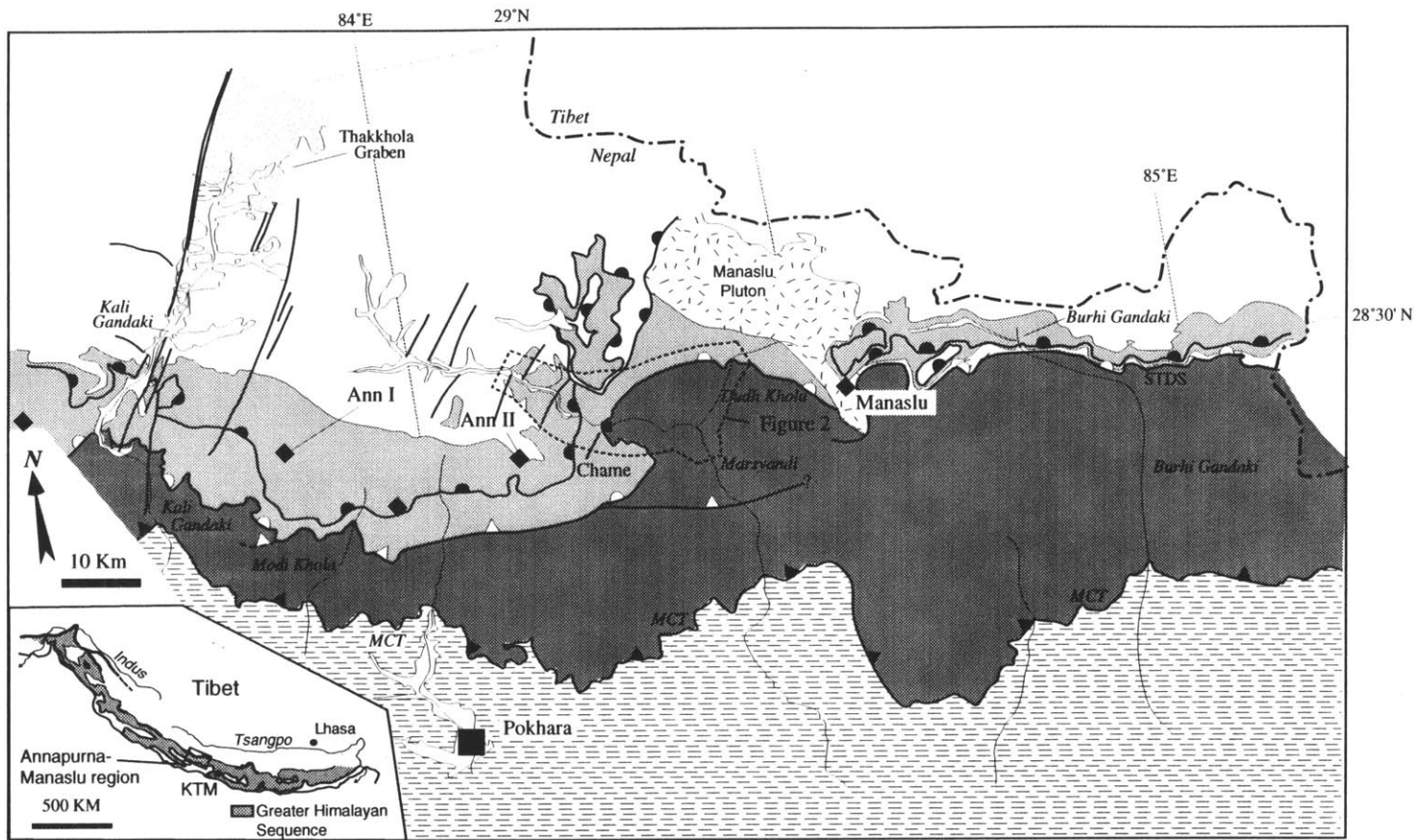


Figure 1



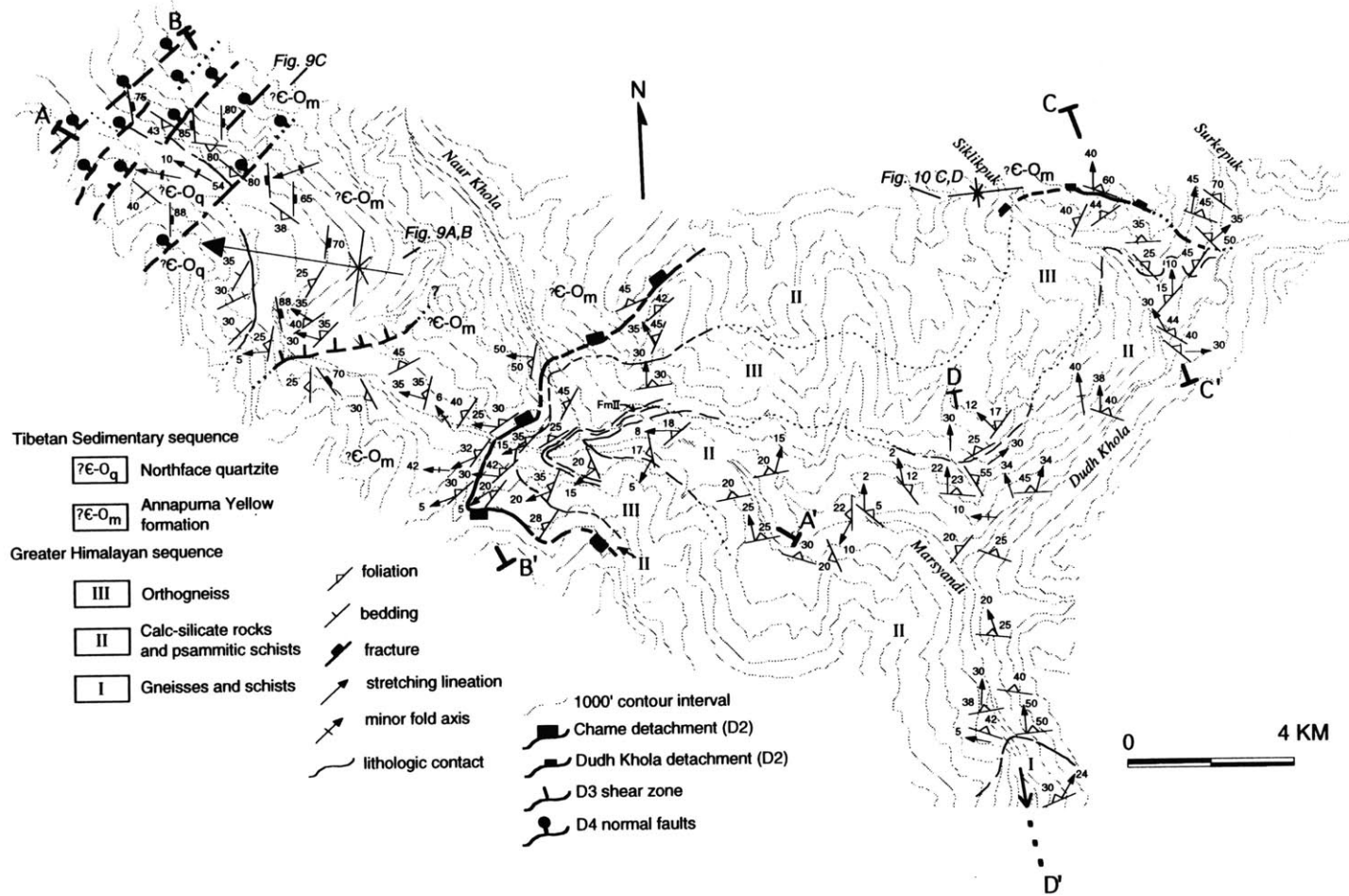


Figure 2





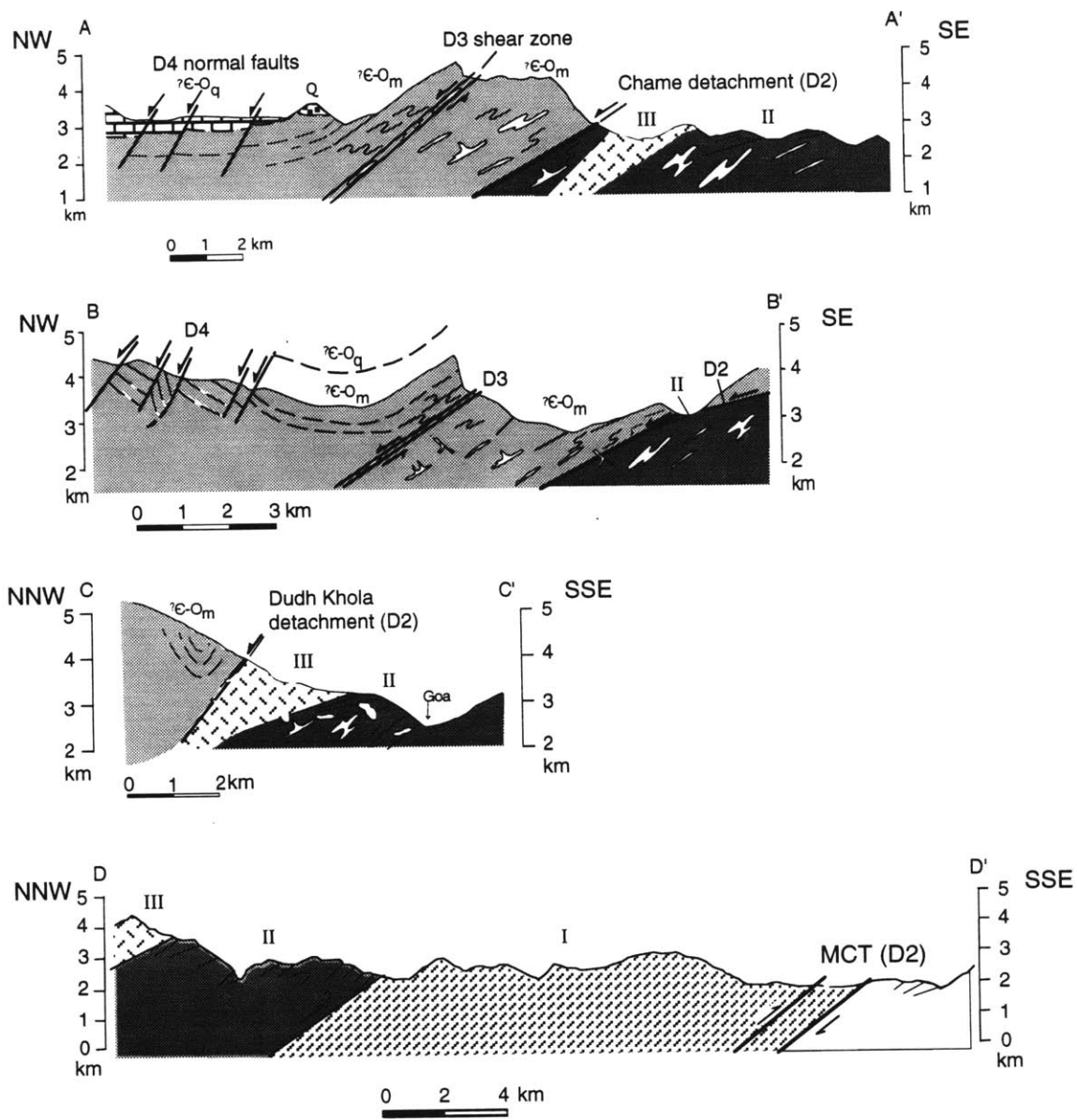
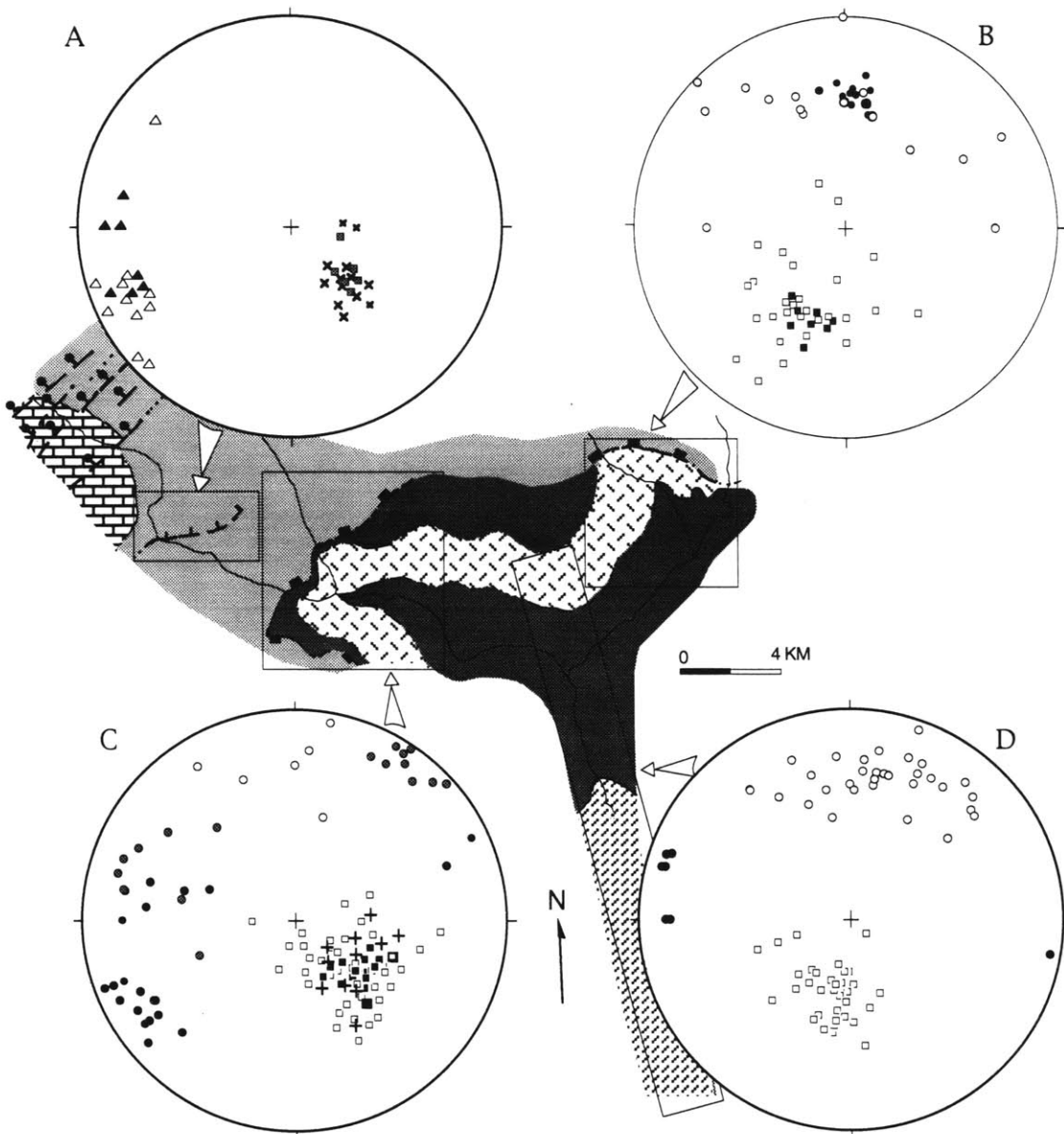


Figure 3





Deformation	Foliation	Lineation
D1	□ S1	○ L1
D2	■ S2	● L2
D1 + D2 (indistinct)	+ S1 + S2	● L1 + L2
D3	■ S3	▲ L3
D2 + D3 (indistinct)	x S2 + S3	△ L2 + L3

**Tibetan Sedimentary sequence**

- Northface quartzite (?C-0)
- Annapurna Yellow Formation (?C-0)

**Greater Himalayan sequence**

- Unit III
- Unit II
- Unit I

Figure 4



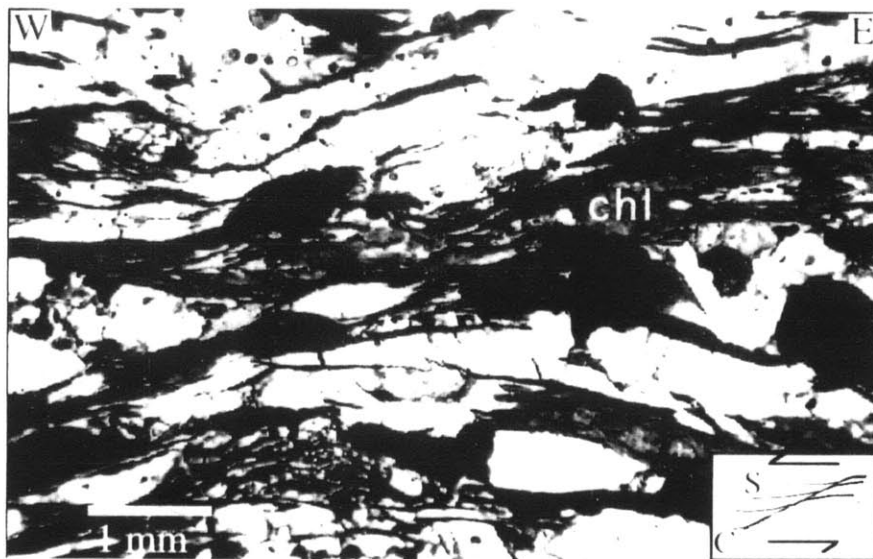
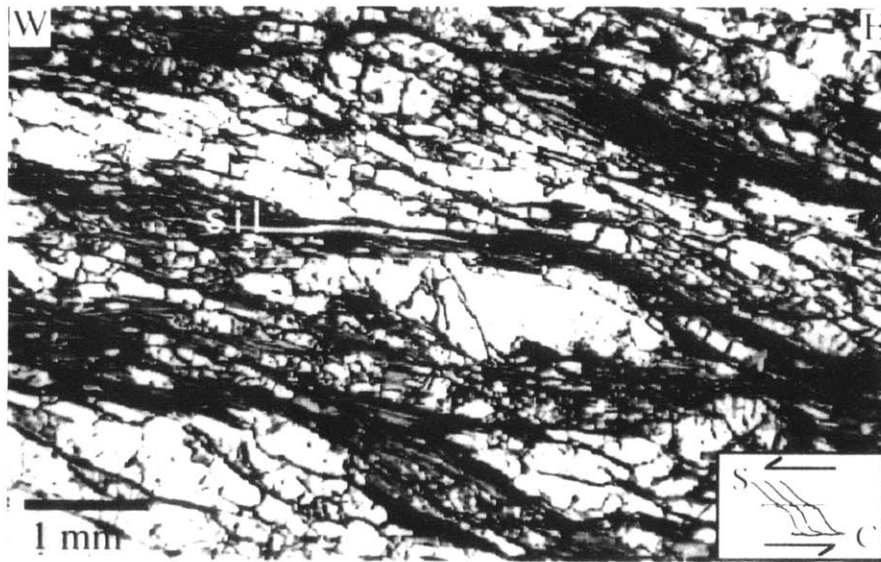
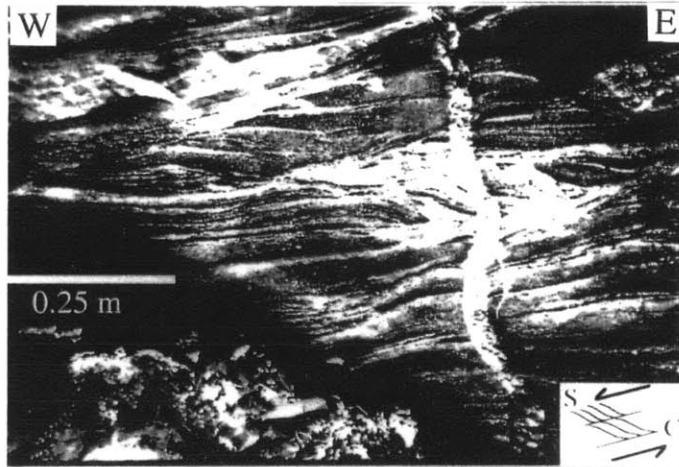
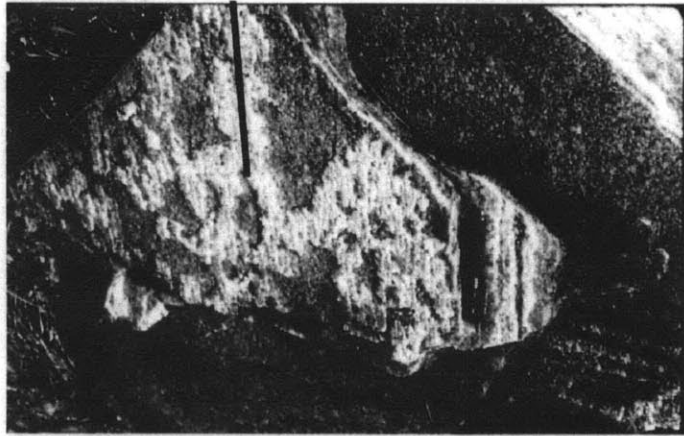


Figure 5



L<sub>s2</sub>



L<sub>m1</sub>

Figure 6





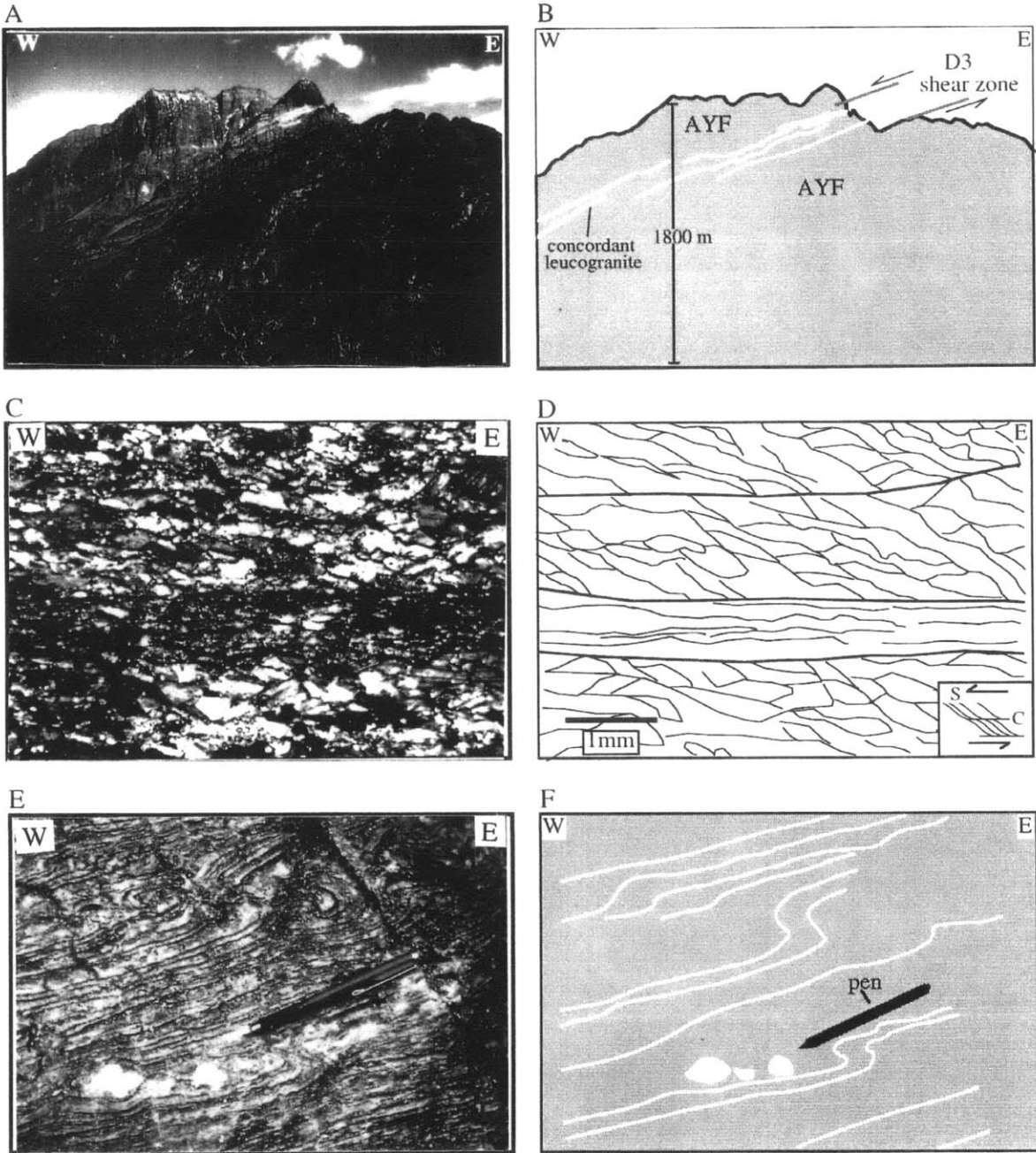


Figure 7



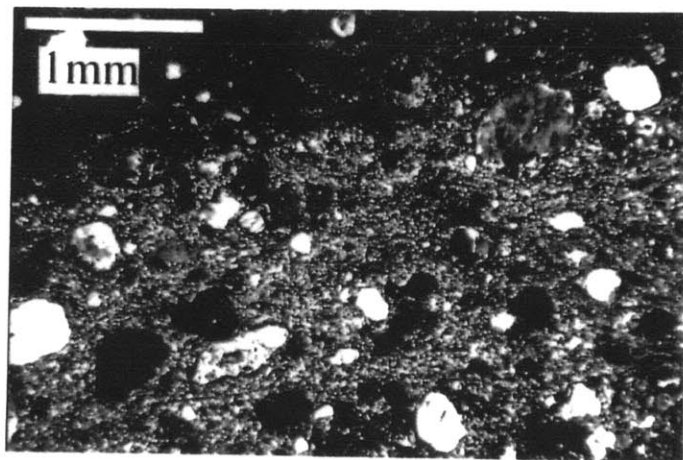


Figure 8



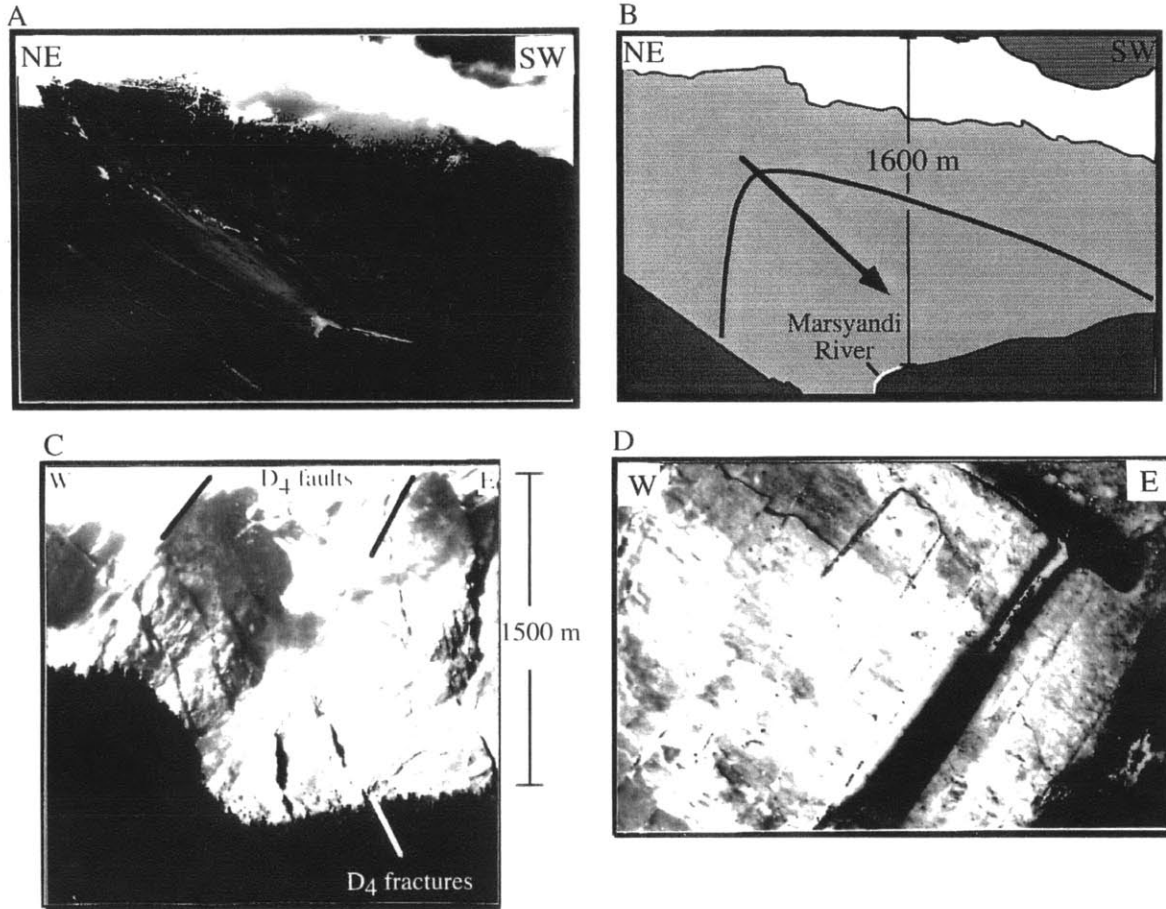


Figure 9



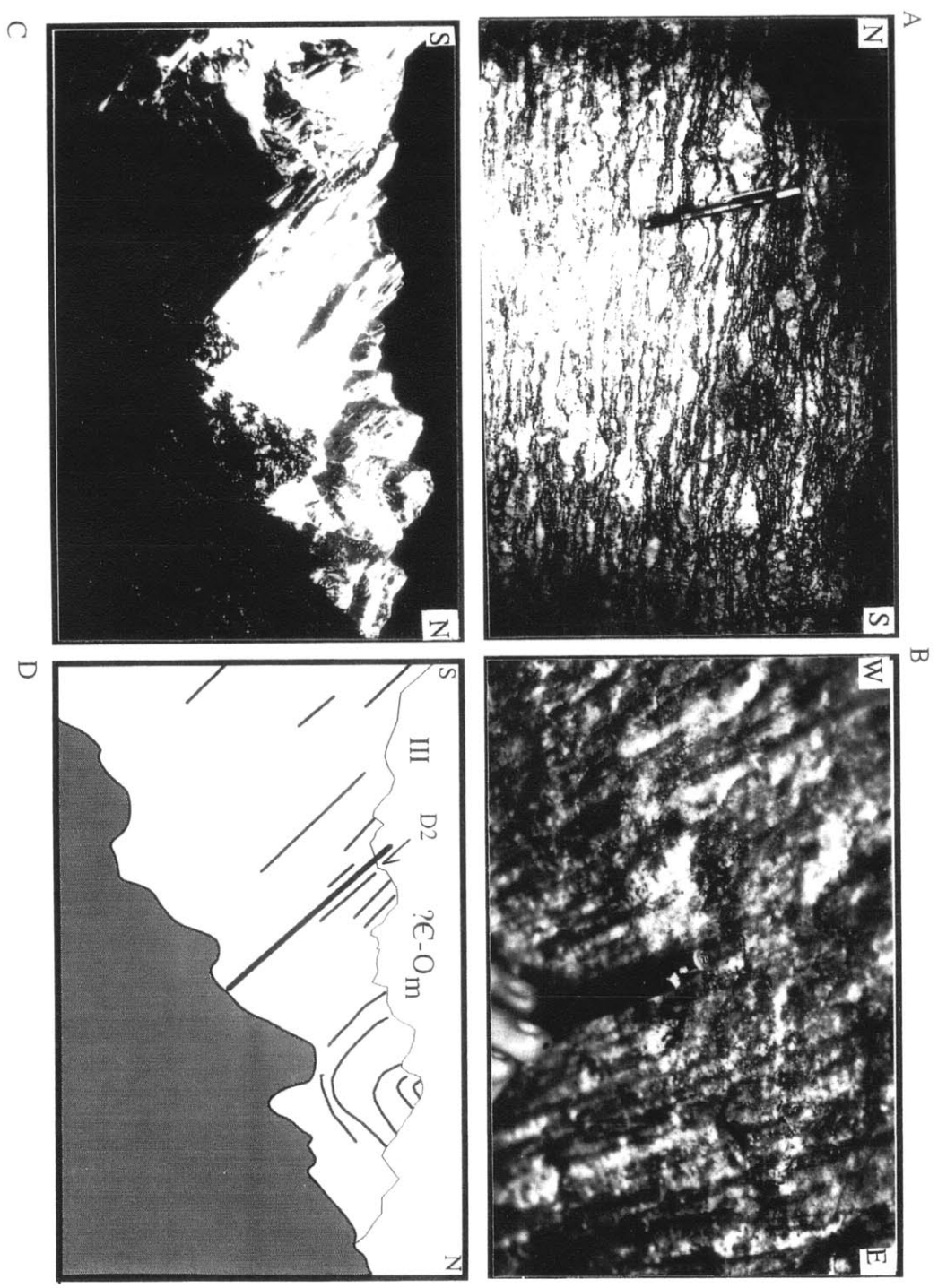


Figure 10





## Chapter 3

### **U-Pb Constraints on Oligocene - Miocene Deformation and Anatexis, Marsyandi Valley, central Nepalese Himalaya**

#### **Abstract**

In the Marsyandi and Dudh Khola valleys of central Nepal a 12 km thick section of amphibolite-facies gneisses, the Greater Himalayan sequence, is completely exposed, and can be described as a metamorphic wedge. It is bound by the Miocene north-dipping Main Central Thrust (MCT) at its base, and roofed by the roughly coeval north-dipping normal faults of the South Tibetan detachment system. Monazite and zircon U-Pb analyses indicate that migmatization at the base of the Greater Himalayan sequence was coeval with migmatization and leucogranite emplacement at the top of the section. Metamorphic monazite ages from mylonitic migmatitic schists within the MCT-zone indicate syn-tectonic amphibolite-grade metamorphism at ~22 Ma, possibly lasting until 18 Ma. Within the upper Greater Himalayan sequence, foliated migmatitic leucogranites yield complicated U-Pb systematics, but are interpreted to have formed at ~22 Ma. Monazite data from the ~22 Ma migmatite have a ~35 Ma inherited component which may reflect Oligocene metamorphism or magmatism. Undeformed leucogranite dikes transect all foliations and intrude the contact between the Greater Himalayan sequence and the overlying Tibetan sedimentary sequence; they yield ~18 Ma ages, placing a lower bound on the age of regional metamorphism and high-temperature deformation.

Field relationships and the ages of migmatization and leucogranite intrusion support models for melt-enhanced deformation (Hollister and Crawford, 1986) along the South Tibetan detachment system, but also allow for late syn-tectonic granite melting to be enhanced by decompression associated with normal faulting. Previous suggestions that

leucogranite generation within the upper Greater Himalayan sequence is temporally unrelated to the formation of migmatites or high-temperature deformation associated with the MCT are inconsistent with the age constraints presented here. Although fundamental distinctions are made between the migmatites and the leucogranites based on trace-element geochemistry, it seems unlikely that they are not genetically related considering their close proximity and timing.

### **Introduction**

The Himalaya host several examples of anatectic granites that intruded during the peak of syn-orogenic metamorphism. As in other continent-continent collisional settings, the mechanism for granite genesis is difficult to determine and there are at least two competing viable models. Whether these granites formed in response to decompression during normal faulting or by wet-melting triggered by thrusting emplacement of hot rocks onto cooler rocks is a fundamental unresolved issue relevant not only for the Himalaya but for magma genesis in compressional orogens in general.

Competing geochemical models that explain anatexis within the Himalaya rely on unique tectonic conditions which, to a certain degree, are testable. In the case of wet melting, granites are produced when fluids are advected from a cool footwall to a relatively hot hanging wall during thrust faulting (e.g. LeFort, 1975). Conversely, for dry melting to occur, significant decompression along normal faults immediately prior to granite emplacement is required in order to produce the volume of melt observed (e.g. Harris and Inger, 1992). The dry melting model introduces an additional controversy of whether magma intrusion triggered extensional faulting (i.e. Hollister and Crawford, 1986) or visa versa. Establishing the relative timing of metamorphism, deformation, and anatexis is a key step toward understanding how these tectonic processes are related. The central

Himalaya which have nearly continuous exposure of the metamorphic core, provide an ideal place to explore the genesis of alpine granites.

The metamorphic core of the Himalaya hosts a thick section of plastically deformed medium to high grade migmatitic schists and gneisses intruded by anatectic granites. The base of the core is a north-dipping crustal scale thrust fault system, the Main Central thrust (MCT), and its roof is marked by gravitationally-driven north-dipping normal faults of the South Tibetan detachment system. The upper half of the metamorphic core is intruded by abundant leucogranites that are both deformed by and cut across ductile fabrics within the metamorphic rock. The combined results of several studies demonstrate rapid and largely contemporaneous thrust faulting, extension, peak metamorphism and anatexis during the early Miocene (e.g. LeFort, 1975, 1981; Pêcher, 1989; Hubbard and Harrison, 1989; Burchfiel et al., 1992; Hodges et al., 1992). However, despite these efforts, many aspects the thermal evolution of the core region remain enigmatic.

Geochronologic data presented here are for leucogranites and gneisses from the metamorphic core of the central Nepalese Himalaya in the Marsyandi and Dudh Khola valleys (Figure 1). The main reason for establishing the ages of leucogranite intrusion and migmatization in this region was to establish the absolute and relative ages of MCT and South Tibetan detachment deformation. A detailed structural analysis of deformation in the upper portion of the Greater Himalayan sequence is given in Chapter 2.

### **Geologic setting**

In the Marsyandi valley the metamorphic core of the orogen, the Greater Himalayan sequence, is exposed in a 12 km-thick section of north-dipping gneisses (Figure 1). The gneisses are subdivided into three mappable formations (Colchen et al., 1986). Formation I consists of pelitic gneisses and migmatites. Formation II is primarily comprised of calc-silicate rocks, and Formation III is a distinctive augen orthogneiss found

at the top of the Greater Himalaya sequence in most transects through the orogen (Colchen et al., 1986). The Greater Himalayan sequence was derived from Indian crust accreted during northward intercontinental subduction (Gansser, 1964).

The MCT at the base of the Greater Himalayan sequence in the Marsyandi region was described in detail by Pêcher (1977, 1989), who documented top to the south thrust faulting penecontemporaneous with kyanite-grade metamorphism. Along the entire orogen, the MCT is associated with an inverted metamorphic sequence (Gansser, 1964; Bordet, 1973; LeFort, 1975). In the central Himalaya, most MCT displacement was syn-metamorphic and the thrust is clearly linked to the configuration of metamorphic isograds within the upper Lesser Himalayan sequence and in the lower section of the Greater Himalayan sequence (LeFort, 1975, 1981; Pêcher, 1978, 1989; Hubbard, 1989). However, where the Greater Himalayan sequence is relatively thick, a second inverted metamorphic gradient occurs within it (e.g. Hubbard, 1989; Pêcher, 1989; Macfarlane, 1992), and this thermal structure cannot be explained in any simple way by syn-metamorphic displacement.

Peraluminous leucogranites are distributed along the strike of the High Himalaya for at least 1000 km. They form discreet sills, dikes, or laccoliths emplaced within the upper Greater Himalayan sequence at or near its upper contact. Although the mechanism that triggered the formation of the granites is controversial, it is generally agreed that they represent intracrustal anatexis. In the Marsyandi valley, the metamorphic grade increases along a Barrovian field gradient from chlorite grade structurally below the Greater Himalayan sequence, to kyanite-grade near the MCT, to sillimanite-grade within the MCT-zone. Accompanying the apparent upward increase in grade within the Greater Himalayan sequence is a noticeable increase in the amount of migmatization within the pelitic gneisses of Formation I, from 5-10% within the MCT zone to ~ 30% at a position 1-2 km higher.

Abundant deformed and undeformed leucogranite intrudes the top 4 km of the Greater Himalayan sequence and the basal part of the Tibetan sedimentary sequence.

The top 1-3 km of the Greater Himalayan sequence is deformed by extensional shear zones, penecontemporaneous with sillimanite-grade metamorphism (Pêcher, 1991; Coleman, in press). North-directed extensional faulting at the top of the Greater Himalayan sequence is recognized along the length of the orogen (Burchfiel et al., 1992; and references therein) and it is coeval with early Miocene thrusting on the MCT in the Everest region (Hodges et al., 1992). Ductile extensional structures in the Marsyandi region are in part coeval with peak metamorphism and pre- to late- kinematic with respect to anatexites and leucogranite plutons, the largest of which is the Manaslu pluton (LeFort, 1981; Pêcher, 1989; Guillot, 1993).

The Manaslu pluton was emplaced between gneisses of the Greater Himalayan sequence and lower grade metamorphosed marble of the Tibetan sedimentary sequence (Le Fort, 1975; 1981). The pluton truncates deformational structures within the Tibetan sedimentary sequence that are associated with north-directed displacement on the South Tibetan detachment system. However, parts of the granite are foliated, and the base of the pluton is both concordant and in metamorphic equilibrium with the Greater Himalayan sequence (Le Fort, 1981).

#### Metamorphism and anatectic melting

The metamorphic history of the Greater Himalaya in central Nepal has been described as a two-stage process commonly referred to as Eohimalayan ( $M_1$ ) and Neohimalayan ( $M_2$ ) (see Hodges et al. 1988; and Pêcher, 1989; for a review of pressure-temperature constraints and tectonic evolution). Initially, rocks at the base of the Greater Himalayan sequence were buried to about 30 km depth during inter-continental subduction, at which time high-pressure, moderate-temperature assemblages equilibrated at the base of

the Greater Himalayan sequence ( $M_1$ ). Neohimalayan metamorphism took place at lower pressures and higher temperatures during displacement on the MCT. Anatexis within the Greater Himalayan sequence, sillimanite-grade metamorphism, and leucogranite emplacement are all thought to be signatures of the  $M_2$  phase of metamorphism.

The existence of large volumes of leucogranite melt at the top of the Greater Himalayan sequence has been explained in a variety of ways. It is generally agreed that the leucogranites were derived from a pelitic crustal protolith; geochemical and field studies suggest that metasedimentary rocks of the Greater Himalayan sequence are the probable source (Dietrich and Gansser, 1981; LeFort, 1981; Vidal et al., 1982; Deniel et al., 1987; LeFort et al., 1987; France-Lanord et al., 1988). However, there is lack of agreement over what section of the Greater Himalayan sequence they were derived from and whether they were produced by “wet” or “dry” melting (e.g., LeFort et al., 1981; Inger and Harris, 1993). These opposing melting models are of interest because they not only require different geochemical processes but are also linked to different tectonic events.

The “wet” melting model of LeFort et al. (1981) requires thrust emplacement along the MCT. In this model, fluids are advected from the footwall of the MCT into the relatively hot hanging wall during thrust emplacement. The fluids trigger anatexis within the Greater Himalayan sequence during sillimanite-grade metamorphism and ultimately lead to emplacement of the leucogranites. In this model the source for leucogranites is within the sillimanite-grade migmatitic gneisses immediately below the granites. It gains support from field relationships that demonstrate synkinematic to late-synkinematic emplacement of the leucogranites with respect to MCT movement (LeFort et al., 1981).

In the “dry” melting model, leucogranites are formed under vapor-absent conditions, as suggested by trace-element systematics (Harris and Inger, 1992; Harris et al., 1993). In this case, decompressional melting, accomplished by normal faulting along

the South Tibetan detachment system, is required to produce the necessary melt fraction (Harris and Inger, 1992; Inger and Harris, 1993). This model does not require syn-anatectic thrusting along the MCT, but suggests that most leucogranites would be synchronous with or postdate South Tibetan Detachment displacement. Additionally, on the basis of contrasting Sr and Nd isotopic signatures, Inger and Harris (1993) argue that the large leucogranite bodies and distributed migmatites are from different sources, and that the latter may be significantly older than Miocene movement on the MCT.

The link between the South Tibetan detachment system and the leucogranites has important implications for the competing geochemical models. The close proximity of the leucogranites to the South Tibetan Detachment system along the length of the orogen is remarkable. However, it remains an unresolved issue as to whether the granites triggered normal faulting (i.e. Hollister and Crawford, 1986) or the converse is true (e.g., Inger and Harris, 1992). Scaillet et al. (1995) concluded that *emplacement* of leucogranite from the Garhwal Himalaya must be genetically related to normal faulting, but that magma generation could still be related to thrusting.

In order to rigorously test the link between leucogranite emplacement at the top of the Greater Himalayan sequence and formation of migmatites 12 km down section, we must obtain direct age constraints from both the leucogranite and the MCT. A recent study interpreted the crystallization age of the Manaslu pluton to be  $22.4 \pm 0.5$  Ma based on  $^{232}\text{Th}/^{208}\text{Pb}$  ion-microprobe dating of monazite (Harrison et al., 1995), and these results are consistent with the conclusions of Guillot et al. (1994) for the crystallization age of the granite based on  $^{40}\text{Ar}/^{39}\text{Ar}$  cooling ages from the metamorphic aureole. Past studies cite isotopic age determinations from the Manaslu pluton as the age of syn-metamorphic displacement on the MCT (Copeland et al., 1990; Harrison et al., 1995). However,

because there are alternative models for anatexis, it is essential to determine separately the ages of the Manaslu pluton, MCT-related metamorphism, and migmatization.

### **Sampling strategy**

In the lower Marsyandi valley, a migmatitic pelitic schist was collected from the MCT mylonite-zone in an attempt to constrain the age of migmatization and syn-metamorphic displacement on the MCT. In the upper Marsyandi and Dudh Khola valleys (Figure 1) samples were collected from both deformed and undeformed leucogranite dikes at the Greater Himalayan sequence-Tibetan Sedimentary sequence boundary, in order to constrain the age of anatexis as well as to bracket the age of sillimanite-grade deformation and extensional faulting at this structural level.

The sample from the MCT zone (MCT-1) contained garnet, staurolite, kyanite, biotite, muscovite, plagioclase, and quartz. The outcrop displayed ~5% leucogranite melt by volume, and both migmatitic and schistose layers are deformed by well-developed mylonitic fabrics with a top to the south shear-sense (Figure 2A ). Mylonitic textures, including “rolled” garnets with asymmetric pressure shadows and kyanite aligned in the stretching direction of the mylonitic foliation, indicate synkinematic growth of the peak metamorphic assemblage (Gt+Bt+Ky+H<sub>2</sub>O). Pressure and temperature calculations based on rim thermobarometry (Chapter 5) indicate pressures of  $1100 \pm 110$  MPa and temperatures of  $640 \pm 30$  °C for the peak equilibrium assemblage. Accessory phases included monazite and zircon. The closure temperature for monazite (720-750 °C from Copeland et al., 1988) is close to or above the peak temperatures obtained by thermobarometry, so that the age of metamorphic monazite provides a potential constraint on the time of staurolite- to kyanite-grade mylonitization within the MCT. Although monazite is ubiquitous, there are commonly concentrations of it in contact with staurolite, suggesting that the growth of these minerals was coeval. Staurolite within MCT-1 is



typically embayed or anhedral (Figure 2B) and mineralogical textures indicate that the sample was quenched during the prograde reaction  $St = Gt + Bt + Ky \pm Sil + H_2O$  (Figure 2C).

#### Deformed leucogranite (MC-93-88 & MC-94-36)

Deformed leucogranite sills (MC-93-88 and MC-94-36) were collected from near Chame in the upper Marsyandi valley within sillimanite-grade gneisses (Figure 1). In the upper Marsyandi valley the top 2-3 kilometers of the Greater Himalayan sequence is deformed by sillimanite-grade, obliquely down-dip top-to-the-west ductile shear related to the Chame detachment (Chapter 2). The sampled sills, each less than a meter thick and separated by about 500 meters of section, contain foliation associated with west-directed shearing (Figure 3A). Both are two mica tourmaline granites containing potassium feldspar, quartz, plagioclase, tourmaline, muscovite, and biotite. The Formation III host to sample MC-93-88 is composed of potassium feldspar, plagioclase, quartz, biotite, muscovite,  $\pm$  garnet,  $\pm$  sillimanite. The MC-94-36 dike intrudes Formation II gneiss, which contains biotite, plagioclase, potassium feldspar, quartz, sillimanite, tourmaline, and garnet. Migmatitic tourmaline-bearing felsic layers (0.5 cm to 0.5 m thick) within the Formation II gneiss have the same mineralogy as the leucogranite sills, indicating that the sills are anatectic in origin.

#### Undeformed leucogranite (DK-1 & DK-2)

Two dikes were sampled from an abundant network of undeformed leucogranite dikes and sills that intrude both hanging wall and footwall rocks of the South Tibetan detachment system in the Dudh Khola valley, adjacent to the Manaslu pluton (Figure 1). These dikes clearly cross-cut all fabric development within both the Greater Himalayan sequence and the Tibetan sedimentary sequence (Figure 3B). A similar network of “aplopegmatitic” dikes is described by Le Fort (1981) about 10 km to the northwest where

they extend at least 10 km from the pluton into marble of the Tibetan sedimentary sequence. The samples include DK-1 which intrudes sillimanite-grade augen gneiss (Formation III) of the Greater Himalayan sequence, and DK-2, which intrudes marble of the Annapurna Yellow formation (Tibetan sedimentary sequence). DK-1 is a medium-grained leucocratic rock that consists of quartz, plagioclase, potassium feldspar, muscovite and biotite, and tourmaline. DK-2 is a fine-grained leucogranite with the same mineralogy as DK-1 except that it contains neither muscovite nor biotite.

### **U-Pb analytical methods**

Final mineral separates of monazite and zircon were hand picked and analyzed at the Geochronology laboratory at the Geological Survey of Canada and analytical methods follow those outlined by Parrish et al. (1987). Initial separation of U-Pb minerals from samples weighing 1.0-2.0 kg was done at M.I.T. using standard heavy liquid and magnetic separation techniques.

### **Results**

#### Main Central Thrust zone

##### *Sample MCT-1*

Seven monazite fractions from MCT-1 show a significant spread on the concordia diagram (Figure 4, Table 1). Three of the fractions (b, f, and g) fall on a chord with an upper intercept of  $760 \pm 20$  Ma and a lower intercept of  $21.5 \pm 0.3$  Ma with an MSWD of 0.64. Although this is a well defined line, the lower intercept age is not necessarily precise considering that the remaining fractions (a, c, e, and d) fall on or very close to concordia between 22 Ma and 18 Ma. The two strongly discordant fractions (f and g) were preliminary analyses comprised of multi-grain populations (15 and 20 grains, respectively) with visible inclusions probably delineating older cores. The position of f and g relative to concordia most likely reflects mixing between an older Precambrian component and a

younger 20-22 Ma metamorphic component. Previous U-Pb constraints on detrital zircons from the Greater Himalayas sequence require that the sequence is no older than Neoproterozoic and no younger than Cambrian (~900-570 Ma) (Parrish and Hodges, in press). The ~760 Ma upper intercept from the line defined by b, f, and g is consistent with this age range and strengthens the argument that it represents inheritance from an originally detrital sedimentary source.

The fractions that plot close to concordia comprised three single-grain analyses (a,b, and c) and two fractions (d and e) relatively free of inclusions. Two of the single-grain analyses plot slightly above concordia (a and c) indicating that the pure metamorphic end-member component of monazite initially incorporated an excess amount of  $^{230}\text{Th}$  (e.g., Scharer, 1984). Therefore the concordant analyses may be a fortuitous mixture of inheritance and Th- disequilibrium, and if the analyses were free of inheritance they would plot above concordia.

There are several possible explanations for the spread in slightly discordant analyses between 21 and 18 Ma. These possibilities include continuous or episodic monazite growth at elevated temperatures, growth of secondary monazite from late-stage hydrothermal fluids, high-temperature Pb-loss, or inheritance. It is also possible that the observed pattern results from some combination of these processes such as a mixture of minor amounts of inheritance and initial Th-disequilibrium combined with prolonged high-temperature Pb-loss. Prolonged monazite growth near or below the closure temperature of monazite over a > 1 Ma period from hydrothermal fluids is also a possibility and has been documented in Proterozoic rocks of the southwestern U.S. (Hawkins, 1996). From the observed pattern in monazite data, it is impossible to resolve a precise age of metamorphic monazite growth without additional single and/or sub grain analyses. However the data

argue strongly that high-temperature metamorphism between 21.5 and 18 Ma accompanied top to south displacement on the MCT.

### Deformed Granites

Monazite and zircon were separated from samples MC-94-36 and MC-93-88. In both samples, two distinct monazite morphologies were divided into separate populations. One consists of large ( $\geq 200\mu\text{m}$ ) dark green irregularly shaped crystals (Figure 5A), and the other has smaller ( $\leq 100\mu\text{m}$ ), light green to clear, rounded to gem-like crystals, with minor inclusions (Figure 5B). Although both populations of monazite are ubiquitous throughout the samples, the large irregularly shaped grains are most abundant as inclusions within muscovite grains (Figure 6A) and the smaller more gem-like grains are more typically concentrated at reaction boundaries between muscovite and quartz (Figure 6B). Zircons from MC-94-36 and MC-93-88 were clear and prismatic; some of them had visible inclusion-rich cores.

### *Sample MC-94-36*

The monazite analyses for sample MC-94-36 plot in a fairly even distribution of reversely discordant ellipses that sit above concordia between 22 Ma and 34 Ma (Figure 7). The reversely discordant pattern is common for young monazite and most likely results from excess  $^{230}\text{Th}$ -derived  $^{206}\text{Pb}$ . The  $^{207}\text{Pb}/^{235}\text{U}$  ages of such samples are typically interpreted as the best estimate of the crystallization age of the mineral (Parrish, 1990). Although initial Th-disequilibrium is a likely cause for reverse discordance in this case, the spread in analyses precludes the possibility of assigning a single crystallization age, and instead leaves several possible interpretations for the observed U-Pb systematics. Two possible explanations are that either 1) the analyses plot on a mixing line between an older inherited component and a younger metamorphic or magmatic component, or that 2) the monazites in this sample are ca. 34 Ma and have experienced variable amounts of Pb loss.

Although some degree of Pb-loss cannot be ruled out, there is a correlation between grain morphology and age; the two single-grain analyses of large, dark green, and irregularly shaped monazites plot towards the “older” end of the array (fractions a and b, Figure 7), whereas the single-grain analyses of clear gem-like monazites plot towards the “younger” end (fractions c, d, and e, Figure 7). This indicates that the distribution most likely reflects mixing between an older  $\geq 34$  Ma and a younger  $\leq 24$  Ma component both of which plot above concordia due to Th disequilibrium. Inheritance in monazite from peraluminous granites is not unusual and was first described in Miocene Himalayan leucogranites (Copeland et al., 1988).

#### *Sample MC-93-88*

Three multi-grain fractions and one single grain fraction of monazite were analyzed from sample MC-93-88. The multi-grain fractions overlap slightly above concordia at ~28 Ma and the single-grain analysis plots slightly above concordia at 34 Ma (Figure 7). It is possible that the grouping of analyses at 28 Ma is indicative of a metamorphic event, however attaching geological significance to these analyses is dangerous. The monazite results for MC-94-36 suggest instead that each fraction represents a mixed population that may overlap fortuitously on concordia. Although both samples MC-93-88 and MC-94-36 have a similar inheritance pattern, the degree of reverse discordance is noticeably different between samples, but consistent within each sample. The two leucogranites are within distinct lithologies, indicating a possible correlation between the amount of excess  $^{230}\text{Th}$  derived  $^{206}\text{Pb}$  and the host rock.

Because of the relatively low probability of obtaining resolvable zircon ages from metamorphosed Himalayan leucogranite due to inheritance problems, only two preliminary multi-grain zircon fractions were analyzed from both samples MC-93-88 and MC-94-36. The results are plotted in Figure 7B. There is a linear relationship between these points

which most likely represents a mixing line with an upper intercept between 400 and 500 Ma and a Tertiary lower intercept, however the linear fit to the data is relatively poor (MSWD = 110) and I regard the lower intercept as having no geological significance.

### Undeformed leucogranite

#### *Sample DK-1*

Five zircon fractions for DK-1 define a linear array with a lower intercept between 17 and 19 Ma. Three of the analyses are slightly discordant between 18 and 19 Ma, and the other two are highly discordant. The three analyses that plot close to concordia consist of clear flat equant crystals with very few visible inclusions (Figure 8B). In contrast, the two discordant fractions are multi-grain populations of long prismatic crystals, some having visible clusters of inclusions probably delineating older cores (Figure 8C). The linear array defined by the latter population is most easily explained as a mixture of an older inherited component with a younger (18-19 Ma) magmatic component. The nearly concordant population most likely represents crystallization age of the leucogranite. The slight discordance may be explained either by minor Pb loss or by initial Th disequilibrium, which in the case of zircons causes an initial deficit of  $^{206}\text{Pb}$  (e.g. Mattinson, 1973; Coleman and Parrish, 1991). The <1 Ma spread in ages of the three nearly concordant fractions may either be explained by differing amounts of Pb-loss or minor inheritance. Three monazite fractions (4 to 5 grains each) with clear gem-like grains (Figure 8A) overlap slightly above concordia at ~19 Ma (Figure 9). The tightly clustered data and the good agreement between zircon and monazite dates in this case justifies interpreting  $18.8 \pm 0.1$  Ma as the crystallization age of the mineral (i.e. Parrish, 1990).

#### *Sample DK-2*

Monazite was the only U-Pb bearing accessory phase separated from sample DK-2. These monazites have very low concentrations of U and Pb relative to those in sample

DK-1 (>0.1 ppm Pb vs. 10-100 ppm Pb), and therefore required the analysis of relatively large multi-grain fractions (ca. 50 grains each). These samples yielded  $^{207}\text{Pb}/^{235}\text{U}$  ages with relatively large analytical errors ( $17.6\pm 3.4$  Ma and  $17.4\pm 3.4$  Ma, Figure 9). Despite their relatively poor precision, they reinforce the interpretation that some of the undeformed granite dikes in the Dudh Khola drainage crystallized at 18-19 Ma.

## **Discussion**

### Implications for Eohimalayan metamorphism

Most petrographic evidence for the existence of an Eohimalayan event comes from samples at the base of the Greater Himalayan sequence (e.g., Hodges et al., 1988; Pecher, 1989). The MCT-1 data show no evidence of an inherited Oligocene component. However, the migmatites at the top of the section (MC-94-36 and MC-93-88) show a clear indication of an Oligocene monazite crystallization event that may be related to Eohimalayan metamorphism. Oligocene ages of ca. 36 Ma from monazite obtained from Formation III in the Modhi Khola (Hodges et al., in press) about 40 km to the west of Chame, provide important supporting evidence that the older inherited component from samples MC-93-88 and MC-94-36 is in fact Oligocene. Sample MC-93-88 is from a sill within the Formation III augen gneiss and MC-94-36 was sampled less than 300 meters down section from the basal contact of Formation III. Formation III is continuous along strike over most of the length of the Himalaya and the ~36 Ma monazite ages from the Modi Khola augen gneiss have been interpreted as either the result of Oligocene magmatism or high-temperature metamorphism (Hodges et al., in press). Either scenario could produce high enough temperatures in the adjacent Formation II gneiss for monazite growth at ~36 Ma.

### Miocene leucogranite generation

There is abundant evidence throughout the Himalaya for ca. 22 Ma high-temperature metamorphism and anatexis at the top of the Greater Himalayan sequence. In the Annapurna-Manaslu region leucogranites of this age have been found in the Kali Gandaki valley (Nazarchuk, 1993), the Modi Khola drainage (Parrish and Hodges, in press; Hodges and Parrish, in press), and as one phase of the Manaslu pluton (Copeland et al., 1990; Guillot et al., 1994; Harrison et al., 1995). However there are at least two temporally distinct phases of granite emplacement in the upper Marsyandi-Dudh Khola valleys: an 18 My old phase (this study) and a 22 My old phase (Harrison et al., 1995). This age range is similar to those reported from eastern Nepal and southern Tibet (e.g. Scharer et al., 1986; Hodges et al., 1992). The combined U-Pb results in the Annapurna-Manaslu region indicate that granite was emplaced either over a prolonged period of time (at least 4 My) or in distinct pulses at ~22 Ma and at 18 Ma. Distinguishing between these two possibilities requires more data.

Different phases of the Manaslu pluton are distinguished on the basis of cross-cutting field relationships (e.g. Guillot, 1993) and also by different geochemical signatures of mineralogically distinct phases (Guillot and LeFort, 1995). Guillot and LeFort (1995) determined the source rock for tourmaline granite to be metapelite and the source rock for two-mica granite to be metagreywacke. Both the 18 Ma leucogranite from this study (DK-1) and the 22 Ma leucogranite from Harrison et al. (1995) are two-mica tourmaline leucogranites, implying that there is no obvious transition in bulk mineralogy over the 22-18 Ma period, arguing against fundamentally different petrogenetic mechanisms.

#### Implications for melting models

Field relationships allow for ~22 Ma migmatization at the top of the Greater Himalayan sequence before or during early stages of extensional faulting. The ~18 Ma ages on cross cutting dikes from the Dudh Khola, and the large volume of Manaslu pluton



that cross cuts the South Tibetan detachment system, also allow for models in which melting is enhanced by decompression. High-temperature deformation within the MCT zone is the same age as migmatization at the top of the Greater Himalayan sequence and is, at least in part, coeval with the South Tibetan detachment. These results demonstrate that the migmatites cannot be significantly older than the leucogranites as suggested by Inger and Harris (1993), and it is clear that migmatization within the MCT was coeval with migmatization ~10 km above within the upper Greater Himalayan sequence.

Migmatization within the lower and upper portions of the Greater Himalayan sequence at ~22 Ma is consistent with the existence of a steep thermal gradient throughout the entire sequence at this time, similar to that documented in the Everest, Nyalam and Burhi Gandaki regions (Hodges et al., 1988; Hubbard, 1989; Hodges et al., 1992). Although the source of heat responsible for this thermal structure is controversial, recent results from thermal modeling (Huerta et al., in press) demonstrate that the radiogenic material in the upper plate of a subduction complex, the amount of which is controlled by the rates of accretion and erosion, can dominate the thermal structure of the upper plate, and in fact, result in an inverted thermal gradient at temperatures consistent with those observed in the Himalaya. The timing constraints presented here cannot unequivocally rule out either granite melting model; however, it seems likely that in situ melting within the Greater Himalayan sequence during syn-metamorphic displacement on the MCT facilitated normal faulting which in turn may well have contributed to further melting by decompression.

## **Conclusions**

U-Pb monazite ages provide evidence for high-temperature deformation and migmatization within the MCT-zone between 18 and 22 Ma. Migmatization within the upper Greater Himalayan sequence is loosely constrained to ~22 Ma with additional evidence for Oligocene regional metamorphism within the upper Formations of the Greater

Himalayan sequence. However, these data do not provide evidence of metamorphism prior to 22 Ma within the lower Greater Himalayan sequence. Extension at the top of the Greater Himalayan sequence was roughly coeval with 18-22 Ma thrusting on the MCT. All foliation and ductile deformational structures are cut by an ~18 Ma leucogranite dike that intrudes both the Greater Himalayan sequence and the Tibetan Sedimentary sequence and postdates all ductile fabrics in the area and limits the age of regional metamorphism and high-temperature deformation within the upper Greater Himalayan sequence.

### **Acknowledgments**

M. Coleman is grateful to the staff of the Geochronology Lab at the Geological Survey of Canada in Ottawa, in particular R. Parrish for sharing his expertise in mineral selection of Himalayan samples and help with all stages of the U-Pb analyses; V. McNicoll, J. Crowley, K. Santowski, and M. Villeneuve for assistance with chemistry, mass spectrometry, and data reduction. Reviews of earlier drafts by K. Hodges and D. Coleman are greatly appreciated. This research has been supported by National Science Foundation Grant No. EAR-9104291 awarded to K. Hodges.

### **References**

- Besse, J., Courtillot, V., Pozzi, J.P., Westphal, M., and Zhou, Y.X., 1984, Paleomagnetic estimates of crustal shortening in the Himalayan thrusts and Zangbo suture: *Nature*, v. 311, p. 621-625.
- Brunel, M., 1975, La nappe du Mahabharat Himalaya du Nepal central: Paris, *Academie des Sciences Comptes Rendus*, v. 280, p. 551-554.
- Burchfiel, B.C., Zhiliang, C., Hodges, K.V., Yuping, L., Royden, L.H., Changrong, D., Jiene, X., 1992, The South Tibetan Detachment System, Himalayan Orogen: Extension contemporaneous with and parallel to shortening in a Collisional Mountain Belt: *Geological Society of America, Special Paper 269*, 41 p.

- Burg, J.P., Brunel, M., Gapais, D., Chen, G.M. and Liu, G.H., 1984, Deformation of leucogranites of the crystalline Main Central Thrust Sheet in southern Tibet (China): *Journal of Structural Geology*, v.6, p.535-542.
- Colchen, M., LeFort, P., Pecher, A., 1986, *Annapurna - Manaslu - Ganesh Himal*: Centre Nationale de la Recherche Scientifique, Paris, 1986.
- Coleman, M.E., in press. Orogen-parallel and orogen-perpendicular extension in the central Nepalese Himalaya: *Geological Society of America Bulletin*.
- Coleman, M.E., and Parrish, R.R., 1990, Eocene dextral strike-slip and extensional faulting in the Bridge River Terrane, southeast British Columbia: *Tectonics*, v. 10, n.6, p.1222-1238.
- Copeland, P., Parrish, R.R., and Harrison, T.M., 1988, Identification of inherited radiogenic Pb in monazite and its implications for U-Pb systematics, *Nature*, v. 333, p.760-763.
- Copeland, P., Harrison, T.M., and Le Fort, P., 1990, Age and cooling of the Manaslu granite: implications for Himalayan tectonics; *Journal of Volcanology and Geothermal Research*, v. 44, p. 33-50.
- Deniel, C., Vidal, P.F., A., Le Fort, P. and Peucat, J.-J., 1987, Isotopic study of the Manaslu granite (Himalaya, Nepal): inferences on the age and source of the Himalayan leucogranites: *Contribution to Mineralogy and Petrology*, v. 96, p.78-92.
- Dietrich, V., and Gansser, A., 1981, The leucogranites of the Bhutan Himalaya (Crustal anatexis versus mantle melting): *Schweiz. Mineral. Petrol.*, V.96, p. 177-202.
- France-Lanord, C., Sheppard, S.M.F., and Le Fort, P., 1988, Hydrogen and oxygen isotope variations in the High Himalaya peraluminous Manaslu leucogranite: evidence for heterogeneous sedimentary source: *Geochemica et Cosmochimica Acta*, v. 52, p. 513-526.
- Gansser, A., 1964, *Geology of the Himalaya*, London, England, Interscience Publishers, 289 p.
- Guillot, S., 1993, *Le Granite du Manaslu (Nepal Central), Marqueur de la Subduction et de l'Extension Intracontinentale Himalayenne*. These de doctorat, Univ. Grenoble, Geologique Alpine, Memoirs hors serie, v. 19, 97 pp.
- Guillot, S., Pecher, A., Rochette, P., and Le Fort, P., 1993, The emplacement of the Manaslu granite (Central Nepal): field and magnetic susceptibility constraints, In: P.J. Treloar and M. Searle (Editors), *Himalayan Tectonics*, Geological Society of London Special Publication, v.74, p.413-428.
- Guillot, S., Hodges, K.V., Le Fort, P. and Pêcher, A., 1994, New constraints on the age of the Manaslu leucogranite: evidence for episodic tectonic denudation in the central Himalaya. *Geology*, v. 22, p.559-562.

- Guillot, S., and Le Fort, 1995, Geochemical constraints on the bimodal origin of High Himalayan leucogranites, *Lithos*, v. 35, p. 221-234.
- Harris, N., Inger, S., and Massey, J., 1993, The role of fluids in the formation of High Himalayan leucogranites: In: P.J. Treloar and M. Searle (Editors), *Himalayan Tectonics*, Geological Society of London Special Publication, v. 74, p. 391-400.
- Harris, N., and Inger, S., 1992, Trace element modeling of pelite-derived granites: *Contributions to Mineralogy and Petrology*, v. 110, p.46-56.
- Harrison, T.M., and Watson, E.B., 1983, Kinetics of zircon dissolution and zirconium diffusion in granite melts of variable water content: *Contributions to Mineralogy and Petrology*, v. 84, p.66-72.
- Harrison, T.M., McKeegan, K.D. and Le Fort, P., 1995, Detection of inherited monazite in the Manaslu leucogranite by  $^{208}\text{Pb}/^{232}\text{Th}$  ion microprobe dating: crystallization age and tectonic implications: *Earth and Planetary Science Letters*, v. 133, p. 271-282.
- Hawkins, D., 1996, U-Pb Geochronological Constraints on the Tectonic and Thermal Evolution of Paleoproterozoic Crust in Grand Canyon, Arizona. PhD Thesis, Massachusetts Institute of Technology, Cambridge.
- Herren, E., 1987, Zaskar shear zone: northeast-southwest extension within the Higher Himalaya (Ladakh, India): *Geology*, v. 15, p.409-413.
- Hodges, K.V., Le Fort, P., and Pecher, A., 1986, Possible evidence for anatectic buffering of the thermal structure of the Tibetan Slab (Central nepalese Himalaya): *Geological Society of America, Abstracts with Programs*, v.18, p. 638.
- Hodges, K.V., Hubbard, M.S., Silverburg, D.S., 1988, Metamorphic constraints on the thermal evolution of the central Himalayan Orogen: *Philosophical Transactions of the Royal Society of London*, v. A326, p. 257-280.
- Hodges, K.V., Parrish, R.R., Housh, T.B., Lux, D.R., Burchfiel, B.C., Royden, L.H. and Chen, Z., 1992, Simultaneous Miocene extension and shortening in the Himalayan orogen: *Science*, v.258, p.1466-1470.
- Hodges, K.V., Parrish, R.R., Searle, M.P., in press, Tectonic evolution of the Central Annapurna Range, Nepalese Himalaya: *Tectonics*.
- Hollister, L.S., and Crawford, M.L., 1986, Melt-enhanced deformation: A major tectonic process: *Geology*, v. 14, p.558-561.
- Hubbard, M.S., 1989, Thermobarometric constraints on the thermal history of the Main Central Thrust Zone and Tibetan Slab, eastern Nepal Himalaya: *Journal of Metamorphic Geology*, v. 7, p. 19-30.

- Hubbard, M.S. and Harrison, T.M., 1989,  $^{40}\text{Ar}/^{39}\text{Ar}$  constraints on deformation and metamorphism in the Main Central Thrust zone and Tibetan Slab, eastern Nepal Himalaya: *Tectonics*, v.8, p.865-880.
- Huerta, A.D., and Royden, L.H., 1995, Thermal Evolution of Collisional Orogens: Effects of Accretion and Erosion [Abs]: *Eos (Transactions, American Geophysical Union)*, v.76, No.46, p.567.
- Huerta, A.D., Royden, L.H., and Hodges, K.V., submitted, The interdependence of deformational and thermal processes in mountain belts, *Science*.
- Inger, S., and Harris, N., 1993, Geochemical constraints on leucogranite magmatism in the Langtang valley, Nepal Himalaya: *Journal of Petrology*, v.34, p. 345-368.
- Le Fort, P., 1975, Himalaya: the collided range. Present knowledge of the continental arc: *American Journal of Science*, v. 275A, p.1-44.
- Le Fort, P., 1981, Manaslu Leucogranite: a collision signature of the Himalaya. A model for its genesis and emplacement: *Journal of Geophysical Research*, v.86, p.10545-10568.
- Le Fort, P., Cuney, C., Deniel, C., France-Lanord, C., Sheppard, S.M.F., Upreti, B.N., and Vidal, P., 1987, Crustal generation of the Himalayan leucogranites: *Tectonophysics*, v.134, p. 39-57.
- Macfarlane, A.M., The Tectonic Evolution of the Core of the Himalaya, Langtang National Park, Central Nepal, Ph.D. thesis, Massachusetts Institute of Technology.
- Mattinson, J.M., 1973, Anomalous isotopic composition of lead in young zircons: *Yearbook, Carnegie Institute, Washington*, v. 72, p. 613-616.
- Montel, J.M., 1993, A model for monazite/melt equilibrium and application to the generation of granitic magmas: *Chemical Geology*, v. 119, p. 127-146.
- Nazarchuk, J.H., 1993, Structure and geochronology of the Greater Himalaya, Kali Gandaki region, west-central Nepal [Master's thesis]: Ottawa, Carleton University, 157 p.
- Parrish, R.R., Roddick, J.C., Loveridge, W.D., and Sullivan, R.W., 1987, Uranium-lead analytical techniques at the Geochronology laboratory, Geological Survey of Canada: in *Radiogenic age and isotopic studies: Report 1, Geological Survey of Canada Paper 87-2*, Ottawa.
- Parrish, R.R., and Hodges, K.V., submitted, Isotopic Constraints on the Age and Provenance of the Lesser and Greater Himalayan Sequences, Nepalese Himalaya: *Geological Society of America*.

- Pêcher, A., 1977, Geology of the Nepal Himalaya: deformation and petrography in the Main Central Thrust zone: in *Ecologie et Géologie de L'Himalaya, Colloques Internationaux du Centre National de la Recherche Scientifique, Paris*, v. 268, p. 301-318.
- Pêcher, A., 1978, Deformations et métamorphisme associées à une zone de cisaillement, exemple du Grand Chevauchement Central himalayen (MCT), transversale des Annapurnas et du Manaslu, Nepal. PhD Thesis, Grenoble.
- Pêcher, A., 1989, The metamorphism in the Central Himalaya: *Journal of Metamorphic Geology*, v.7, p.31-41.
- Pêcher, A., 1991, The contact between the higher Himalaya crystallines and the Tibetan sedimentary series: Miocene large-scale dextral shearing: *Tectonics*, v. 10, p.587-598.
- Scaillet, B., Pêcher, A., Rochette, P., and Champenois, M., 1995, The Gangotri granite (Garhwal Himalaya): Laccolithic emplacement in an extending collisional belt, *Journal of Geophysical Research*, v. 10, N.B1, p. 585-607.
- Scharer, U., 1984, The effect of initial  $^{230}\text{Th}$  disequilibrium on young U-Pb ages: The Makalu case: *Earth and Planetary Science Letters*, v. 67, p.191-204.
- Scharer, U., Xu, R., and Allegre, C.J., 1986, U-(Th)-Pb systematics and ages of Himalayan leucogranites, South Tibet; *Earth and Planetary Science Letter*, v. 77, p. 35-48.
- Smith, H.A., and Barreiro, B., 1990, Monazite U-Pb dating of staurolite grade metamorphism in pelitic schists, *Contributions to Mineralogy and Petrology*, v. 105, p. 602-615.
- Vidal, P., Cocherie, A., and Le Fort, P., 1982, Geochemical investigations of the origin of the Manaslu leucogranite (Himalaya, Nepal): *Geochimica et Cosmochimica Acta*, v. 46, p. 2279-2292.



**Table 1.** U-Pb isotopic data for monazites and zircons.

Fractions** & Properties	Weight (µg)	Concentrations		Atomic ratios						Ages (Ma)				corr. coef.	Total Common Pb (pg)		
		U (ppm)	Pb* (ppm)	<sup>206</sup> Pb† / <sup>204</sup> Pb	<sup>208</sup> Pb* / <sup>206</sup> Pb	<sup>206</sup> Pb‡ / <sup>238</sup> U	% err	<sup>207</sup> Pb‡ / <sup>235</sup> U	% err	<sup>207</sup> Pb‡ / <sup>206</sup> Pb	% err	<sup>206</sup> Pb / <sup>238</sup> U	<sup>207</sup> Pb / <sup>235</sup> U			<sup>207</sup> Pb / <sup>206</sup> Pb	err
<u>Sample MCT-1, migmatitic pelitic schist from the Main Central Thrust zone, lower Marsyandi river valley</u>																	
a,M(1),cl,in	17.2	9869.7	63.64	2096.5	1.2394	0.00325	0.23	0.02064	0.32	0.04606	0.18	20.9	20.7	0.8	±4.4	0.828	16.7
b,M(1),cl,in	9.3	7176.9	60.94	1358.1	1.8993	0.00334	0.22	0.02131	0.48	0.04634	0.40	21.5	21.4	15.3	±9.5	0.571	10.4
c,M(1),cl,in	10.3	8013.1	60.16	1004.8	2.0161	0.00284	0.21	0.01809	0.50	0.04626	0.41	18.3	18.2	11.3	±9.9	0.594	14.9
d,M(3),cl,in	14.4	9008.7	70.72	1907.7	1.6640	0.00333	0.24	0.02160	0.35	0.04699	0.23	21.5	21.7	48.7	±5.4	0.762	14.4
e,M(5),cl,in	25.3	9818.9	74.42	2428.5	1.6817	0.00319	0.28	0.02036	0.33	0.04622	0.17	20.6	20.5	9.1	±4.1	0.850	20.7
f,M(15),cl,in	27.9	7704.1	96.84	2379.7	2.2601	0.00436	0.23	0.03046	0.28	0.05069	0.14	28.0	30.5	226.5	±3.1	0.882	24.9
g,M(20),cl,in	27.2	7174.8	65.12	1598.7	1.7882	0.00371	0.26	0.02460	0.34	0.04814	0.19	23.8	24.7	106.2	±4.4	0.843	28.7
<u>Sample MC-94-36, foliated leucogranite from Formation II gneiss, upper Marsyandi river valley</u>																	
1a, M(1),dg	35.1	12609	147.4	3546.8	1.6302	0.00504	0.38	0.02836	0.41	0.04083	0.12	32.4	28.4	-298.5	±3.0	0.958	39.6
1b,M(1),dg	29.1	13117	177.9	3248.2	1.4488	0.00549	0.49	0.03155	0.51	0.04170	0.12	35.3	31.5	-244.8	±3.1	0.513	40.7
1c,M(1),lg,cl	14.7	19959	156.3	4259.4	1.0810	0.00429	0.28	0.02381	0.32	0.04031	0.13	27.6	23.9	-331.2	±3.3	0.912	18.6
1d,M(1),lg,cl	27.5	18391	142.2	3721.2	1.1446	0.00408	0.42	0.02262	0.45	0.04026	0.15	26.2	22.7	-334.4	±3.8	0.943	34.9
1e,M(1),lg,cl	39.3	14158	155.6	3688.1	1.5523	0.00488	0.49	0.02766	0.51	0.04114	0.12	31.4	27.7	-279.0	±3.0	0.973	46.4
1f,M(4),lg,cl	17.7	13725	151.7	3066.0	1.5598	0.00489	0.26	0.02845	0.31	0.04221	0.13	31.4	28.5	-214.2	±3.2	0.912	24.4
1e,M(6),lg,cl	28.0	14249	139.2	3414.9	1.4753	0.00446	0.39	0.02566	0.43	0.04175	0.13	28.7	25.7	-248.1	±3.4	0.950	39.9
1f,M(3),lg,cl	135.4	13158	169.3	4099.8	1.7356	0.00533	2.57	0.03115	2.57	0.04240	0.11	34.3	31.1	-202.8	±2.6	0.999	146.0
1e,Z(5),vc	11.0	4842.6	33.18	2418.8	0.0349	0.00736	0.22	0.05482	0.30	0.05403	0.22	47.3	54.2	372.3	±4.9	0.682	10.2
1f,Z(16),cl	6.0	4001.5	28.19	2461.7	0.0596	0.00745	0.28	0.05684	0.32	0.05533	0.25	47.9	56.1	425.5	±5.6	0.658	4.6
<u>Sample MC-93-88, foliated leucogranite from formation III gneiss, upper Marsyandi river valley</u>																	
2a,M(9),cl	10.3	10856	144.1	1914.8	2.3598	0.00447	0.26	0.02792	0.34	0.04528	0.34	28.8	28.0	-40.5	±6.2	0.674	16.5
2b,M(4),cl,in	8.2	7692.0	105.4	533.19	2.3931	0.00444	0.31	0.02823	1.52	0.04611	1.38	28.6	28.3	3.1	±33.0	0.513	34.2
2c,M(5),cl,in		66498	978.1	704.36	2.6315	0.00448	0.29	0.02794	0.59	0.04526	0.45	28.8	28.0	-41.9	±10.9	0.664	245.0
2d,M(1),cl,in	8.9	16139	173.3	4641.7	1.2803	0.00534	0.26	0.03390	0.31	0.04602	0.17	34.3	33.9	-1.3	±4.0	0.839	10.4
2e,Z(8),vc,in	6.0	565.67	36.1	2710.8	0.0593	0.06701	0.31	0.52288	0.39	0.05660	0.29	418.1	427.1	475.8	±6.4	0.685	5.3
2f,Z(11),vc	17.0	1392.2	53.4	8838.4	0.0384	0.04087	0.20	0.31558	0.24	0.05600	0.13	258.2	278.5	452.5	±2.9	0.833	6.9



**Table 1. (continued)**

Sample DK-1, undeformed leucogranite from Formation III gneiss, Dudh Khola

a,Z(1),cl,f	24.8	5029.5	13.96	916.92	0.0468	0.00291	0.23	0.01880	0.46	0.04680	0.35	18.8	18.9	39.3	±8.4	0.664	25.4
b,Z(2),cl,f	6.9	4892.7	12.73	741.9	0.0545	0.00288	0.53	0.01850	4.57	0.04662	4.28	18.6	18.6	29.6	±103.0	0.570	8.4
c,Z(5),cl,f	1.0	87256	222.3	2382.7	0.019	0.0028	0.22	0.01822	0.34	0.04679	0.25	18.2	18.3	38.7	±6.0	0.677	6.5
d,Z(10),cl,p	41.0	4029.9	12.02	3690.1	0.0246	0.00325	0.24	0.02194	0.30	0.04899	0.18	20.9	22.0	147.1	±4.2	0.803	9.2
e,Z(20), p,in	59.0	4978.1	19.07	9804.7	0.0201	0.00417	0.31	0.03004	0.33	0.05226	0.10	26.8	30.1	297.0	±2.2	0.955	7.8
f,M(5),cl	11.9	10123	73.02	751.95	1.6742	0.00299	0.27	0.01862	0.55	0.04511	0.42	19.3	18.7	-49.7	±10.3	0.664	30.9
g,M(4),cl	11.3	11158	82.61	650.66	1.7104	0.00302	0.30	0.01892	0.65	0.04550	0.52	19.4	19.0	-28.6	±12.6	0.626	37.9
h,M(5),cl	16.9	10119	73.1	633.85	1.6480	0.003	0.29	0.01874	0.66	0.04529	0.52	19.3	18.9	-39.9	±12.8	0.640	52.3

Sample DK-2, undeformed leucogranite from the Annapurna Yellow Formation, Dudh Khola

a,M(>50),in	719.4	142.1	0.656	48.78	1.1958	0.003	1.00	0.01745	17.70	0.04244	17.03	19.2	17.6	-200.6	±380	0.695	639.0
b,M(>50),in	602.2	150.64	0.684	52.94	1.1865	0.0003	0.96	0.01771	16.74	0.04234	16.06	19.5	17.8	-206.2	±360	0.725	505.0

\*\* Z=zircon, M=monazite. Number of grains analyzed in each fraction shown in parantheses. cl=clear, dg=dark green, lg=light green, in=inclusions, vc=visible cores, f=flat crystals, p=prismatic crystals.

\* Radiogenic Pb.

† Measured ratio corrected for spike and fractionation only.

‡ Corrected for fractionation, spike, blank, and initial common Pb

All errors are reported as  $2\sigma$ . Zircons and monazites analyzed using mixed  $^{205}\text{Pb}$ - $^{233}\text{U}$ - $^{235}\text{U}$  spike. Zircon and monazite dissolution and chemistry followed methods of Krogh (1973) and Parrish (1987). Decay constants used are  $^{238}\text{U} = 0.15513 \times 10^{-9} \text{ yr}^{-1}$ , and  $^{235}\text{U} = 0.98485 \times 10^{-9} \text{ yr}^{-1}$  (Steiger and Jäger, 1977). Common Pb corrections were calculated using the model of Stacey and Kramers (1975) and the interpreted age of the sample. Pb blank ranged from 7 to 8 pg and U blank ranged from 0 to 2 pg during this study. Data reduction and error analysis was accomplished using the algorithms of Ludwig (1989, 1990).



## Figure captions

Figure 1) Simplified regional tectonic map of central Nepal from Colchen et al. (1980) with minor modifications from this study. The major structures include the Main Central thrust (MCT), the South Tibetan detachment system (STDS), and the Thakkola graben. The summits of Annapurna I (Ann I) Annapurna II (Ann II), and Manaslu are located by black diamonds. The village of Chame and the city of Pokhara are marked by black squares. The sample locations for U-Pb age determinations are labeled according to sample numbers MCT-1, MC-93-88, MC-94-36, DK-1, and DK-2. The inset map shows the location of the Annapurna-Manaslu region within the Himalaya.

Figure 2) (A) Mylonitic pelitic-schist (Grt+St+Ky +Bt+Ms+Pl+Qtz) from the Main Central Thrust zone (Sample MCT-1 site). S-C mylonitic textures indicate a top-to-the-south shear-sense. Pencil for scale. (B) Embayed staurolite crystal. (C) Garnet with inclusion rich core. Textures within this assemblage indicate that the rock was quenched during the prograde reaction  $St=Gr+bt+ky+H_2O$ .

Figure 3) (A) Deformed leucogranite (sample MC-94-36) within sillimanite-grade biotite-gneiss of Formation II. Hammer for scale. (B) Undeformed leucogranite intrudes sillimanite-grade gneiss of the Greater Himalayan sequence.

Figure 4) Concordia plot from U-Pb monazite analyses obtained from mylonitic pelitic schist sample MCT-1. Four nearly concordant monazite analyses plot between 20 and 21 Ma indicating metamorphic monazite growth at this time. The single concordant analyses

at 18 Ma is either the result of Pb-loss while the rock remained at elevated temperatures or continued monazite growth at 18 Ma.

Figure 5) **(A)** Large dark green irregularly shaped monazite found both within leucogranite sample MC-94-36 and within thin sections of Formation III augen gneiss and Formation II biotite-gneiss. These grains yield analyses within the “older” half of the spread of monazite analyses from this sample (Figure 7) and are thought to be inherited from the parent gneiss. **(B)** Light green gem-like monazites from leucogranite sample MC-94-36 plot within the younger half of the spread of analyses and are thought to have crystallized during anatexis and contain an inherited component from the larger dark green crystals shown in Figure 5A.

Figure 6) **(A)** Large dark green anhedral monazite (similar to those shown in Figure 5 A) surrounded by muscovite. **(B)** Monazite concentrated at the reaction boundary of muscovite and quartz. Clear gem-like monazites are typical of the “younger” analyses from sample MC-94-36.

Figure 7) Concordia plots from U-Pb monazite and zircon analyses obtained from two deformed leucogranite samples. Note that error ellipses are for the most part smaller than symbols used for location of plotted analyses. See text for explanation and discussion of data.

Figure 8) **(A)** Gem-like monazites analyzed from undeformed leucogranite sample DK-1. **(B)** Clear, flat, semi-equant zircons analyzed from sample DK-1. These zircons seem to be among the few zircons from Himalayan leucogranites that yield nearly concordant

results (see Figure 9, fractions a, b, and c). (C) Zircons from sample DK-1 with a large degree of inheritance.

Figure 9) Monazite and zircon analyses from undeformed leucogranite dike samples DK-1 and DK-2 from the Dudh Khola valley.



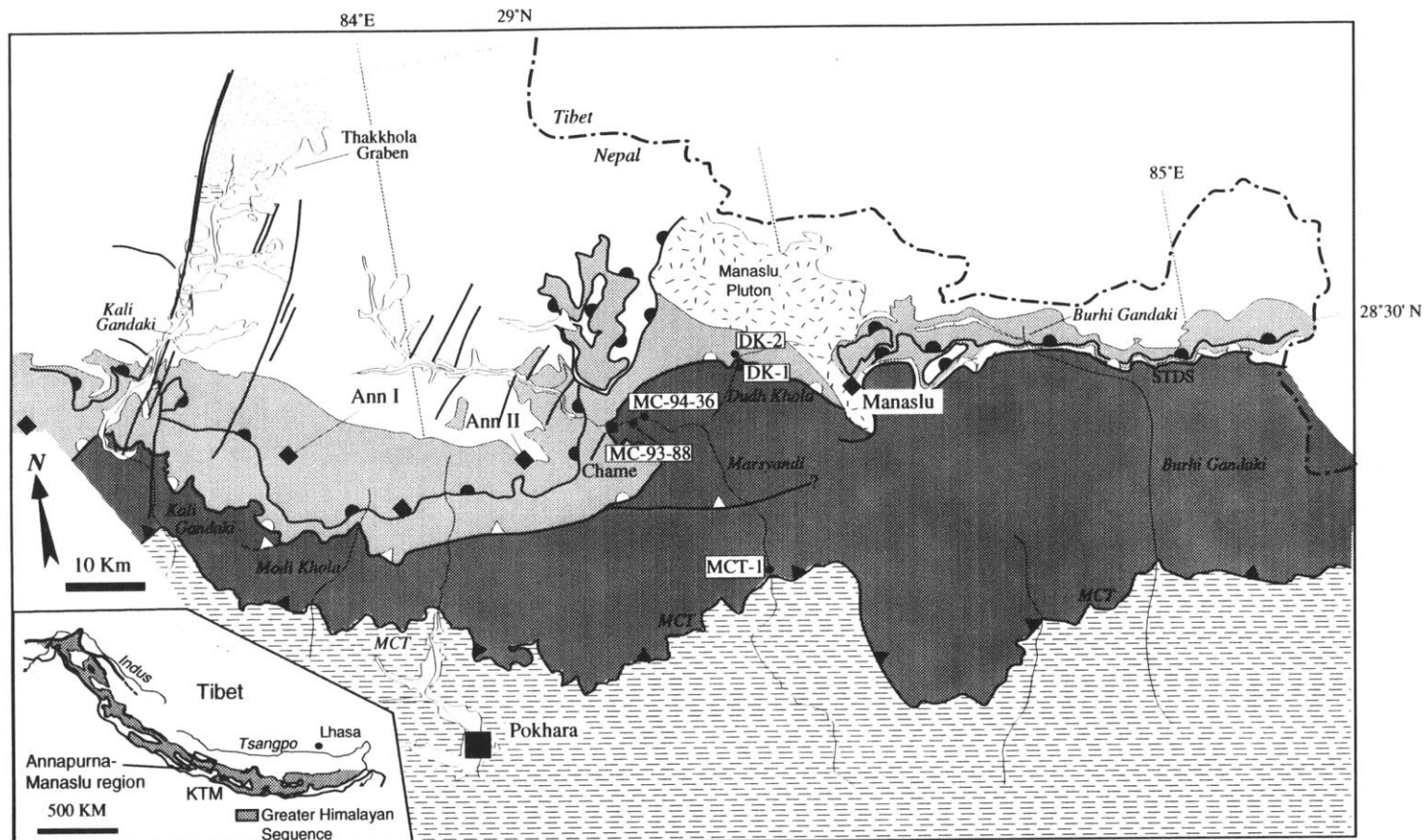
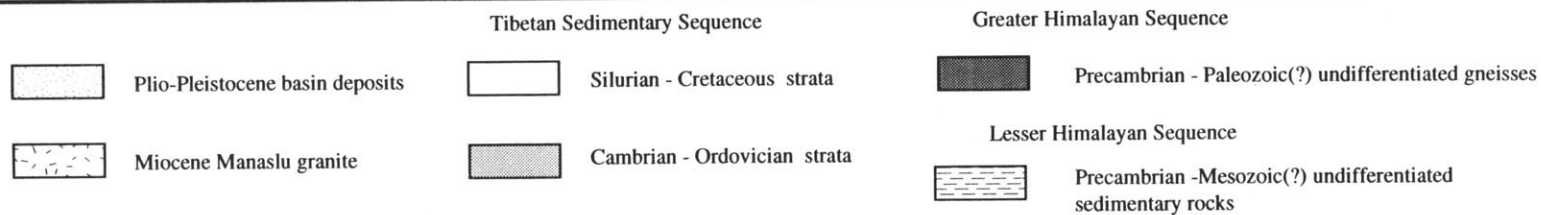


Figure 1







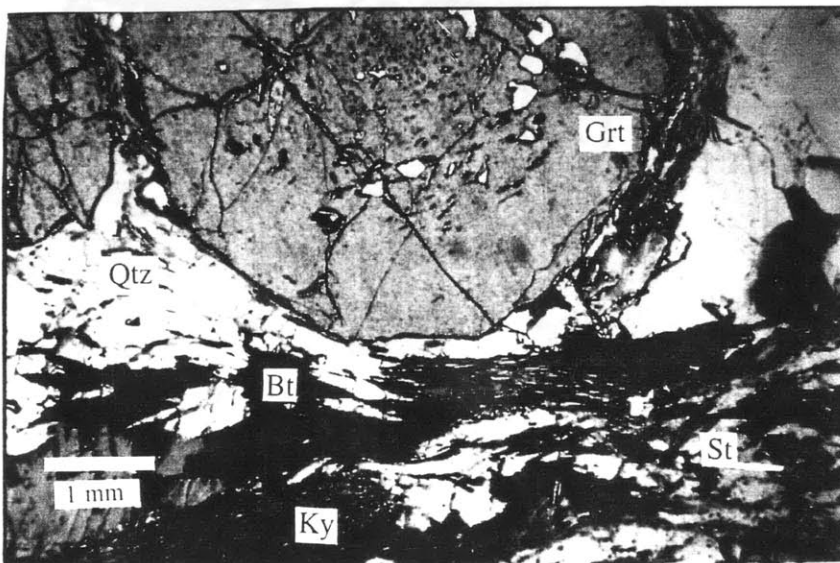
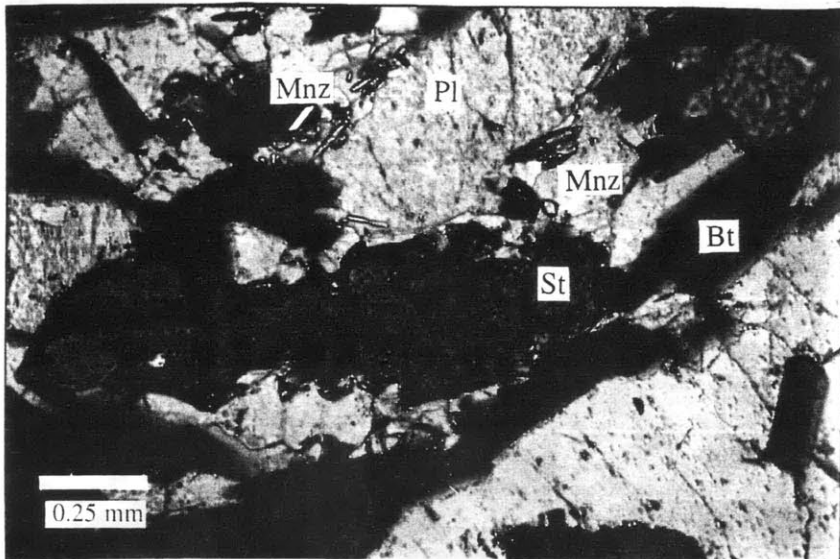
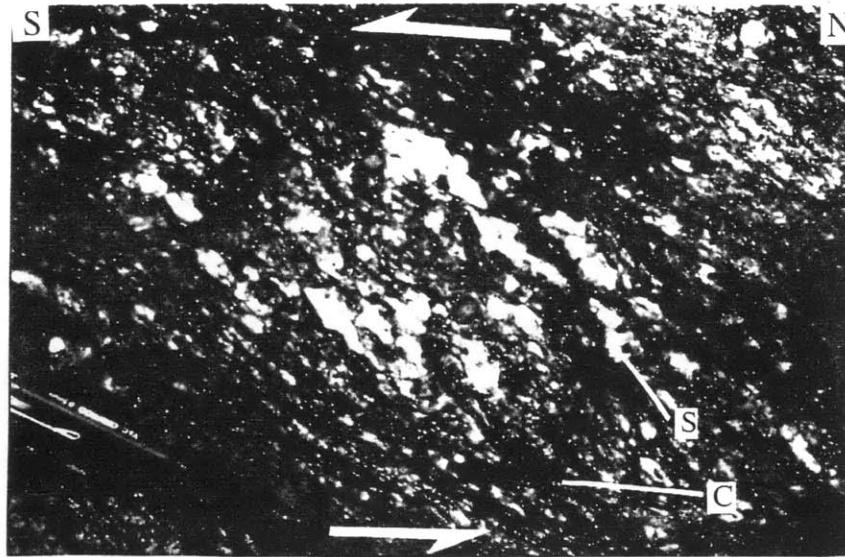


Figure 2



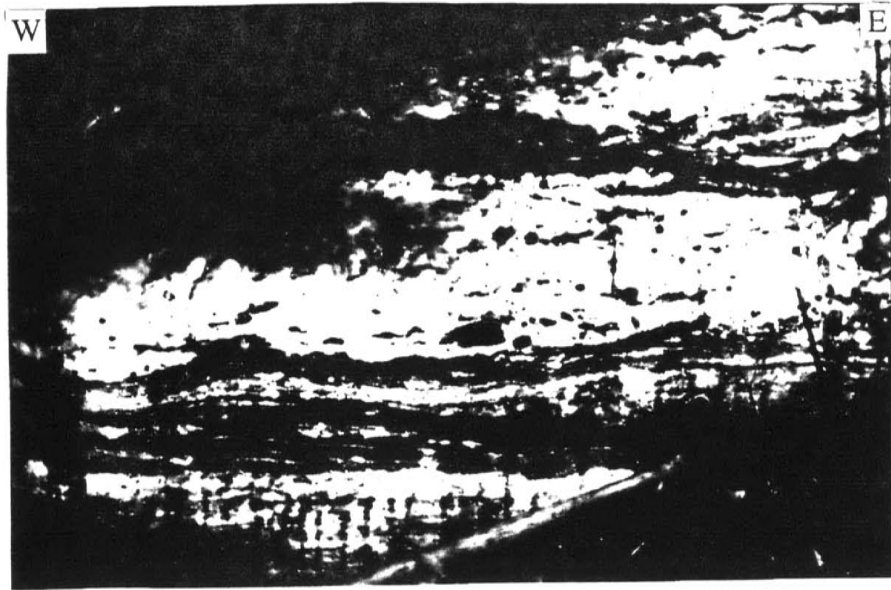


Figure 3



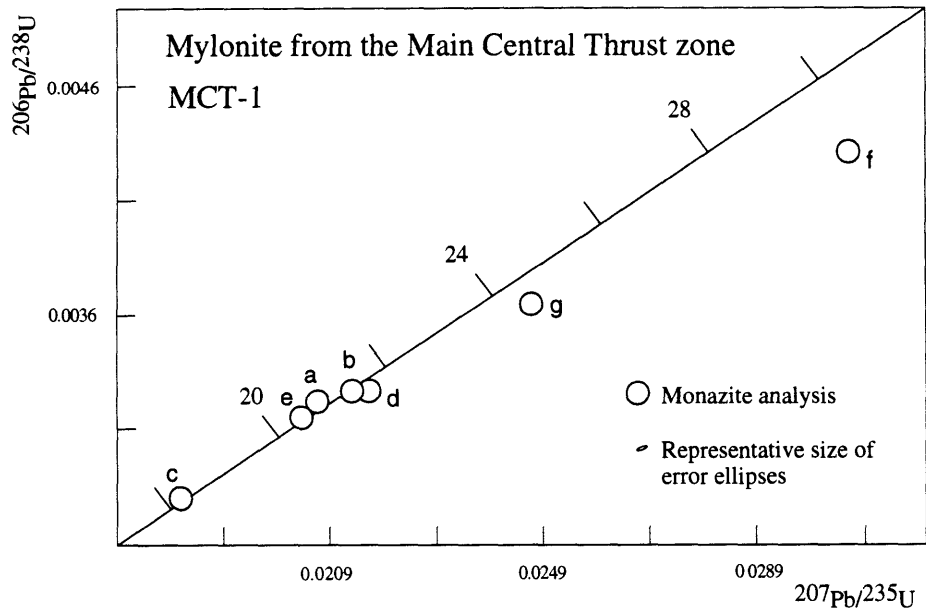
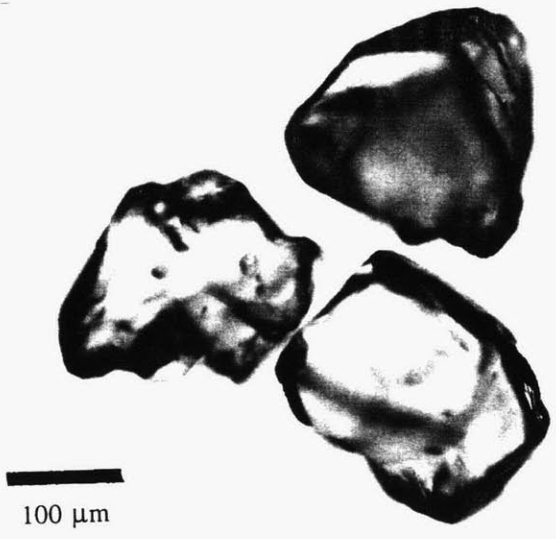
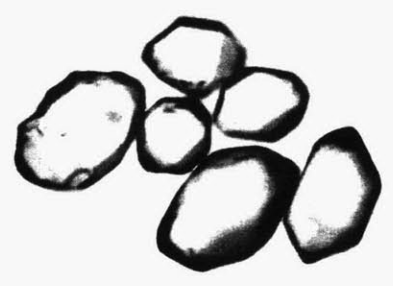


Figure 4





100  $\mu\text{m}$



100  $\mu\text{m}$

Figure 5





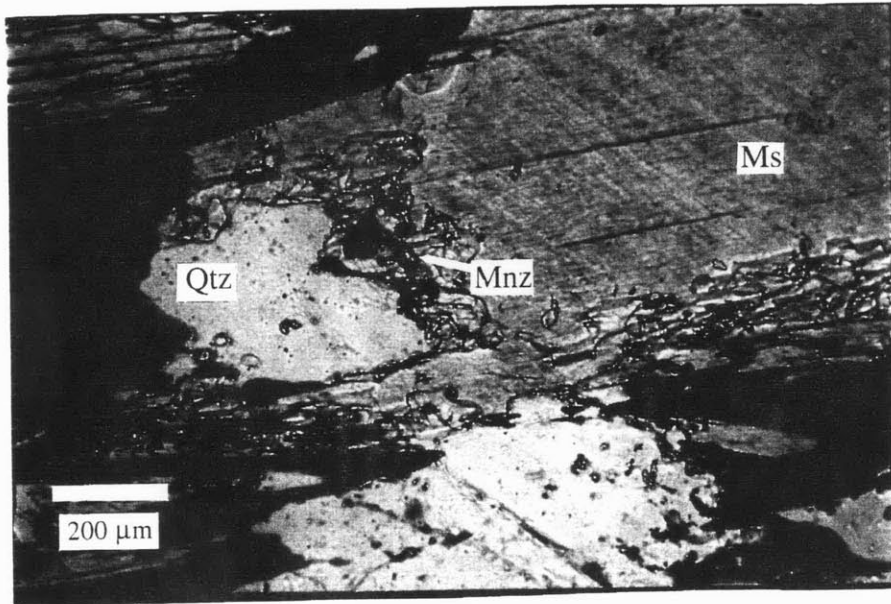
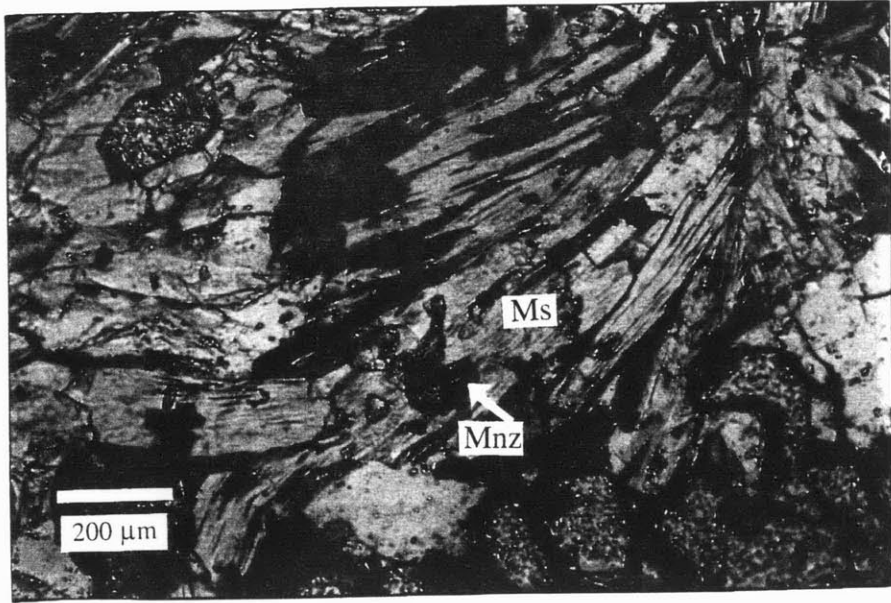


Figure 6



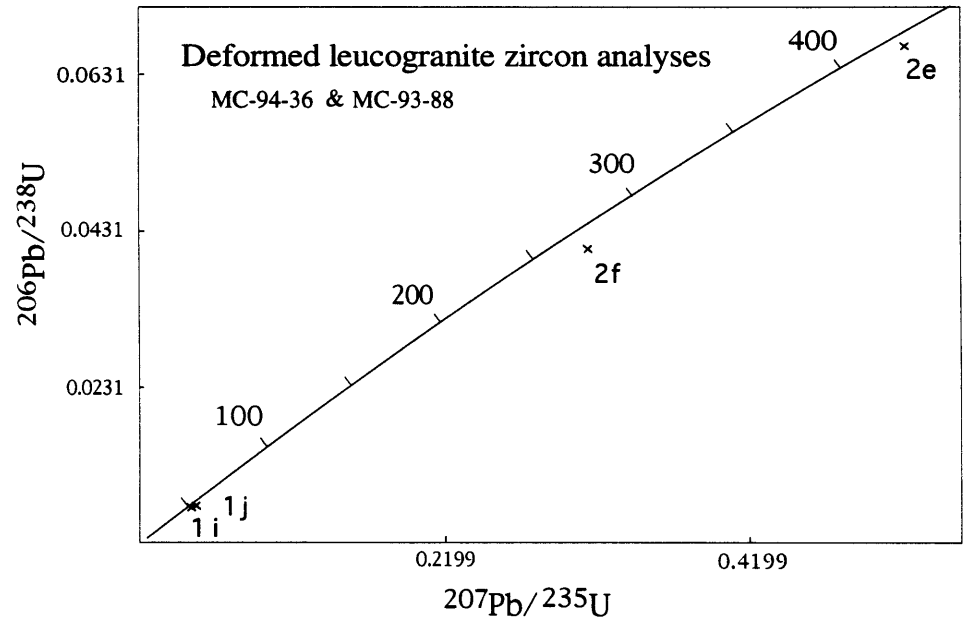
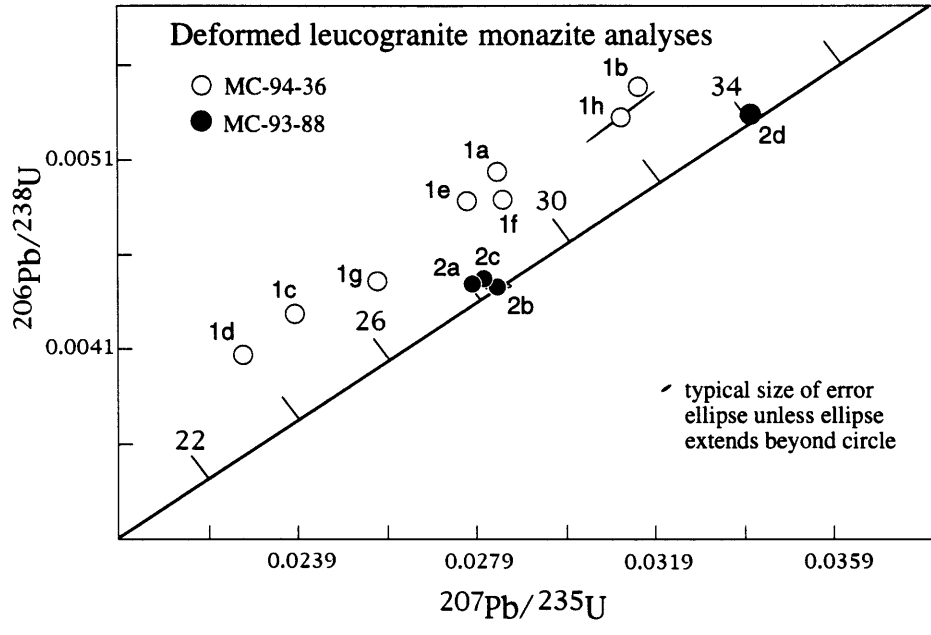


Figure 7



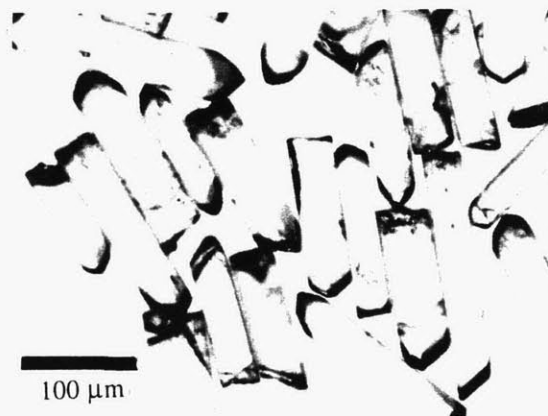
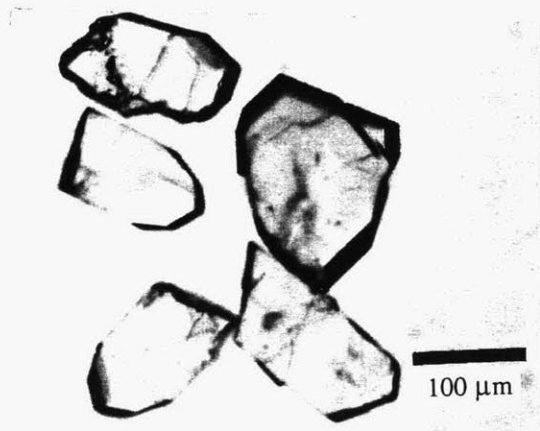
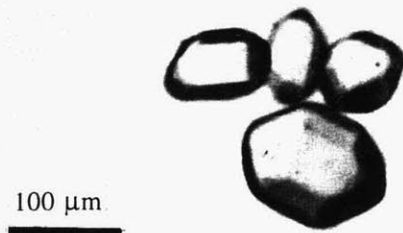


Figure 8



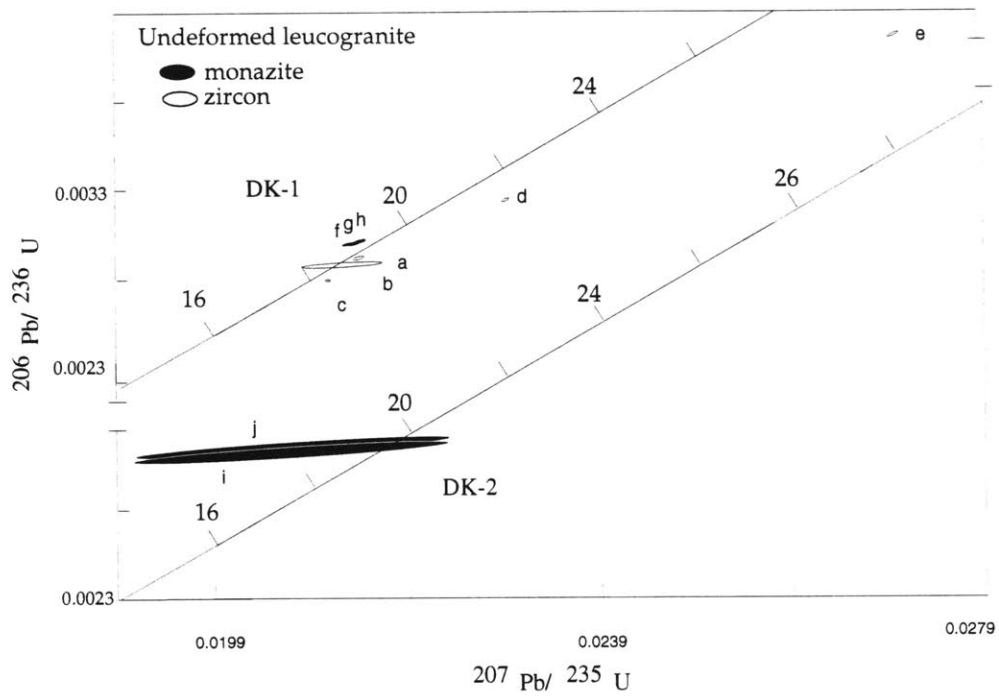


Figure 9





## Chapter 4

### Insights into the Oligocene thermal history of the central Himalaya from $^{40}\text{Ar}/^{39}\text{Ar}$ thermochronology, Marsyandi Valley, central Nepal

#### Abstract

In the Marsyandi valley of central Nepal, a major strand of the South Tibetan detachment system - the 18-22 Ma Chame detachment - places epidote-amphibolite to amphibolite facies calc-silicate rocks and marbles of the Tibetan sedimentary sequence on amphibolite facies pelitic gneisses and calc-silicate rocks of the Greater Himalayan sequence. Although the resulting metamorphic discontinuity is minor and sometimes cryptic,  $^{40}\text{Ar}/^{39}\text{Ar}$  thermochronologic results from the area reveal that the hanging wall and footwall of the detachment had distinctive thermal histories. Hanging wall phlogopites and biotites yield cooling ages of 27.1 to 29.9 Ma, compared with footwall biotite ages of 14.1 to 16.6 Ma. U-Pb monazite thermochronology demonstrates that the Greater Himalayan sequence experienced peak amphibolite facies conditions ca. 22 Ma, but the  $^{40}\text{Ar}/^{39}\text{Ar}$  results require hanging wall metamorphism to be an Oligocene (or older) phenomenon. These events represent the “Neohimalayan” and “Eohimalayan” metamorphic phases proposed by previous workers in the central Himalaya. Some of the dated hanging wall phlogopites grew synchronously with development of SW-vergent macroscopic folds in the Tibetan sedimentary sequence, implying that Eohimalayan metamorphism was associated with an important phase of crustal shortening in this sector of the Himalaya.

Despite the intensity of Neohimalayan metamorphism below the Chame detachment, evidence for Eohimalayan metamorphism and igneous activity is preserved in the footwall rocks of the Marsyandi drainage. Inherited ca. 35 Ma monazites of either metamorphic or igneous origin have been found in the upper Greater Himalayan sequence,

and one hornblende separate from the uppermost footwall yields a  $^{40}\text{Ar}/^{39}\text{Ar}$  age of  $30.0 \pm 3.0$  Ma. This hornblende date and a similar result from the same structural level in the nearby Kali Gandaki valley, if robust, suggest that the duration of the Neohimalayan event was extremely short, probably less than 1 million years, and that peak temperatures in the upper part of the Greater Himalayan sequence were not substantially greater than about 900K.

### **Introduction**

The Himalayan orogen is the result of roughly 50 million years of continental collision between the Indian and Eurasian plates (Patriat and Achache, 1984; Dewey et al., 1988). The high part of the range, the Greater Himalayan sequence, comprises a thick section of accreted continental crust derived from the subducting Indian plate (LeFort, 1975). The Greater Himalayan sequence was metamorphosed at temperatures of 870-1070K at mid-crustal depths during intracontinental subduction (see Hodges et al., 1988, and Pecher, 1989, for reviews). Most thermochronologic data from the central part of the range record cooling after Miocene or "Neohimalayan" metamorphism and anatexis, and there is very little known about the previous 30 million years of convergent tectonics. There is petrographic evidence for an earlier period of regional metamorphism, commonly referred to as the "Eohimalayan" phase (Brunel and Kienast, 1986; Hodges et al., 1988; Pecher, 1989). However both phases could have been part of a single protracted metamorphic event, and without supporting geochronologic data it has remained unclear whether or not there was significant crustal thickening within the Indian plate prior to the Miocene.

Over the past decade, a few isolated Oligocene hornblende and monazite cooling ages have been obtained from the Greater Himalayan sequence (Treloar et al., 1986; Hodges et al., 1994; Hodges et al., in press; Vannay and Hodges, in press; Chapter 3). In

the central part of the orogen, 35-36 Ma monazite ages from two separate locations (but within the same orthogneiss horizon), suggest that there was either Oligocene metamorphism or magmatism within the upper Greater Himalayan sequence (Hodges et al., in press; Chapter 3). In addition, a 37 Ma hornblende cooling age from a similar structural level (Vannay and Hodges, in press) provides further evidence of a pre-Miocene thermal event. However, the same rocks that have the Oligocene hornblende and monazite ages have a strong Miocene metamorphic and structural overprint. Miocene monazite ages for leucogranitic melt layers that are concordant with the oldest deformational fabric in the Greater Himalayan sequence make it very difficult to correlate the Oligocene ages with any structures (Chapter 3; Hodges et al., in press).

In this paper, we present  $^{40}\text{Ar}/^{39}\text{Ar}$  thermochronologic data for a suite of samples collected from the hanging wall and footwall of an extensional shear zone at the top of the Greater Himalayan sequence, the Chame detachment. The Chame detachment is part of the South Tibetan detachment system (Burchfiel et al., 1992), a family of primarily north-dipping extensional faults that form the upper boundary of the Greater Himalayan sequence along the length of the orogen. They are thought to have developed through gravitational instability of the Himalayan topographic front in Early Miocene time (Burchfiel and Royden, 1985). The South Tibetan detachment in other parts of the Himalaya, such as in eastern Nepal and southern Tibet, juxtaposes unmetamorphosed rocks of the Tibetan Sedimentary sequence against upper amphibolite facies rocks of the Greater Himalayan sequence (Burchfiel et al., 1992). In contrast, although there is structural evidence for normal faulting along the Chame detachment (Chapter 2), there is not an obvious break in metamorphic grade across the fault. However, thermochronologic results from the Chame detachment transect indicate a dramatic contrast in cooling histories across the fault. Data from the upper plate rocks provide clear evidence of Oligocene regional metamorphism

synchronous with the development of major deformational structures in the Tibetan Sedimentary sequence.

### **Geologic setting**

The upper Marsyandi valley is a major drainage that lies between the Annapurna and Manaslu massifs in central Nepal (Figures 1 and 2). The uppermost samples collected for thermochronology are from the basal unit of the Tibetan sedimentary sequence known as the Cambrian(?) Annapurna Yellow Formation. This unit is a 5 km-thick section of complexly folded amphibolite- to epidote-amphibolite-facies marble. Carbonate solvus thermometry indicates temperatures of 780-800K for prograde metamorphic conditions within the upper half of the Annapurna Yellow Formation (Schneider and Masch, 1993). Throughout the unit, the preferred alignment of phlogopite defines an S<sub>1</sub> foliation. This fabric is deformed by open to tight F<sub>2</sub> folds that verge primarily to the W and SW. An S<sub>2</sub> foliation is defined by secondary growth of phlogopite, axial planar to F<sub>2</sub> folds. The S<sub>2</sub> foliation is variably developed throughout the section but is most intense within the basal 200 meters of the Annapurna Yellow Formation, where it strikes NE-SW and dips moderately to the NW, concordant with the mylonitic foliation in the underlying Greater Himalayan sequence. Within this zone, F<sub>2</sub> folds are sheared out parallel to S<sub>2</sub> foliation planes (Chapter 2).

A northwest-dipping shear zone, the Chame detachment, juxtaposes the Annapurna Yellow Formation with calc-silicate gneiss of the Greater Himalayan sequence (Chapter 2). The Chame detachment has a significant component of top down-to-the-west, normal-oblique slip. Synkinematic growth of minerals suggests that shearing occurred at sillimanite-grade and lasted through retrograde conditions at greenschist-grade (Chapter 2).

The remaining samples were collected from the upper 5 km of the Greater Himalayan sequence. In the Marsyandi region this includes a variety of sillimanite-grade

calcareous and pelitic metamorphic rocks intruded by abundant concordant and cross-cutting leucogranites (see Chapter 2 for a detailed description of lithologies).

Thermobarometry of a pelitic gneiss 3 km below the top of the Greater Himalayan sequence indicates final equilibration at  $870 \pm 40$  K and  $630 \pm 80$  MPa (Chapter 5).

Although there is strong evidence that these data do not record equilibrium conditions, phase equilibrium constraints suggest that Neohimalayan temperatures at this level were at least 900 K. The upper 3 km of the Greater Himalayan sequence contains a composite foliation ( $S_2$ ) that strikes NE and dips  $25^\circ$ - $45^\circ$  NW. A mylonitic  $S_2$ (?) foliation, parallel to the Chame detachment deforms the upper 1000 m of the Greater Himalayan sequence, and  $D_2$  S-C fabrics indicate west-directed shearing at sillimanite-grade conditions (Chapter 2).

Previously obtained U-Pb monazite data from both foliated and cross-cutting leucogranites within the footwall gneisses reflect Middle Miocene anatexis and bracket displacement on the Chame detachment to between 18 and  $\sim 22$  Ma (Chapter 3). Monazite analyses have an Oligocene inherited component of  $\sim 35$  Ma (Chapter 3), implying that the Greater Himalayan section experienced Oligocene metamorphism or magmatism.

Previous  $^{40}\text{Ar}/^{39}\text{Ar}$  analysis of muscovite that defines  $S_2$ , indicates that the upper Greater Himalayan sequence passed through the muscovite closure temperature (ca. 625 K; McDougall and Harrison, 1988) at 17.5 Ma (Coleman and Hodges, 1995).

### **Thermochronology**

Thermochronologic analyses of samples from the upper Marsyandi valley were originally intended for comparison of the T-t histories of the footwall and hanging wall of the Chame detachment. The samples collected for thermochronology fall into three categories (see Figure 2 for sample locations). The first category includes metamorphic rocks from the footwall of the Chame detachment (MC-93-88, MC-93-47, MC-93-91, and

MC-93-52); the second includes metamorphic rocks from the hanging wall of the detachment (MC-93-54, MC-93-98, and MC-93-92); and the third includes one sample from a cross-cutting and undeformed leucogranite dike that intrudes the hanging wall (MC-93-92). Minerals analyzed by the  $^{40}\text{Ar}/^{39}\text{Ar}$  method include biotite, phlogopite, and hornblende. Estimated closure temperatures are 580K for biotite, 680K for phlogopite, and 780K for hornblende (McDougall and Harrison, 1988). Analytical procedures are given in the Appendix and results are summarized in Table 1. Complete data for each sample may be found in Table 2. All ages and isotopic ratios are reported at the  $2\sigma$  uncertainty level.

#### *Footwall samples*

Footwall samples include biotite-bearing gneiss and schist (MC-93-47 and MC-93-91), foliated leucogranite (MC-93-88), and amphibolite gneiss (MC-93-52). Biotite and hornblende define well-developed  $S_2$  and  $L_2$  fabrics in these rocks and can be used to constrain the minimum age of deformation.

#### Biotite $^{40}\text{Ar}/^{39}\text{Ar}$ results

Biotites from MC-93-88, MC-93-47, and MC-93-91 were analyzed by incremental laser step heating. All three samples yield flat release spectra with plateau ages ranging from  $15.53 \pm 0.31$  Ma to  $16.9 \pm 0.2$  Ma (Figures 3a - 6a). Inverse isochron ages range from  $14.87 \pm 0.69$  Ma and  $16.63 \pm 0.65$  Ma (Figures 3b - 6b). While within uncertainty of the plateau ages, the isochron ages are substantially less precise because most data cluster near the  $^{39}\text{Ar}/^{40}\text{Ar}$  axis, resulting in poorly constrained (but essentially atmospheric) initial  $^{40}\text{Ar}/^{36}\text{Ar}$  ratios of  $358 \pm 38$ ,  $280 \pm 300$ , and  $380 \pm 120$ .

#### Hornblende $^{40}\text{Ar}/^{39}\text{Ar}$ results

Sample MC-93-52 is a layered amphibolite gneiss containing hornblende, plagioclase, biotite and quartz. Hornblende was analyzed by furnace incremental heating

(Table 2). The release spectrum (Figure 7a) is characterized by a flat central region (defining a plateau age of  $35.28 \pm 0.88$  Ma) but inconsistent results at the lowest and highest temperatures of the experiment. Much of the last 20% of  $^{39}\text{Ar}_k$  released was associated with significantly older ages ( $>50$  Ma). Since these ages are improbably old (nominally as old as India-Asia collision in this sector of the range), the sample almost certainly contains a significant amount of excess  $^{40}\text{Ar}$ . Unfortunately, the high concentration of  $^{40}\text{Ar}$  in the trapped component makes it difficult to estimate the true cooling age of this sample more precisely than  $30.0 \pm 3.0$  Ma.

#### *Hanging wall samples*

Samples from the hanging wall include a biotite schist from the upper half of the Chame detachment shear zone (MC-93-54), a coarse-grained phlogopite marble in the immediate hanging wall of the Chame detachment (MC-93-93), and a fine-grained phlogopite marble (MC-93-98) from 3 km above the detachment. Phlogopite in MC-93-98 defines an  $S_1$  foliation that is folded by SW-verging F2-folds.

#### Phlogopite $^{40}\text{Ar}/^{39}\text{Ar}$ results

Laser step heating of MC-93-93 phlogopite resulted in a relatively flat release spectrum (Figure 8) with a plateau age of  $29.9 \pm 0.7$  Ma (57% of the total  $^{39}\text{Ar}_k$  released). Nine of the ten increments (80%  $^{39}\text{Ar}_k$ ) define an isochron age of  $29.7 \pm 1.2$  Ma, within uncertainty of the plateau age. Furnace step heating of sample MC-93-98 phlogopite also resulted in a robust plateau (100%  $^{39}\text{Ar}_k$ ) (Figure 9) with an age of  $27.4 \pm 0.5$  Ma and a similar but less precise isochron age of  $26.7 \pm 1.4$  Ma.

#### Biotite $^{40}\text{Ar}/^{39}\text{Ar}$ results

Laser step heating of MC-93-54 biotite resulted in a well-defined inverse isochron with an MSWD of 1.32 and a  $^{40}\text{Ar}/^{36}\text{Ar}$  intercept of  $280 \pm 10$ , close to the modern

atmospheric value (Figure 10). The isochron age is  $29.5 \pm 1.2$  Ma, within uncertainty of the plateau age for this samples  $28.7 \pm 0.5$  Ma ( $98\% \text{ }^{39}\text{Ar}_k$ ).

#### *Cross-cutting leucogranite within hanging wall*

#### Biotite $^{40}\text{Ar}/^{39}\text{Ar}$ results

Roughly 97% of the gas released by laser incremental heating of MC-93-92 biotite define a plateau age of  $16.4 \pm 0.3$  (Figure 10a). On the isotope correlation diagram (Figure 10b), all but the last three increments fall on an isochron, indicating an age of  $16.3 \pm 0.7$  Ma.

#### **Discussion**

The combined results imply a significant contrast in cooling histories between foliated rocks from the footwall and hanging wall of the Chame detachment. Footwall mica cooling ages range from  $\sim 14$  to  $17$  Ma, while hanging wall ages range from  $\sim 27$  to  $30$  Ma. Given that trioctahedral micas have a propensity to incorporate excess  $^{40}\text{Ar}$  in many environments (e.g., Roddick et al., 1980), one interpretation of the observed age discrepancy in the Marsyandi transect is that the hanging wall micas preferentially incorporated an unconstrained excess component. However, this possibility can be discounted using the isotope correlation diagrams in Figures 7-9. The hanging wall data *consistently* suggest either an atmospheric or a well defined excess component, and isochron ages for the hanging wall samples are virtually indistinguishable from plateau ages (which assume a  $^{40}\text{Ar}/^{36}\text{Ar}$  ratio of 295.5). We conclude that prograde metamorphism of the Tibetan sedimentary sequence in this transect is at least 30 Million years old.

The footwall hornblende analysis may provide further evidence of Oligocene metamorphism. In this case, the isotope correlation diagram provides evidence of significant contamination with an excess  $^{40}\text{Ar}$  component, and the result is a  $2\sigma$  error of



about 10% on the calculated age of the sample. However, the hornblende age is significantly greater than the ca. 22 Ma age of prograde Miocene metamorphism at this structural level, implying that the hornblende is not Neohimalayan. This conclusion is supported by another pre-Miocene  $^{40}\text{Ar}/^{39}\text{Ar}$  hornblende age obtained at roughly the same structural level in the nearby Kali Gandaki transect by Vannay and Hodges (in press), and by Oligocene U-Pb monazite ages from the Modi Khola transect (Hodges et al., in press, Figure 1). More importantly, a deformed leucogranite collected about 1.5 km structurally below the Marsyandi hornblende contained ~ 35 Ma metamorphic or igneous monazite (Chapter 3).

The preservation of Ordovician  $^{40}\text{Ar}/^{39}\text{Ar}$  hornblende ages in rocks that experienced sillimanite grade Miocene metamorphism presents an interesting thermal problem. Given our knowledge of the diffusivity of Ar in hornblende, the Miocene Neohimalayan event must have been very brief; otherwise, the hornblendes would have been reset. We have explored this in a semi-quantitative way using the MacArgon software package of Lister and Baldwin (in press). MacArgon permits the forward modeling of release spectra for minerals based on a user-definable temperature-time history. The approach is based on straightforward diffusion theory that is described in detail by McDougall and Harrison (1988), Giletti (1974), Harrison et al. (1985), and Lister and Baldwin (in press).

By trial and error, we found that the temperature-time trajectory shown in Figure 11, which is consistent with all petrologic and U-Pb geochronologic data from the Marsyandi transect, would produce hornblende, muscovite, and biotite ages such as those reported in this paper and in Coleman and Hodges (1995). Specific modeled release spectra are shown in Figures 12-14. It is important to note that the exact forms of these spectra are dependent on the assumption that Ar is released from these minerals in the laboratory exclusively through volume diffusion. This is certainly incorrect, because

hydrous phases undergo a series of dehydroxylation reactions that release Ar during vacuum heating (Lee et al., 1991; Wartho et al., 1991; Hodges et al., 1994). However, the relatively flat, high-temperature segments of the modeled spectra probably correspond to plateau (or near-plateau) ages that would be obtained for samples subjected to the assumed T-t trajectory.

The modeled results should not be regarded as unique; ages similar to those obtained for Marsyandi samples could almost certainly be produced by somewhat different T-t histories. However, all viable histories that we examined shared some characteristics:

- An initial period of high-grade Eohimalayan metamorphism prior to 35 Ma.
- Relatively rapid cooling from the Eohimalayan metamorphic peak.
- Extremely rapid heating (>500K/m.y.) to peak Neohimalayan temperatures (assumed to be at least 900K based on petrologic constraints in Chapter 5).
- Cooling from the Neohimalayan peak to less than 800K in less than 1 million years
- Maintenance of temperatures roughly corresponding to greenschist facies for at least five million years after the Neohimalayan peak.

The exact mechanism by which the upper part of the Greater Himalayan sequence could have been heated to Neohimalayan temperatures in such a short time remains enigmatic. In any case, the hornblende data suggest strongly that the Neohimalayan event in this part of the Himalaya was short lived.

### **Tectonic Implications**

The  $^{40}\text{Ar}/^{39}\text{Ar}$  thermochronologic results presented here indicate that the Chame detachment juxtaposes rocks with very different temperature-time histories. The hanging wall retains evidence of an Oligocene metamorphic history, but such evidence has been all but obliterated in the footwall by a strong Miocene overprint. There is no evidence of Miocene metamorphism in the cooling ages of metamorphic micas from the hanging wall,

indicating that these rocks preserve syn-metamorphic deformation that is at least ~30 Ma. The hanging wall lithologies preserve an Oligocene  $S_1$  foliation defined by the preferred alignment of phlogopite. Throughout the Annapurna Yellow Formation,  $S_1$  is folded by SW and W verging  $F_2$  folds. In some areas a second generation of phlogopite is axial planar to the  $F_2$  folds, suggesting that the phlogopite grew both prior to and during folding. Cooling ages from both phlogopite that defines  $S_1$  and  $S_2$  demonstrate that  $S_1$  foliation development and  $F_2$  folding are both Oligocene phenomena. This conclusion is consistent with the observation that south-west verging  $F_2$  folds are sheared out at the base of the Annapurna Yellow formation by the Chame detachment (Chapter 2). Oligocene hornblende ages and monazite ages from the upper Greater Himalayan sequence, in the footwall of the Chame detachment, provide evidence of regional metamorphism at a deeper structural level during thrusting. The conclusion that southwest-directed thrusting occurred along the leading edge of the Indian plate prior to Miocene time is inconsistent with the tectonic model proposed by Yin et al. (1994), which maintained that the last major thrusting prior to MCT development occurred along the 27-23 Ma Gangdese thrust, more than 200 km to the north of the high Himalaya and within the Eurasian plate. Our data suggest a more complicated history of foreland propagating thrusts.

A separate but equally important tectonic problem is understanding what mechanism cooled the Greater Himalayan sequence during the Miocene. The Greater Himalayan sequence preserves a steep to inverted Miocene metamorphic field gradient with temperatures of at least 900K from the base of the section to the top (Chapters 3 and 4; Hubbard, 1989). The two main mechanisms by which orogens are unroofed and cooled are erosion and tectonic denudation. Thermal models demonstrate that the unroofing rate of an evolving orogen plays a key role in the resulting thermal structure (Ruppel et al., 1988; Royden, 1993; Huerta et al., in press). It is also known that rates of surficial erosion

in mountain ranges with rapid uplift rates are comparable to rates of tectonic erosion (e.g., Adams, 1980; Burbank, et al., 1996). Thus, in an orogen such as the Himalaya, where present and past surficial erosion rates are high (1 to 10 mm/yr) (Burbank et al., 1996; Copeland and Harrison, 1990) and where extension was active during convergence (Burchfiel and Royden, 1985; Hodges et al., 1992), it is not necessarily clear which mechanism was more important. Although our data do not constrain the cooling or unroofing rate on the Chame detachment, it seems most reasonable to attribute the cooling of the Greater Himalayan sequence in the Marsyandi transect to unroofing along the Chame detachment. This interpretation is supported by the close agreement in cooling ages (~16.5 Ma) between biotite from a leucogranite dike which cross cuts foliation within the hanging wall and biotite from the footwall foliation.

### **Acknowledgments**

I thank D. Applegate and M. House for sharing their expertise in mineral separation techniques and data reduction, W. Olszewski for assistance with sample preparation and sample analysis, and K.V Hodges for help with running the analyses, for writing new and improved reduction software and re-reducing the data, and for sound advise with the interpretation. Special thanks also to K. Bull, M. Sherpa, and D.R. Thulung for assistance with field mapping and sample collection.

### **Appendix**

#### *Analytical methods*

Samples were crushed using standard crushing and grinding techniques and sieved to obtain fractions close to the actual grain sizes of micas, and smaller than the actual grain sizes of hornblendes (in order to avoid composite grains). Pure mineral separates were prepared using standard heavy liquid, magnetic, and paper shaking methods. Hornblendes were also cleaned with a high-power ultrasonic probe. Hornblende and some of the mica

separates were hand picked to achieve the desired purity (>99%). The separates were washed in water, acetone, and ethanol prior to being wrapped in individual Al foil packets for irradiation. Samples were irradiated in position 8D of the McMaster University reactor for 7 hours with Cd shielding. Ca, K, and Cl production factors during irradiation were established by analyzing reagent grade  $\text{CaF}_2$ ,  $\text{K}_2\text{SO}_4$ , and KCl included in the irradiation package. The fast neutron flux was monitored using Mmhb-1 hornblende (520.4 Ma, Samson and Alexander 1987) and Fish Canyon sanidine (20.8 Ma, Cebula et al. 1986). Irradiated samples were analyzed at the Cambridge Laboratory for Argon Isotope Research at MIT using a MAP 215-50 mass spectrometer. Gas was extracted using either a 10 W Ar-ion laser or a double-vacuum resistance furnace. During the course of these analyses, laser blanks for M/e 40 and 36 (moles) were  $3 \times 10^{-16}$  and  $5 \times 10^{-18}$ , respectively. For furnace analyses, over the 800 - 1500 K range, M/e 40 and 36 blanks (moles) ranged from  $6 \times 10^{-15}$  and  $1 \times 10^{-16}$ , to  $3 \times 10^{-15}$  and  $3 \times 10^{-18}$ , respectively. Additional details of laboratory procedures, descriptions of facilities, and propagation of uncertainties can be found in Hodges et al. (1994).

## References

- Adams, J., 1980, Contemporary uplift and erosion of the Southern Alps, New Zealand: Geological Society of America Bulletin, Part II, v. 91, p. 1-114.
- Brunel, M. and Kienast, J.R., 1986, Etude petro-structurale des chevauchements ductiles himalayens sur la transversale de l'Everest-Makalu (Nepal oriental): Canadian Journal of Earth Science, v. 23, p. 1117-1137.
- Burbank, D.W., Leland, J., Fielding, E., Anderson, R.S., Brozovic, N., Reid, M., and Duncan, C., 1996, Bedrock incision, rock uplift and threshold hillslopes in the northwestern Himalaya: Nature, v.379, p. 505-510.
- Burchfiel, B.C. and Royden, L., 1985, North-south extension within the convergent Himalayan region: Geology, v. 13, p. 679-682.
- Burchfiel, B.C., Zhiliang, C., Hodges, K.V., Yuping, L., Royden, L.H., Changrong, D., Jiene, X., 1992, The South Tibetan Detachment System, Himalayan Orogen: Extension contemporaneous with and parallel to shortening in a Collisional Mountain Belt: Geological Society of America, Special Paper 269, 41 p.
- Cebula, G.T., Kunk, M.J., Mehnert, H.H., Naeser, C.W., Obradich, J.D., and Sutter, J.F., 1986, The Fish Canyon Tuff, a potential standard for the  $^{40}\text{Ar}$ - $^{39}\text{Ar}$  and fission-track methods: Terra Cognita, v. 6, p.139-140.
- Coleman, M.E., and Hodges, K.V., 1995, Evidence for Tibetan plateau uplift before 14 Myr ago from a new minimum age for east-west extension: Nature, v. 374, p. 49-52.
- Copeland, P., and Harrison, T.M., 1990, Episodic rapid uplift in the Himalaya revealed by  $^{40}\text{Ar}/^{39}\text{Ar}$  analysis of detrital K-feldspar and muscovite, Bengal fan: Geology, v. 18, p. 354-357.
- Dewey, J.F., Shackleton, R.M., Chang Chengfa and Sun Yiyin, 1988, Tectonic evolution of the Tibetan Plateau: Philosophical Transactions of the Royal Society of London, Series A, v. 327, p. 379-413.
- Giletti, B.J., 1974, Studies in diffusion I: Argon in phlogopite mica, :In Geochemical transport and kinetics, eds. Hofmann, A.W., Giletti, B.J., Yoder, H.S., and Yund, R.A., Carnegie Institute of Washington, 634, p.61-76.
- Harrison, T.M., 1981, Diffusion of  $^{40}\text{Ar}$  in hornblende: Contributions to Mineralogy and Petrology, v. 78, p. 324-331.
- Harrison, T.M., Duncan, I., and McDougall, I., 1985, Diffusion of  $^{40}\text{Ar}$  in biotite: Temperature, pressure and compositional effects; Geochimica et Cosmochimica Acta, v. 49, p.2461-2468.

- Hodges, K.V., Hubbard, M.S., Silverburg, D.S., 1988, Metamorphic constraints on the thermal evolution of the central Himalayan Orogen: *Philosophical Transactions of the Royal Society of London*, v. A326, p. 257-280.
- Hodges, K.V., Hames, W.E., Olszewski, W., Burchfiel, B.C., Royden, L.H., Chen, Z., 1994, Thermobarometric and  $^{40}\text{Ar}/^{39}\text{Ar}$  geochronologic constraints on Eohimalayan metamorphism in the Dinggye area, southern Tibet: *Contributions to Mineralogy and Petrology*, v. 117, p.151-163.
- Hodges, K.V., Hames, W.E., and Bowring, S. A., 1994,  $^{40}\text{Ar}/^{39}\text{Ar}$  age gradients in micas from a high temperature - low pressure metamorphic terrain: Evidence for very slow cooling and implications for the interpretation of age spectra: *Geology*, v. 22, p. 55-58.
- Hodges, K.V., Parrish, R.R., Searle, M.P., in press, Tectonic evolution of the Central Annapurna Range, Nepalese Himalaya: *Tectonics*.
- Hubbard, M.S., 1989, Thermobarometric constraints on the thermal history of the Main Central Thrust Zone and Tibetan Slab, eastern Nepal Himalaya: *Journal of Metamorphic Geology*, v. 7, p. 19-30.
- Huerta, A.D., Royden, L.H., and Hodges, K.V., in press, The interdependence of deformational and thermal processes in mountain belts: *Science*.
- Lee, J.K.W., Onstott, T.C., Cashman, K.V., Cumbest, R.J., and Johnson, D., 1991, incremental heating of hornblende in vacuo: Implications for  $^{40}\text{Ar}/^{39}\text{Ar}$  geochronology and the interpretation of thermal histories: *Geology*, v. 19, p. 872-876.
- Le Fort, P., 1975, Himalaya: the collided range. Present knowledge of the continental arc: *American Journal of Science*, v. 275A, p.1-44.
- Lister, G. S., and Baldwin, S.L., in press, Modelling the effect of arbitrary P-T-t histories on argon diffusion in minerals using the MacArgon program for the Apple Macintosh: *Tectonics*.
- McDougall, I., and Harrison, T.M., 1988, *Geochronology and Thermochronology by the  $^{40}\text{Ar}/^{39}\text{Ar}$  Method*, Oxford University Press, Oxford. 212 p.
- Patriat, P., and Achache J., 1984, India-Eurasia collision chronology and its implications for crustal shortening and driving mechanisms of plates: *Nature*, v. 311, p.615-621.
- Pêcher, A., 1989, The metamorphism in the Central Himalaya: *Journal of Metamorphic Geology*, v.7, p.31-41.
- Roddick, J.C., Cliff, R.A., and Rex, D.C., 1980, The evolution of excess argon in alpine biotites-a  $^{40}\text{Ar}/^{39}\text{Ar}$  analysis: *Earth and Planetary Science Letters*, v. 48, p. 945-960.

- Royden, L., 1993, The steady state thermal structure of eroding orogenic belts and accretionary prisms: *Journal of Geophysical Research*, v.98, p. 4487-4507.
- Ruppel, C., Royden, L., and Hodges, K.V., 1988, Thermal modeling of extensional tectonics: application to pressure-temperature-time histories of metamorphic rocks: *Tectonics*, v.7, p. 947-957.
- Samson, S.D., and Alexander, E.C., 1987, Calibration of the interlaboratory  $^{40}\text{Ar}/^{39}\text{Ar}$  dating standard, Mmhb-1: *Chemical Geology*, v. 66, p. 27-34.
- Schneider, C. and Masch, L., 1993, The metamorphism of the Tibetan Series from the Manang area, Marsyandi Valley, Central Nepal, *in* P.J. Treloar and M.P. Searle, eds., *Himalayan Tectonics*, the Geological Society, London, Special Publication No. 47, p. 357-374.
- Treloar, P.J., Rex, D.C., Guise, P.G., Coward, M.P., Searle, M.P., Windley, B.F., Petterson, M.G., Jan, M.Q., and Luff, I.W., 1989, K-Ar and Ar-Ar geochronology of the Himalayan collision in NW Pakistan: constraints on the timing of suturing, deformation, metamorphism and uplift: *Tectonics*, v. 8(4), p. 881-909.
- Vannay, J.C., and Hodges, K.V., in press, Tectonometamorphic evolution of the Himalayan metamorphic core between the Annapurna and Dhaulagiri, central Nepal: *Journal of Metamorphic Geology*.
- Wartho, J., Didson, M.H., Rex, D.C., and Guise, P.G, 1991, Mechanisms of Ar release from Himalayan metamorphic hornblende: *American Mineralogist*, v. 76, p. 1446-1448.
- Yin, A., Harrison, T.M., Ryerson, F.J., Wenji, C., Kidd, W.S.F., and Copeland, P., 1994, Tertiary structural evolution of the Gangdese thrust system, southeastern Tibet: *Journal of Geophysical Research*, v. 99, p. 18175-18201.
- York, D., 1966, Least-squares fitting of a straight line: *Canadian Journal of Physics*, v. 44, p. 1079-1086.
- York, D., 1969, Least-squares fitting of a straight line with correlated errors: *Earth and Planetary Science Letters*, v. 5, p. 320-324.



Table 1 Summary of  $^{40}\text{Ar}/^{39}\text{Ar}$  results<sup>a</sup>

Sample	Mineral	Extraction method	Plateau Age (Ma) <sup>b</sup>	$^{39}\text{Ar}$ (%) <sup>c</sup>	Isochron/ Errorchron Age (Ma) <sup>d</sup>	$^{39}\text{Ar}$ (%) <sup>f</sup>	$(^{40}\text{Ar}/^{36}\text{Ar})_0$	MSWD <sup>g</sup>
MC9388	Bt	Laser	16.9±0.2	100	16.6±0.7	98	360±40	1.9
MC9391	Bt	Laser	15.0±0.2	100	14.8±0.7	100	380±120	1.75
MC9347a	Bt	Laser	14.7±0.2	100	13.0±0.9	77	445±67	8.9
MC9347b	Bt	Laser	15.5±0.3	71	15.6±1.1	71	280±300	5.02
MC9352	Hbl	Furnace	35.3±0.9	75	30.0±3.0	100	820±190	1.64
MC9393	Phl	Laser	29.9±0.7	57	29.7±1.2	81	301±53	1.05
MC9398	Phl	Furnace	26.8±0.4	100	26.7±1.4	77	480±400	2.2
MC9354	Bt	Laser	28.7±0.5	98	29.5±1.2	100	250±20	1.32
MC9392	Bt	Laser	16.8±0.3	97	16.6±0.7	56	280±10	1.14

<sup>a</sup> All uncertainties quoted at the  $2\sigma$  confidence level. <sup>b</sup> Calculated following methods outlined in Hodges et al. (1994). <sup>c</sup> Percentage of total  $^{39}\text{Ar}$  in the sample that was released in the heating steps included in the plateau. <sup>d</sup> Calculated using a least squares linear regression with correlated errors (York 1969). <sup>e</sup> Percentage of total  $^{39}\text{Ar}$  in the heating steps used for the regression. <sup>f</sup> Mean squared weighted deviation.

Sample: MC-93-88 biotite  
 J Value: 5.93E-04 ± 2.26E-05

Amps	36/40	(36/40)err	39/40	(39/40)err	39ArK moles	Cum. 39ArK%	40Ar*%	Age (Ma)	err	w/o J	
11.5	2.99E-03	2.88E-04	1.22E-02	1.80E-04	2.38E-14	0.46	11.78	10.3	7	7.41	0.3
12.5	2.21E-03	9.88E-05	2.28E-02	1.11E-04	8.66E-14	2.14	34.74	16.22	1	1.36	0.1
13	7.88E-04	9.67E-05	4.67E-02	3.17E-04	2.25E-13	6.5	76.7	17.49	1	0.66	0.1
13.5	3.88E-04	5.22E-05	5.45E-02	3.97E-04	4.12E-13	14.49	88.53	17.31	1	0.33	0.0
14	2.19E-04	4.41E-05	5.88E-02	3.12E-04	5.26E-13	24.67	93.52	16.94	1	0.25	0.0
14.5	3.08E-04	4.50E-05	5.76E-02	2.28E-04	4.92E-13	34.2	90.87	16.82	1	0.25	0.0
15	2.26E-04	6.29E-05	6.06E-02	2.95E-04	5.24E-13	44.35	93.3	16.4	1	0.33	0.0
16	1.16E-04	3.98E-05	6.08E-02	1.30E-04	8.54E-13	60.89	96.56	16.92	1	0.21	0.0
18	1.20E-04	3.45E-05	6.09E-02	2.87E-04	1.10E-12	82.19	96.43	16.87	1	0.19	0.0
20	7.99E-05	2.54E-05	6.24E-02	1.81E-04	9.19E-13	100	97.62	16.66	1	0.14	0.0

39Ar Wtd. Mean Age: 16.86 ± 0.23

Sample: MC-93-91 biotite  
 J Value: 5.93E-04 ± 2.26E-05

Amps	36/40	(36/40)err	39/40	(39/40)err	39ArK moles	40Ar*%	Age (Ma)	err
13	3.73E-04	1.07E-04	6.26E-02	6.21E-04	1.05E-15	6.25	88.55	15.16 ± 0.56
13.5	2.36E-04	7.62E-05	6.32E-02	3.43E-04	1.49E-15	15.18	92.59	15.69 ± 0.39
14	2.71E-04	3.95E-05	6.52E-02	2.16E-04	1.85E-15	26.22	91.53	15.04 ± 0.2
14.5	1.47E-04	7.26E-05	6.88E-02	1.00E-03	1.75E-15	36.67	95.15	14.82 ± 0.39
15	1.38E-04	6.85E-05	6.77E-02	2.52E-04	1.57E-15	46.03	95.42	15.1 ± 0.32
16	2.04E-04	3.57E-05	6.68E-02	5.43E-04	2.31E-15	59.84	93.5	15 ± 0.21
18	1.59E-04	1.60E-05	6.71E-02	4.06E-04	4.58E-15	87.21	94.83	15.14 ± 0.12
20	1.69E-04	6.13E-05	6.66E-02	3.77E-04	2.14E-15	100	94.54	15.22 ± 0.3

39Ar Wtd. Mean Age: 15.13 ± 0.23

Table 2

Sample: MC-93-47 biotite, Split B  
 J Value: 5.93E-04 ± 2.26E-05

Amps	36/40	(36/40)err	39/40	(39/40)err	39ArK moles	40Ar*%	Age (Ma)	err
13	3.81E-04	9.15E-05	6.22E-02	3.92E-04	1.50E-15	11.09	88.71	15.2 ± 0.47
13.5	1.01E-04	1.09E-04	6.34E-02	4.13E-04	1.43E-15	21.66	97	16.3 ± 0.55
14	1.79E-04	1.02E-04	6.65E-02	3.50E-04	1.31E-15	31.37	94.7	15.18 ± 0.49
14.5	1.47E-04	8.60E-05	6.56E-02	3.03E-04	1.28E-15	40.84	95.63	15.54 ± 0.42
15	2.52E-04	1.31E-04	6.58E-02	3.94E-04	1.35E-15	50.8	92.53	14.98 ± 0.63
16	6.96E-05	5.69E-05	6.57E-02	3.84E-04	2.69E-15	70.69	97.92	15.89 ± 0.29
18	-6.26E-05	4.35E-05	6.46E-02	4.70E-04	3.19E-15	94.26	101.82	16.8 ± 0.24
20	-1.06E-04	1.36E-04	6.51E-02	8.72E-04	7.77E-16	100	103.09	16.89 ± 0.69
39Ar Wtd. Mean Age:							15.84 ±	0.27

Table 2 (continued)

Sample: MC-93-52 hornblende  
J Value: 5.93E-04 ± 2.26E-05

T, K	36/40	(36/40)err	39/40	(39/40)err	39ArK moles	40Ar*%	Age (Ma)	err
1050	7.46E-04	1.34E-04	1.64E-02	2.65E-04	2.22E-14	8.42	77.85	50.13 ± 2.63
1100	4.62E-04	1.21E-04	2.69E-02	1.52E-04	4.63E-14	25.96	86.18	34.09 ± 1.41
1150	2.31E-04	5.45E-05	2.79E-02	1.40E-04	9.48E-14	61.88	92.96	35.37 ± 0.63
1175	2.25E-04	1.73E-04	2.75E-02	1.77E-04	4.34E-14	78.33	93.15	35.95 ± 1.96
1200	1.25E-04	7.62E-04	2.45E-02	9.25E-04	5.86E-15	80.55	96.13	41.57 ± 9.73
1225	4.22E-04	6.26E-04	2.06E-02	9.58E-04	3.78E-15	81.99	87.4	44.98 ± 9.61
1250	5.02E-04	4.56E-04	1.75E-02	5.80E-04	6.01E-15	84.27	85.06	51.46 ± 8.2
1275	3.92E-04	1.83E-04	1.81E-02	2.57E-04	1.89E-14	91.43	88.3	51.69 ± 3.2
1300	3.20E-04	5.47E-04	1.92E-02	3.05E-04	8.06E-15	94.49	90.4	49.83 ± 8.81
1325	-1.37E-05	1.65E-03	1.99E-02	1.24E-03	2.53E-15	95.44	100.25	53.25 ± 25.7
1350	1.20E-03	2.69E-03	1.67E-02	3.03E-03	1.24E-15	95.91	64.55	41.07 ± 50.5
1400	1.37E-03	2.52E-03	1.68E-02	2.12E-03	1.20E-15	96.37	59.45	37.55 ± 46.8
1500	1.74E-03	2.24E-03	1.67E-02	2.08E-03	1.32E-15	96.86	48.55	30.85 ± 41.9
1800	4.09E-04	5.81E-04	2.90E-02	4.99E-04	8.27E-15	100	87.71	32.11 ± 6.24
39Ar Wtd. Mean Age:							37.84 ±	0.67

Table 2 (continued)

Sample: MC-93-93 phlogopite  
J Value: 5.93E-04 ± 2.26E-05

Amps	36/40	(36/40)err	39/40	(39/40)err	39ArK moles	40Ar*%	Age (Ma)	err	
11.5	1.10E-03	2.43E-04	2.45E-02	8.80E-04	3.03E-16	5.85	67.28	29.25 ± 3.26	
12.5	6.11E-04	1.29E-04	2.97E-02	2.53E-04	5.63E-16	16.73	81.76	29.28 ± 1.38	
13	4.19E-04	1.39E-04	3.16E-02	4.09E-04	4.42E-16	25.27	87.4	29.41 ± 1.42	
13.5	2.72E-04	1.10E-04	3.18E-02	4.82E-04	3.93E-16	32.86	91.75	30.71 ± 1.17	
14	1.40E-04	1.09E-04	3.07E-02	3.09E-04	5.25E-16	43	95.65	33.1 ± 1.15	
14.5	2.73E-04	1.18E-04	3.27E-02	2.69E-04	4.69E-16	52.07	91.7	29.88 ± 1.15	
15	3.37E-04	7.98E-05	3.20E-02	8.16E-04	4.34E-16	60.46	89.82	29.84 ± 1.08	
16	1.71E-04	6.40E-05	3.35E-02	2.29E-04	6.42E-16	72.86	94.69	30.1 ± 0.63	
18	1.06E-04	5.21E-05	3.49E-02	2.19E-04	1.25E-15	96.97	96.6	29.46 ± 0.5	
20	9.18E-06	2.52E-04	3.40E-02	4.23E-04	1.57E-16	100	99.47	31.09 ± 2.33	
							39Ar Wtd. Mean Age:	30.17 ± 0.51	

Table 2 (continued)

Sample: MC-93-98 phlogopite  
J Value: 5.93E-04 ± 2.26E-05

T,K	36/40	(36/40)err	39/40	(39/40)err	39ArK moles	40Ar*%	Age (Ma)	err	
900	2.70E-03	9.17E-04	3.59E-03	1.14E-03	6.85E-16	0.09	20.17	59.26 ± 80.5	
950	1.85E-03	4.29E-04	2.46E-02	5.34E-04	1.44E-14	2.02	45.22	19.6 ± 5.47	
1000	4.74E-04	1.28E-04	3.43E-02	2.96E-04	5.29E-14	9.12	85.76	26.62 ± 1.19	
1050	3.23E-04	1.36E-04	3.74E-02	3.80E-04	5.34E-14	16.29	90.19	25.72 ± 1.16	
1100	2.60E-04	1.48E-04	3.80E-02	2.42E-04	4.93E-14	22.91	92.06	25.8 ± 1.22	
1150	1.54E-04	1.27E-04	3.77E-02	3.16E-04	5.33E-14	30.06	95.19	26.94 ± 1.07	
1200	5.74E-05	1.32E-04	3.72E-02	2.25E-04	4.10E-14	35.56	98.03	28.06 ± 1.12	
1250	1.51E-04	8.95E-05	3.77E-02	2.86E-04	7.70E-14	45.89	95.28	26.94 ± 0.77	
1350	4.81E-05	2.46E-05	3.88E-02	2.11E-04	2.96E-13	85.65	98.29	26.98 ± 0.25	
1550	7.16E-05	7.34E-05	3.77E-02	3.33E-04	1.07E-13	100	97.6	27.6 ± 0.65	
							39Ar Wtd. Mean Age:	26.84 ± 0.44	

Table 2 (continued)

Sample: MC-93-54 biotite  
J Value: 5.93E-04 ± 2.26E-05

	36/40	(36/40)err	39/40	(39/40)err	39ArK moles	40Ar*%	Age (Ma)	err
11	3.16E-03	3.58E-04	8.40E-03	5.86E-04	9.67E-17	1.52	6.54	8.33 ± 13.4
11.5	3.05E-03	7.74E-04	1.27E-02	2.80E-03	2.05E-17	1.85	9.88	8.32 ± 19.3
12	1.85E-03	7.27E-04	2.14E-02	1.44E-03	5.66E-17	2.74	45.41	22.64 ± 10.8
12.5	2.48E-03	2.75E-04	1.31E-02	5.29E-04	9.99E-17	4.31	26.6	21.6 ± 6.62
13	1.25E-03	3.61E-04	2.59E-02	7.97E-04	1.33E-16	6.4	63.01	25.95 ± 4.44
13.5	9.28E-04	1.92E-04	2.67E-02	6.67E-04	2.83E-16	10.86	72.43	28.9 ± 2.35
14	6.21E-04	1.51E-04	3.05E-02	5.75E-04	3.78E-16	16.81	81.47	28.47 ± 1.63
14.5	4.76E-04	3.71E-05	3.11E-02	4.59E-04	5.61E-16	25.64	85.74	29.35 ± 0.57
15	4.91E-04	7.29E-05	3.21E-02	3.81E-04	1.20E-15	44.5	85.28	28.24 ± 0.78
16	2.74E-04	2.38E-05	3.35E-02	1.58E-04	3.53E-15	100	91.68	29.09 ± 0.26

39Ar Wtd. Mean Age: 28.67 ± 0.5

Sample: MC-93-92 biotite  
J Value: 5.93E-04 ± 2.26E-05

Amps	36/40	(36/40)err	39/40	(39/40)err	39ArK moles	40Ar*%	Age (Ma)	err
11	2.88E-03	2.02E-04	1.24E-02	7.44E-04	2.73E-16	0.79	14.8	12.7 ± 5.16
12	2.48E-03	7.96E-05	2.02E-02	2.18E-04	5.03E-16	2.25	26.64	14.09 ± 1.25
13	1.13E-03	1.39E-04	4.27E-02	3.32E-03	1.27E-15	5.93	66.41	16.62 ± 1.68
14	5.59E-04	6.34E-05	4.93E-02	5.35E-03	3.53E-15	16.16	83.17	18.04 ± 2.28
15	6.39E-04	2.68E-05	5.30E-02	1.80E-04	4.40E-15	28.91	80.79	16.32 ± 0.17
16	4.35E-04	3.18E-05	5.66E-02	5.65E-04	4.30E-15	41.38	86.79	16.41 ± 0.24
17	4.35E-04	1.80E-05	5.61E-02	3.66E-04	4.98E-15	55.82	86.78	16.54 ± 0.15
18	2.70E-04	3.37E-05	5.78E-02	3.23E-04	3.78E-15	66.8	91.61	16.96 ± 0.21
19	3.86E-04	2.57E-05	5.27E-02	2.20E-03	6.30E-15	85.06	88.23	17.91 ± 0.84
20	1.25E-04	2.00E-05	5.68E-02	2.28E-03	5.15E-15	100	95.9	18.07 ± 0.75

39Ar Wtd. Mean Age: 17.0 ± 0.2

## Figure captions

Figure 1) Simplified regional tectonic map of central Nepal from Colchen et al. (1986) with minor modifications from Coleman (in press). The major structures include the Main Central thrust (MCT), the South Tibetan detachment system (STDS), and the Thakkola graben. The village of Chame and the city of Pokhara are marked by black squares. The inset map shows the location of the Annapurna-Manaslu region within the Himalaya.

Figure 2) Geological map of the upper Marsyandi valley region with  $^{40}\text{Ar}/^{39}\text{Ar}$  sample locations.

Figures 3 -10)  $^{40}\text{Ar}/^{39}\text{Ar}$  Ar release spectra and inverse isotope correlation diagrams. The shaded steps within the release spectra indicate the increments used for calculating plateau ages. The shaded squares on the inverse plots indicate which points were used in the linear regression.

Figure 11) Temperature-time path used for modeling release spectra (Figures 12-14) with the MacArgon software package of Lister and Baldwin (1988). The temperature-time history is consistent with petrologic and geochronologic data from the Marsyandi transect. Temperatures indicated on the vertical axis are in degrees celsius.

Figures 12-14) Modeled release spectra for hornblende, muscovite, and biotite, respectively. The release spectra were modeled using the temperature-time history illustrated in Figure 11.





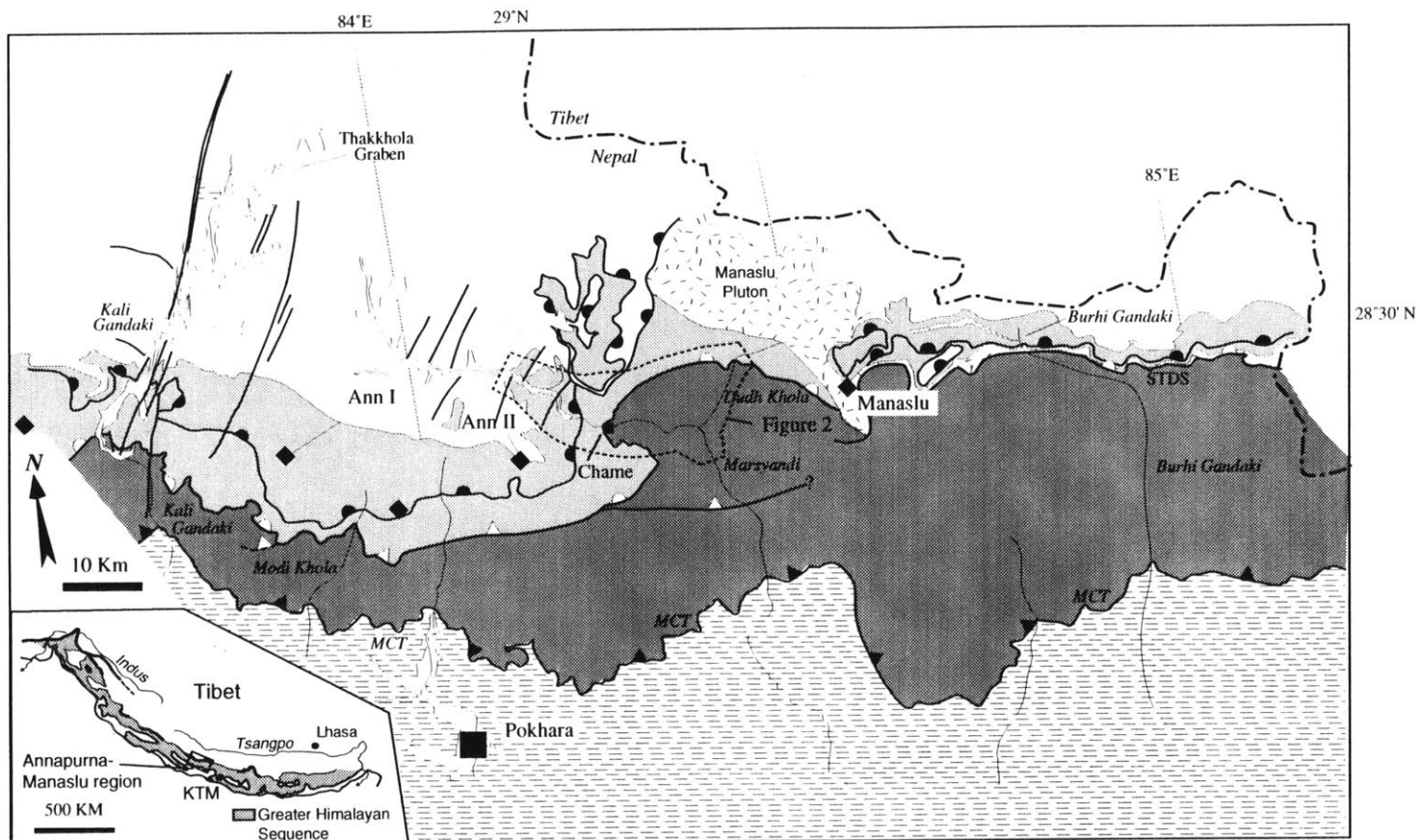
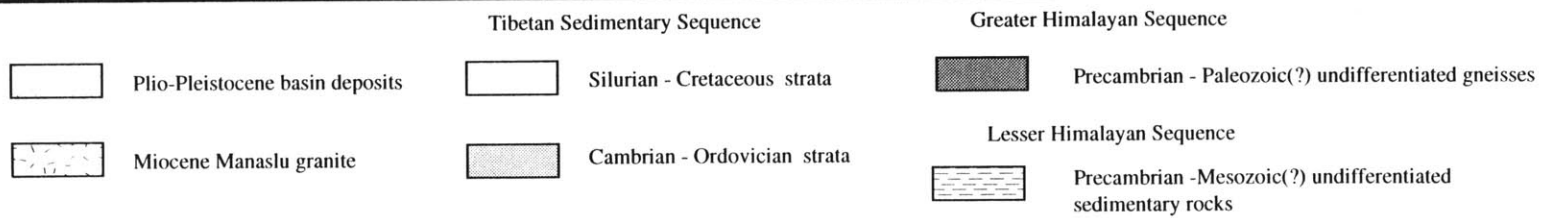


Figure 1





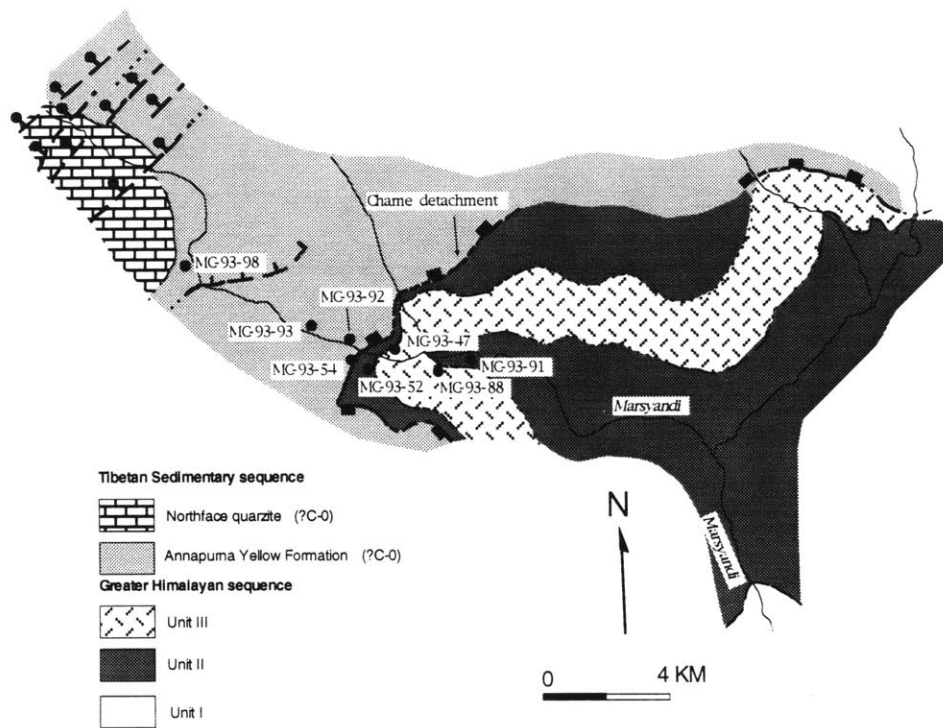


Figure 2



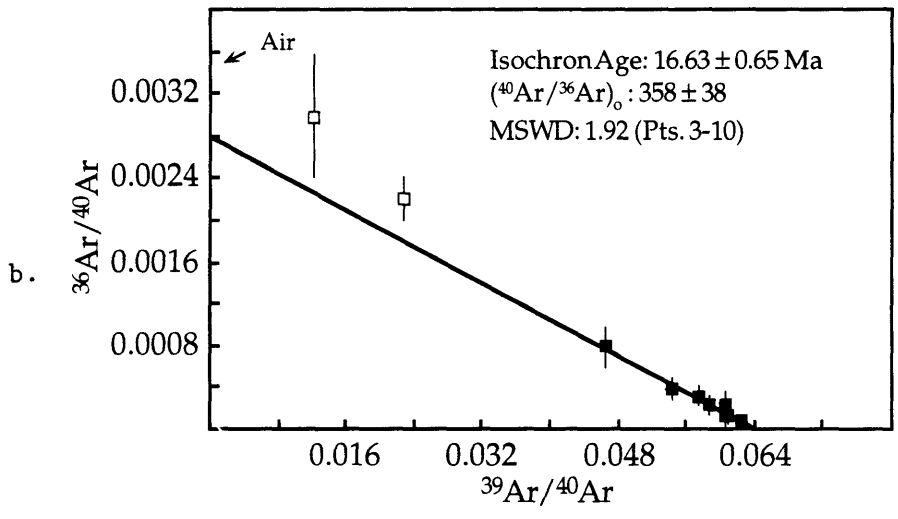
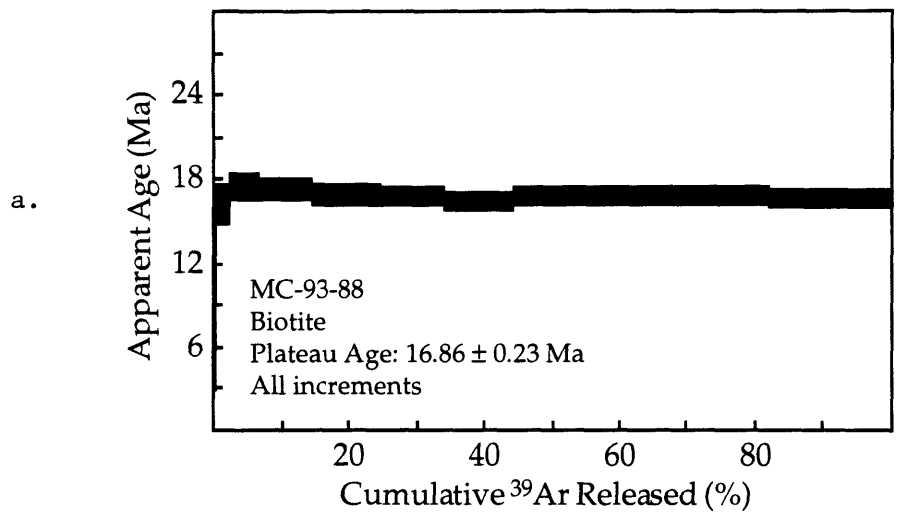


Figure 3.



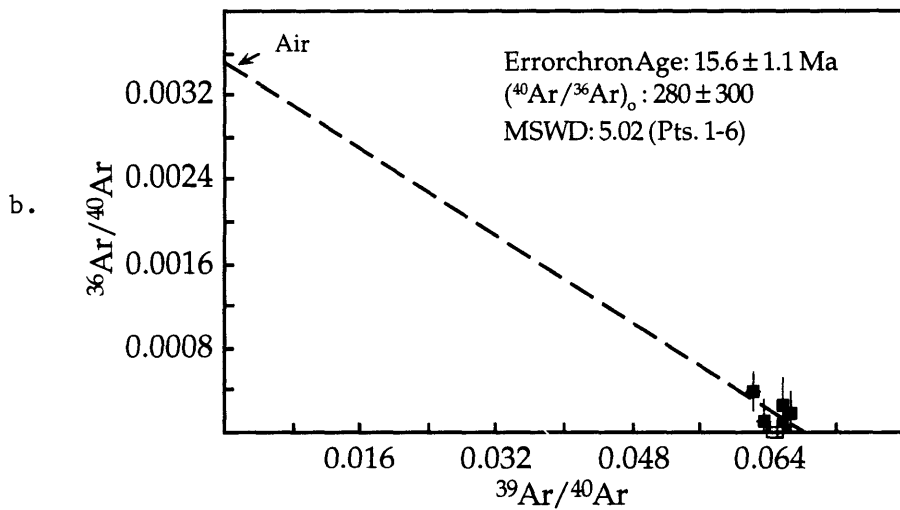
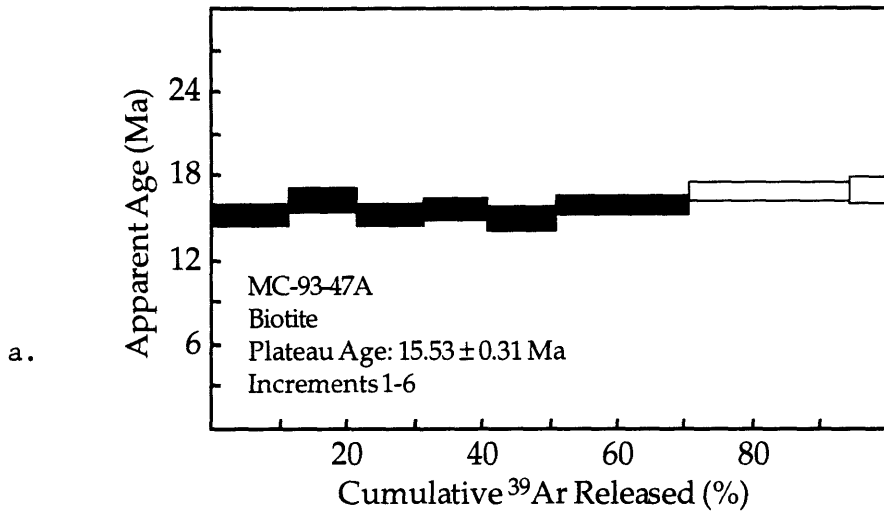


Figure 4





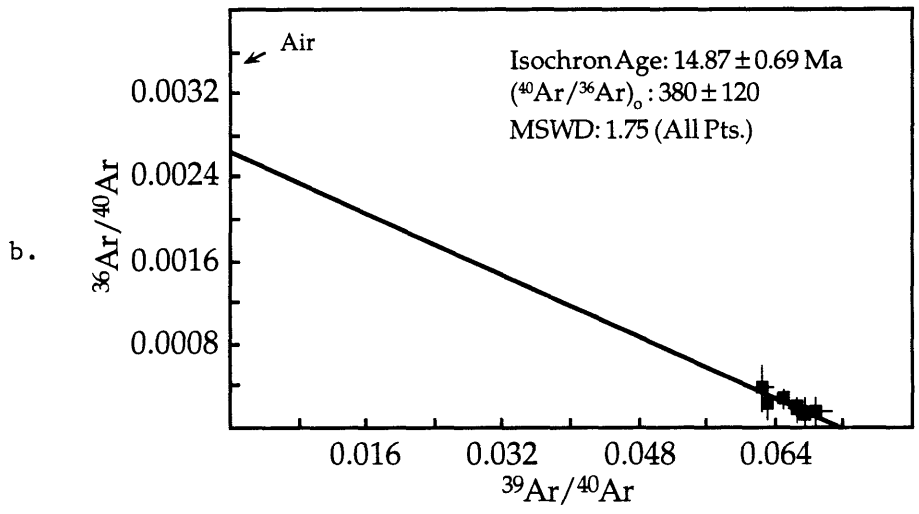
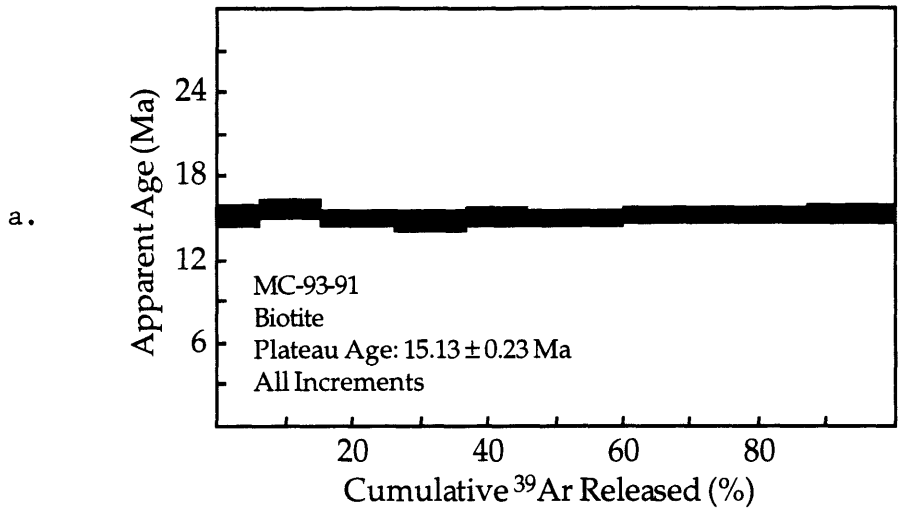


Figure 5



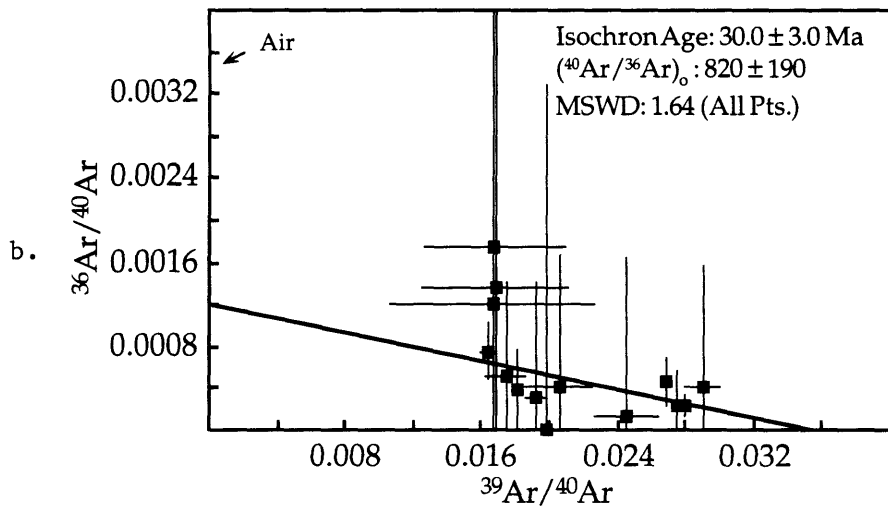
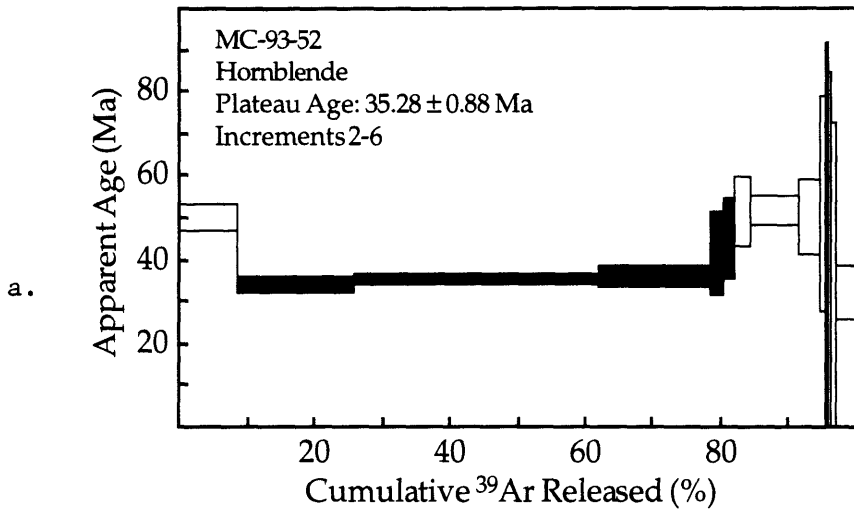


Figure 6



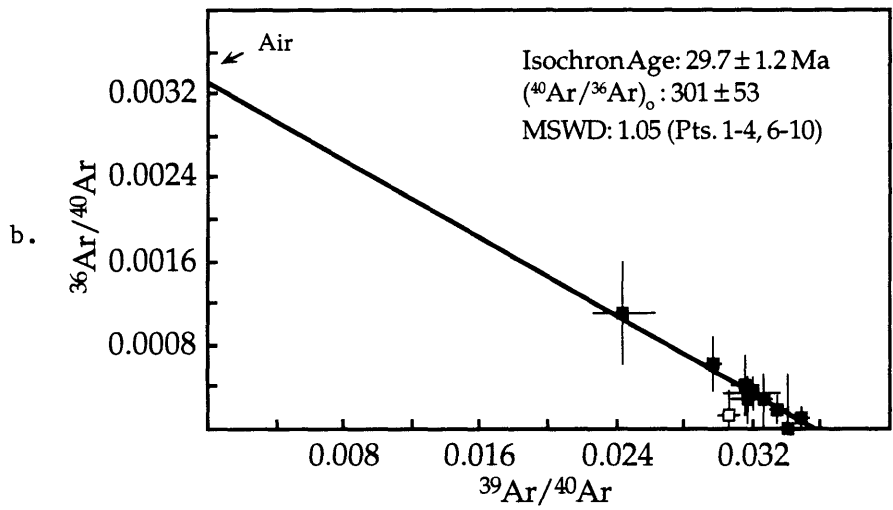
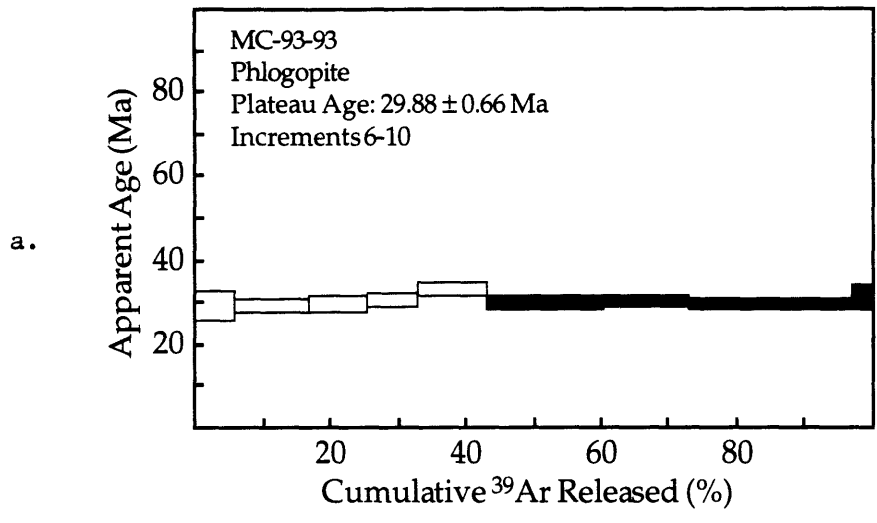


Figure 7



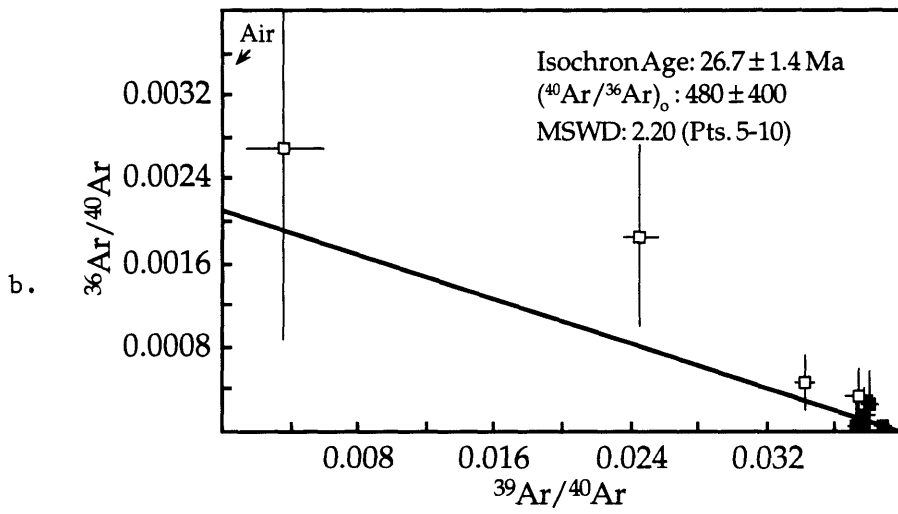
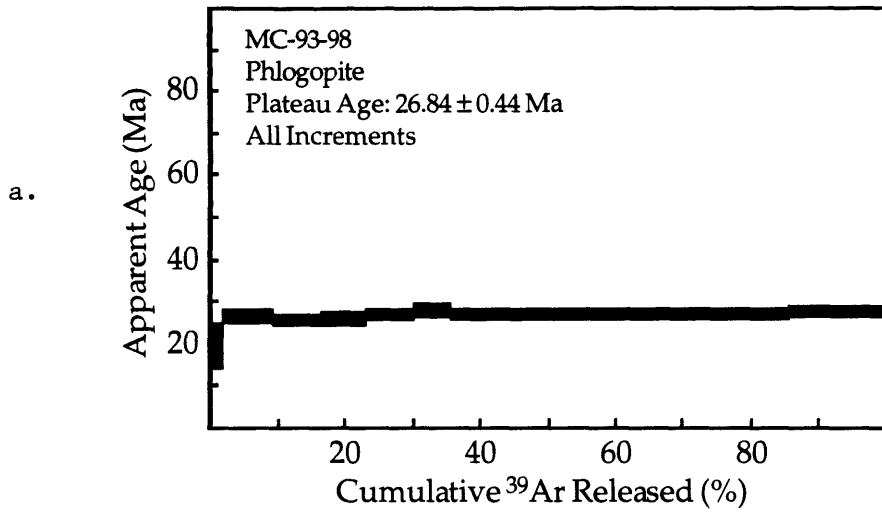


Figure 8





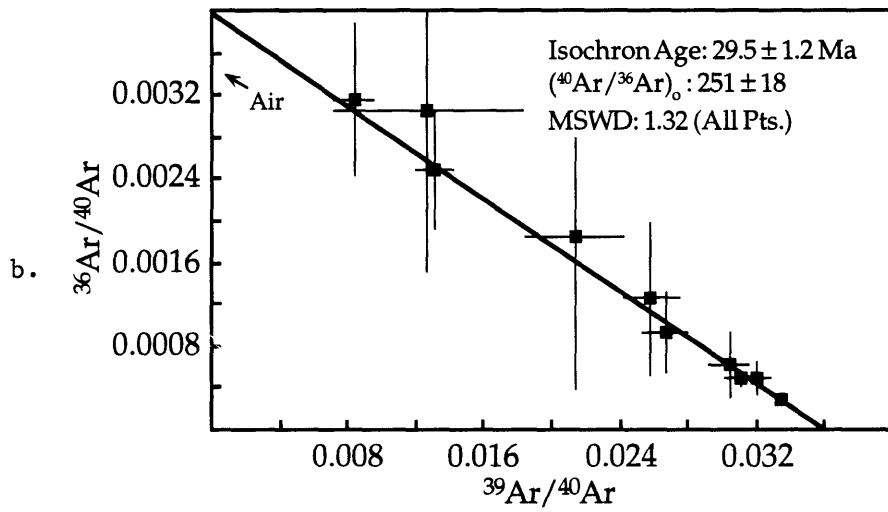
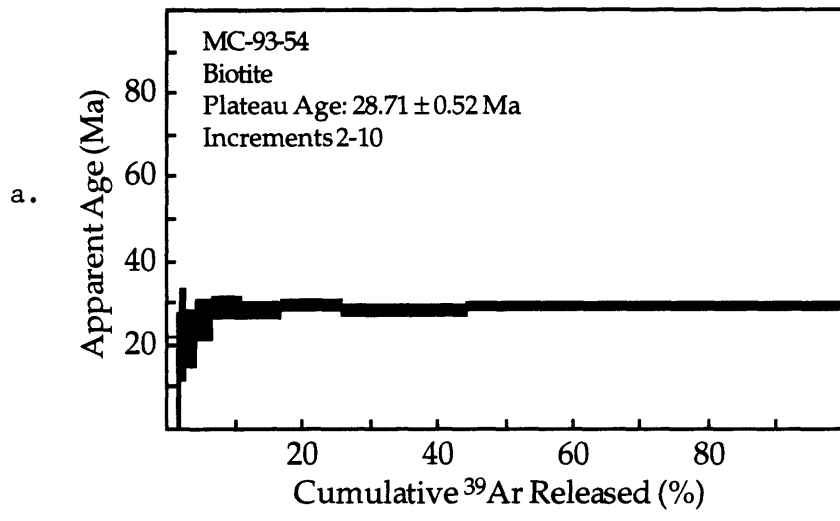


Figure 9



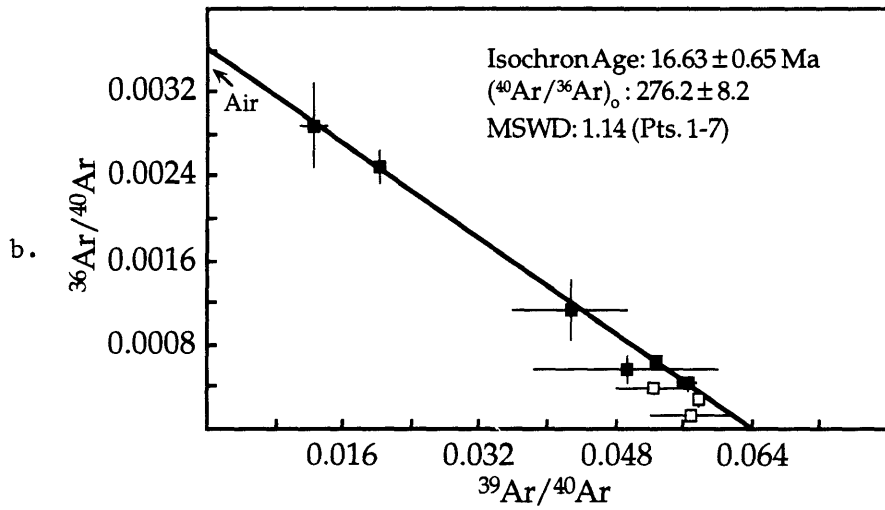
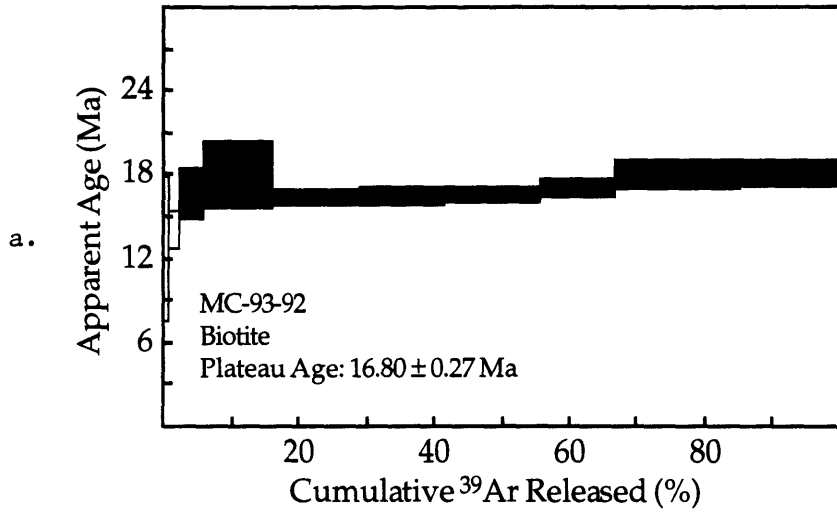


Figure 10



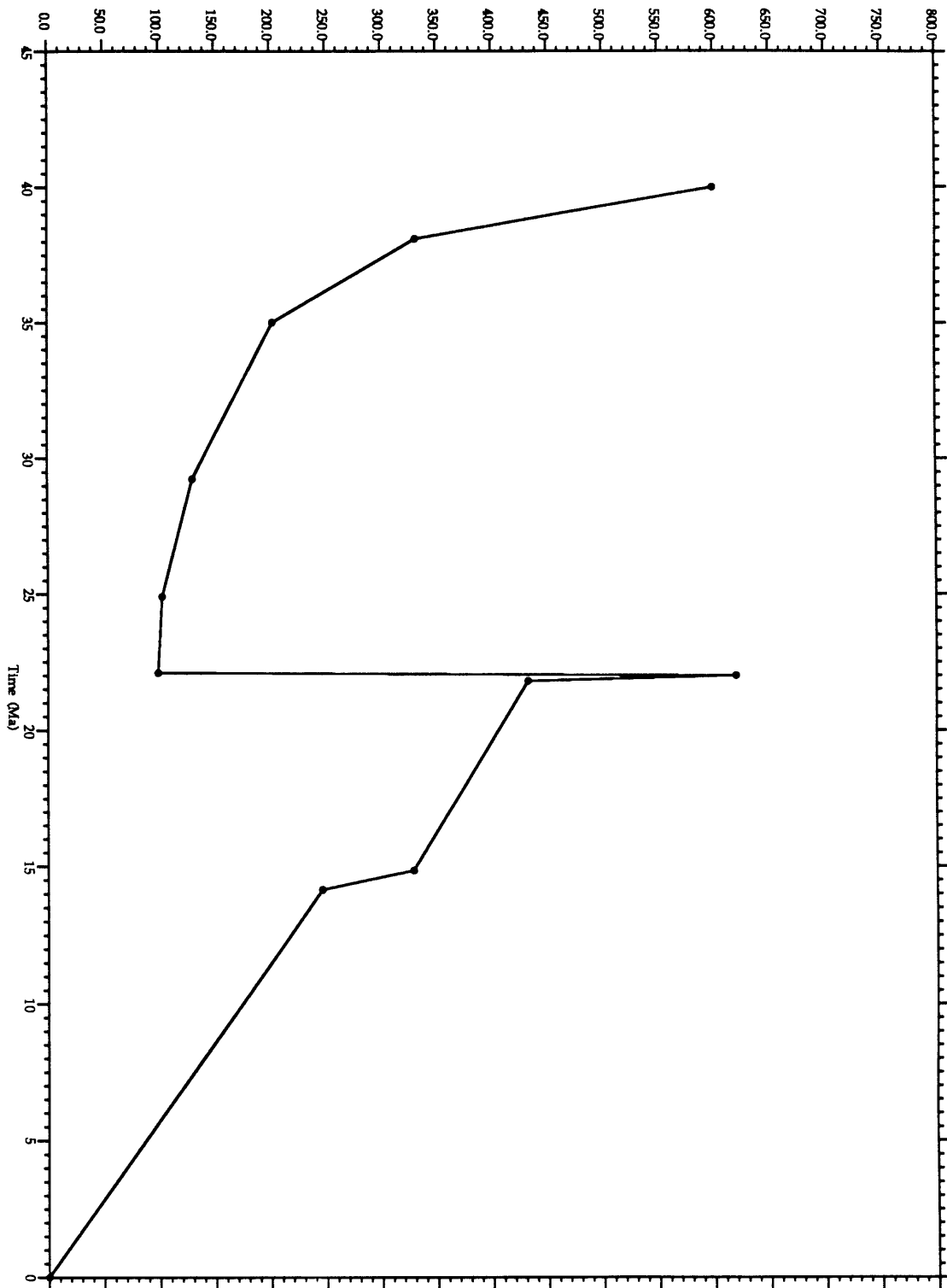


Figure 11



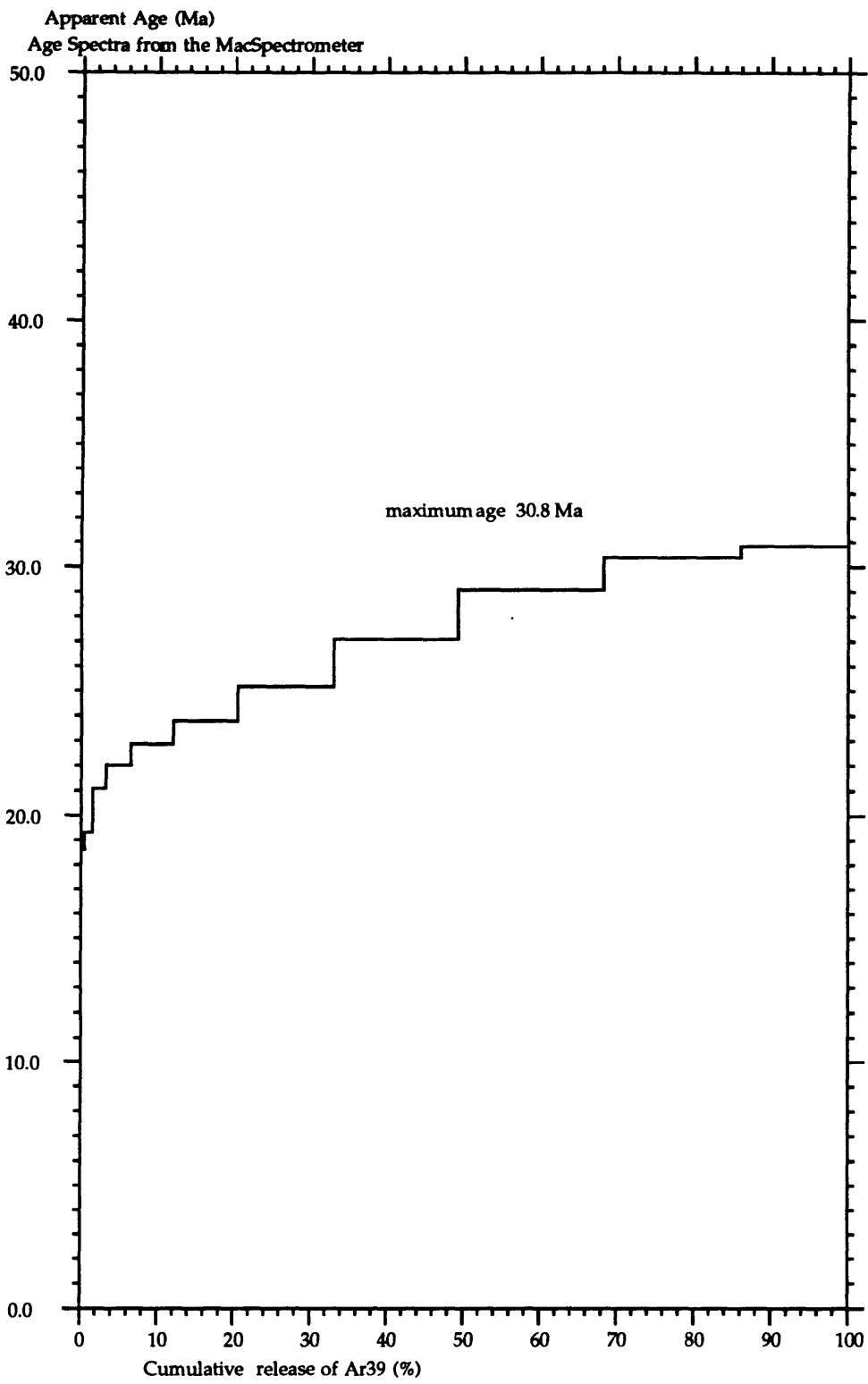


Figure 12





Apparent Age (Ma)  
Age Spectra from the MacSpectrometer

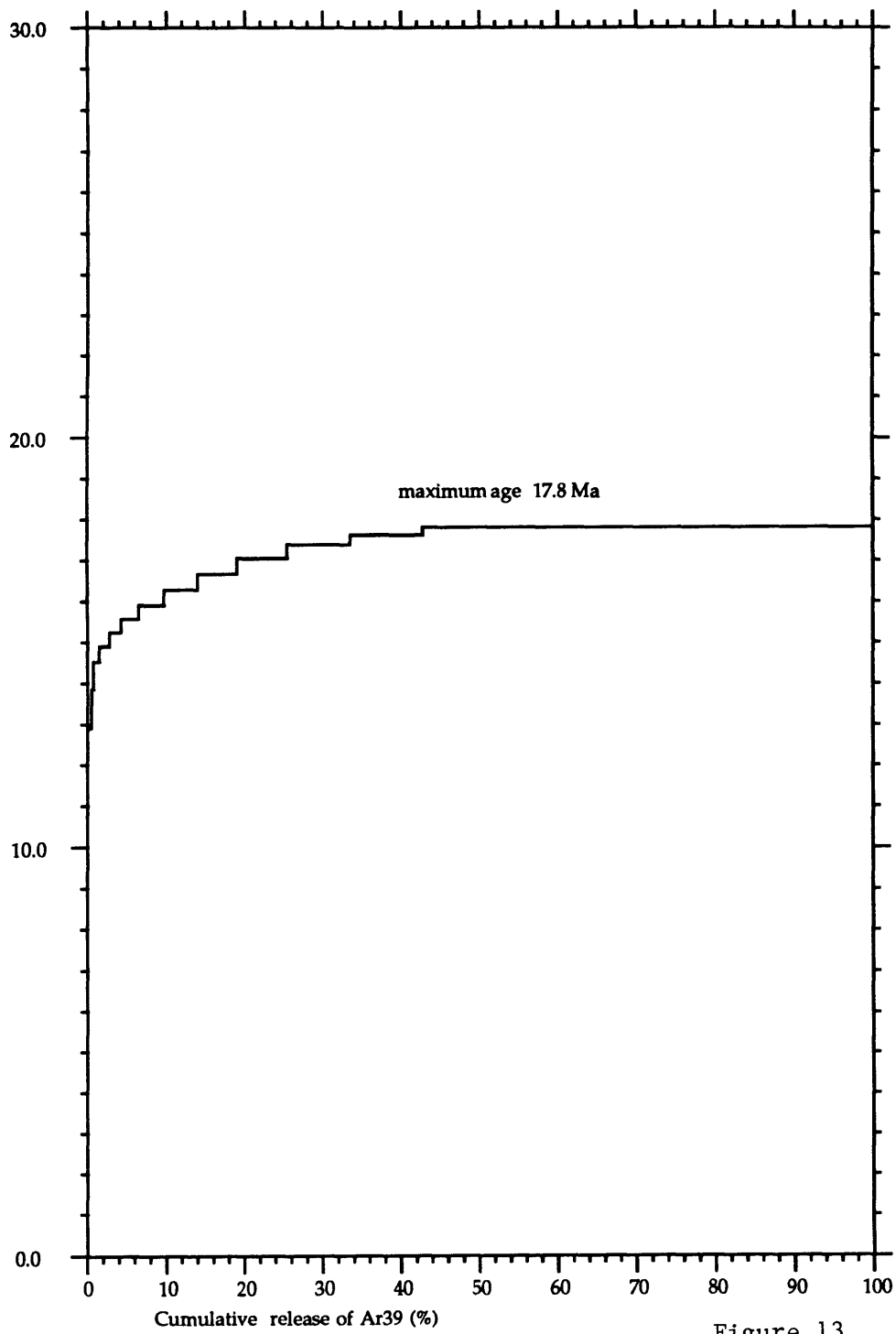


Figure 13



Apparent Age (Ma)  
Age Spectra from the MacSpectrometer

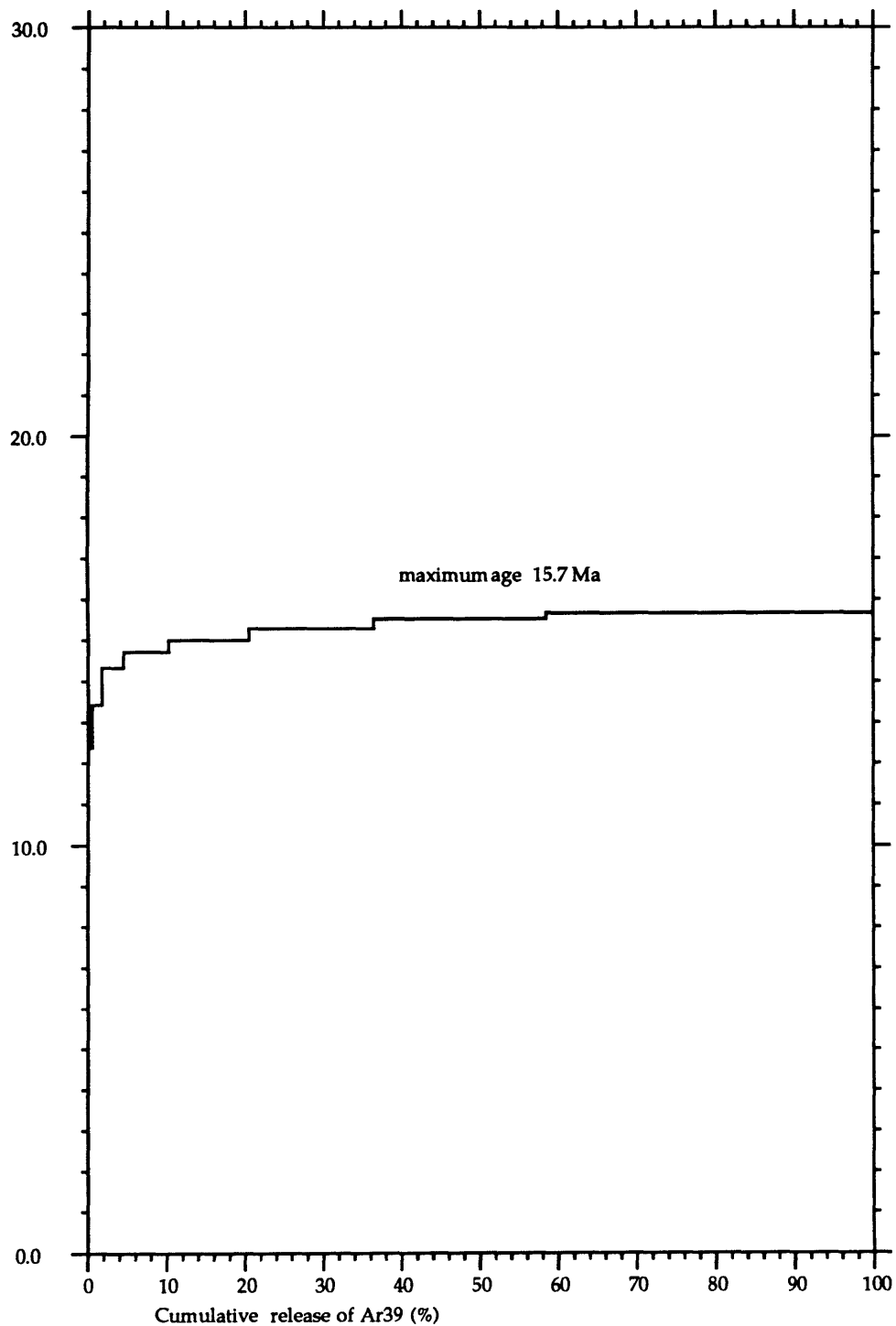


Figure 14



## Chapter 5

### **P-T constraints on metamorphism of the central Greater Himalayan sequence: data from the Marsyandi valley, central Nepal**

#### **Abstract**

The metamorphic core of the Himalaya in the Marsyandi valley of central Nepal is a north dipping section of penetratively deformed schists and gneisses, the Greater Himalayan sequence. The sequence lies above a major south-directed thrust, the MCT, and below a system of north-directed normal faults, the South Tibetan detachment system. The dominant phase of metamorphism ( $M_2$ ) within the sequence produced an inverted metamorphic field gradient. Metamorphic grade increases from kyanite near the MCT to sillimanite + K-feldspar near the South Tibetan detachment system. Thermobarometric results for 9 samples collected over a 16-km-thick section of the Greater Himalayan sequence reflect P-T conditions of 1160-630 MPa and 910-1050K during  $M_2$ . Estimated paleopressures show that the base of the Greater Himalayan sequence was buried to depths in excess of 35 km prior to MCT displacement. Collectively, petrologic data (this study) and geochronologic data (Chapter 3) suggest that  $M_2$  conditions reflect a brief metamorphic event. This phase of metamorphism may have resulted from early Miocene radioactive heating within the tectonically thickened Greater Himalayan sequence.

#### **Introduction**

The metamorphic core of the Himalaya, or Greater Himalayan sequence, comprises a thick section of the middle crust now exposed 1-8 km above sea level. Previous studies from the central Himalaya (Pecher, 1989; Hubbard, 1989; Macfarlane, 1992; Vannay and Hodges, in press) reveal the presence of a steep to inverted metamorphic field gradient within the Greater Himalayan sequence above the basal Main Central Thrust (MCT), a north-dipping, crustal scale thrust fault that is largely syn-metamorphic. The cause of this

thermal structure has been the subject of extensive study and remains controversial (e.g., LeFort, 1975; Pecher, 1989; Hubbard, 1989; Jaupart and Provost, 1985; Molnar and England, 1990).

This paper presents a petrologic and thermobarometric analysis of samples from the Marsyandi valley in central Nepal, which augments a detailed structural and thermochronologic study of the area (Chapters 2, 3, and 4). The Greater Himalayan sequence is a 12 km-thick section of north-dipping amphibolite-facies schists and gneisses (Figure 1). The Main Central Thrust places the Greater Himalayan sequence on the greenschist facies Lesser Himalayan sequence to the south. The Greater Himalayan sequence is roofed by a system of north-dipping normal faults known as the South Tibetan detachment system (Burchfiel et al., 1992). Geochronologic constraints (Chapter 3) demonstrate that the MCT was active in the Marsyandi section sometime between 18 and 22 Ma. Geochronology of both cross-cutting and deformed dikes from the top of the sequence constrain normal displacement on the South Tibetan detachment in this region to the Middle Miocene. The existing timing constraints suggest that thermobarometric techniques can be used to evaluate the conditions of metamorphism within the Greater Himalayan sequence when there was active deformation on the MCT and the South Tibetan detachment.

### **Previous work**

The metamorphic history of the Greater Himalaya in central Nepal has been described as a two-stage process based on textural evidence (see Hodges et al. 1988a, and Pêcher, 1989, for a review of pressure-temperature constraints and tectonic evolution). According to these previous studies, rocks at the base of the Greater Himalayan sequence were buried initially to about 30 km depth during intercontinental subduction, at which time high-pressure, moderate-temperature assemblages equilibrated at the base of the Greater

Himalayan sequence. Following this Barrovian metamorphism ( $M_1$ ), metamorphic conditions changed and were characterized by moderate-pressure, high-temperature metamorphism ( $M_2$ ) during displacement on the MCT. Anatexis within the Greater Himalayan sequence, sillimanite-grade metamorphism, and leucogranite emplacement are all thought to be signatures of the second phase of metamorphism.

One of the first quantitative studies of metamorphism in the Nepalese Himalaya was that of Hubbard (1989), who used thermobarometry to define an inverted metamorphic gradient in the Everest region of eastern Nepal. Metamorphic temperatures increased from approximately 770K about 2 km below the kyanite isograd, at the MCT, to approximately 975K about 5 km above the isograd. Hubbard and Harrison (1989) obtained a  $\sim 21$  Ma  $^{40}\text{Ar}/^{39}\text{Ar}$  age for hornblende that grew within the MCT fabric during thrusting. Pêcher (1978) estimated high-pressure metamorphism at the base of the Greater Himalayan sequence in central Nepal to have occurred at 870-960K and 700-850 MPa based on a simplified petrogenetic grid. Petrogenetic and thermobarometric constraints on the Greater Himalayan sequence in the Burhi Gandaki drainage (Figure 1) record an isothermal temperature structure of about 900K with pressures decreasing monotonically up-section, consistent with a normal lithostatic pressure gradient (Hodges et al., 1988b). The MCT-zone in the Marsyandi and Burhi Gandaki valleys has been described in detail by Pêcher (1977, 1989), who documented south-directed ductile shear-sense indicators that formed synchronously with the main foliation and kyanite-grade metamorphism. One of the goals of my work was to quantify metamorphic P-T conditions during thrusting and normal faulting as a constraint on relationships between the deformational and thermal evolution of this sector of the Himalaya.

### **Sampling strategies**

Nine metapelitic samples were chosen from the Marsyandi transect for thermobarometry (see Figures 1 and 2 for sample localities). Rocks with low variance assemblages, apparent textural equilibrium, and very minor or no retrogression were selected preferentially. There are three main groups of samples based on structural position. They span a 12 km section of the Greater Himalayan sequence (Figure 2). Group I (MC2, MC3, and MCT-1) includes kyanite-grade samples collected from immediately below, within, and above the Main Central Thrust zone at the base of the Greater Himalayan sequence. Group II samples (MC4, MC18, MC19, MC5, and MC7) come from a wide zone in the middle of the Greater Himalayan sequence, it includes samples at kyanite + sillimanite grade in the lower section and samples at second sillimanite grade in the upper section. Group III is represented by sample MC36 from the upper Greater Himalayan sequence, about 2 km beneath the Chame detachment. The sample descriptions below synthesize observations from field work, hand-sample, and thin-section analysis. Fabric nomenclature such as  $S_1$ ,  $S_2$ , etc., follows Chapter 2.

### Group I

Samples MC2 and MCT-1 are both mylonites from the MCT zone that preserve spectacular S-C fabrics indicative of top-to-the-south shear. Sample MC2 contains muscovite (25%), biotite (20%), plagioclase (20%), quartz (20%), garnet(5%), staurolite (5%), and chlorite (5%). Garnet growth was syn-kinematic with respect to  $S_2$  MCT-mylonitic fabric. Garnet porphyroblasts range from 0.1 cm to 1.5 cm in diameter. Biotite, muscovite, and staurolite help define the  $S_2$  foliation. Minor retrograde chlorite is intergrown with biotite and partially rims garnet. Sample MCT-1 is a migmatitic schist with roughly 5-10% leucogranitic leucosome. Schistose layers contain quartz (30%), plagioclase (30%), biotite (20%), muscovite (10%), garnet(5%), kyanite(3%), and staurolite (2%). MCT-1 displays mylonitic textures similar to those in MC2, with the



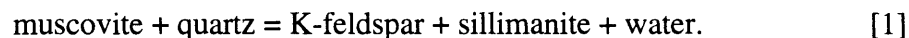
addition of large euhedral blades of kyanite (up to 3 cm-long) which are aligned within the  $S_2$  foliation. In some examples, kyanite blades are folded and deformed by  $D_2$  shear bands and foliation, indicating that kyanite growth is both pre and syn-kinematic with  $S_2$  fabric development. Garnets, 0.1-5.0 cm in diameter. Commonly have inclusion-rich cores with distinct inclusion-free rims.

## Group II

Sample MC3, collected about 1 km above the MCT-mylonite zone, is a medium-grained schist interlayered with ~30% leucogranitic stringers. The schist contains biotite (30%), plagioclase (25%), quartz (25%), muscovite (10%), garnet (3%), and kyanite (5%). Biotite, muscovite, and kyanite are aligned with  $S_1$ .

Sample MC4 is a pelitic schist, collected about 5 km above the base of the MCT. It contains quartz (35%), plagioclase (30%), biotite (25%), garnet (2%), kyanite (5%), and sillimanite (3%).  $S_1$  foliation is defined by the preferred orientation of biotite. Euhedral kyanite is aligned within the  $S_1$  foliation, and fibrolitic sillimanite mats are intergrown with biotite, and appear to be syn to post-kinematic with respect to  $S_1$ .

Samples MC18 and MC19 are pelitic gneisses that contain plagioclase (~25%), muscovite (~20%), quartz (~20%), biotite (~15%), sillimanite (~10%), garnet (~5%), and K-feldspar (~5%). K-feldspar is present only as perthitic intergrowths within plagioclase. Muscovite is embayed and intergrown with sillimanite, indicating that the rock quenched during the muscovite breakdown reaction:



Both samples exhibit  $D_2$  S-C fabric and indicate localized zone of high-strain.

Samples MC5 and MC7 are felsic gneisses that contain plagioclase (25%), quartz (25%), K-feldspar (15%), biotite (15%), sillimanite (10%), garnet (5%), and muscovite (5%). Feldspar and quartz grains are annealed, and K-feldspar occurs not only as

microperthitic intergrowths within plagioclase but also as part of the matrix assemblage. Muscovite appears as remnant, partially resorbed blades, intergrown with fibrolitic sillimanite mats. It appears that the muscovite breakdown reaction [1] progressed more in these samples than in MC18 and MC19. Sample MC7 garnets are 1-2 mm in diameter, euhedral to slightly rounded, and have distinct inclusion-rich cores. Sample MC5 garnets are 3-5 mm in diameter, filled with inclusions, and partially resorbed.

### Group III

Sample MC36 is a layered gneiss with alternating leucocratic layers and pelitic schistose layers. In outcrop, the rock displays top-to-the west  $D_2$  shear-sense indicators related to the Chame detachment (Chapter 2). The pelitic layers contain plagioclase (25%), K-feldspar (20%), biotite (20%), quartz (20%), muscovite (10%), sillimanite (5%), and garnet (~1%). Garnet is partially resorbed and embayed. K-feldspar displays microcline twinning with microperthitic albite lamellae. Felsic layers are largely annealed with randomly oriented feldspar and biotite. Muscovite is partially overgrown by sillimanite indicating that the rocks were quenched during Reaction [1].

### **Mineral rim thermobarometry**

The assemblage  $\text{Grt}+\text{Bt}+\text{Pl}+\text{Qtz}\pm\text{Ky}\pm\text{Sil}\pm\text{Ms}$  in metamorphic pelitic rocks of the Marsyandi section allow application of several, well-calibrated thermobarometers (Table 1). The Marsyandi results reported here are based on the thermobarometric calibrations recommended by Hodges and McKenna (1987) for GARB, McKenna and Hodges (1988) for GASP, and Applegate and Hodges (1994) for GMAP. Non-ideal solution behavior was modeled using the approaches of Chatterjee and Froese (1975), Berman (1990), Elkins and Grove (1990), and Patiño-Douce et al. (1993) for muscovite, garnet, plagioclase, and biotite respectively. Sillimanite, kyanite, and quartz were treated as pure phases.

### Analytical approach

Before discussing the details of the analytical procedures, it is important to explain the philosophy behind them. The study was designed to estimate the P-T conditions at which the major phases in each sample equilibrated for the last time. This does not necessarily mean peak metamorphic conditions. In order to obtain the final P-T conditions, we use rim compositions of the relevant phases (preferably in contact with each other) for thermobarometric calculations. This procedure follows the approach of Hodges and McKenna (1987), such that each rim composition in Table X represents the average of 5-10 spot measurements from at least one domain in each microprobe section. The approach differs slightly from Hodges and McKenna (1987) in that previously obtained element maps (WDS mapping explained below) negated the necessity to probe more than one domain in most of the thin section. Uncertainties in oxide weight percentages were propagated through thermobarometric calculation using a Monte Carlo approach (see Hodges and McKenna, 1987). For further details of the error propagation techniques, see Hodges et al. (1994).

### Analytical Procedure

Prior to acquiring quantitative compositional data for rim thermobarometry, preliminary WDS element-mapping was carried out at the University of Massachusetts using the Cameca SX-50 electron microprobe. At least one 5 x5 mm area was mapped in each sample. These domains contained garnet  $\geq 1$  mm in diameter in contact with biotite, plagioclase,  $\pm$  muscovite. Images for Mg, Ca, Mn, and Na were used for selecting areas suitable for quantitative analyses. Element maps indicated very minor chemical zoning within garnets. We attribute this to high-temperature diffusive reequilibration, which prevents inverse modeling of garnet zoning (e.g., Spear and Selverstone, 1983). Compositions for quantitative rim thermobarometry were measured using the JEOL 733

electron microprobe at MIT with a nominal beam current of 10 nA and an accelerating voltage of 15 kV. They are reported in Table 2.

### Results and interpretation

Rim thermobarometric data with nominal precision limits are presented in Table 3, and uncertainty ellipses obtained through the simultaneous solution of GARB - GASP and/or GARB - GMAP are shown in Figures 3-5. Whenever possible, both pairs of equilibria were applied to each sample.

#### *Group I*

Results from Group I samples (Figure 3) agree well with phase equilibrium constraints on metamorphic conditions. The kyanite-bearing samples MCT-1 and MC3 both plot in the kyanite stability field. Sample MC2 does not contain an aluminum-silicate; however, application of GARB-GMAP results in a P-T ellipse in close agreement with MC96 and MC3. The results from all three samples plot above the nominal, water-saturated, minimum melt curve for pelitic compositions (curve A in Figure 3A; Thompson, 1982) which is consistent with the observation that both samples MC96 and MC3 contain abundant melt layers.

Group I P-T are in the range 1040-1160 MPa at 910-950 K. The three samples are distributed over a 3 km-thick section, and pressures show a gradual increase toward the lowermost sample as expected. These results most likely give accurate determinations of P-T conditions during final equilibration at the base of the Greater Himalayan sequence. Textures within the Group I samples suggest that kyanite, biotite, quartz, and feldspar grew during the development of D2 mylonitic fabrics within the MCT-zone. In addition, garnets in sample MC96 have optically distinct inclusion-rich cores surrounded by inclusion free rims. The garnet rims probably grew synchronously with D<sub>2</sub>. Because these samples may

have continued to equilibrate after mylonitization, the Group I thermobarometric data are interpreted as providing a minimum estimate of P-T conditions during D2.

### *Group II*

Pressure-temperature results from sample MC4, the lowermost sample from Group II, plot within the kyanite stability field. As previously mentioned, this sample contains both euhedral kyanite and fibrolitic sillimanite. However, both GARB-GASP and GARB-GMAP solutions show close agreement within the kyanite field, indicating that kyanite was most likely the phase in equilibrium with the other relevant phases. Results from MC4 yield a P-T estimate of  $720 \pm 100$  MPa and  $880 \pm 40$  K.

Sample MC7, highest of the Group II samples, did not contain muscovite in contact with garnet within the thin section used for analysis. Where muscovite was observed, it appeared only as remnant, partially resorbed blades. Sillimanite is ubiquitous throughout the sample, however, we relied on GARB-GASP for our P-T determination. The results plot within the sillimanite stability field, to the right of the muscovite breakdown curve and consistent with all phase equilibrium constraints. A pressure and temperature of  $860 \pm 60$  MPa at  $1050 \pm 40$  K implies a deeper structural level for MC7 than the rest of the Group II samples, suggesting either that the rest of the Group II samples did not equilibrate at the same time as MC-7, or that there is an unidentified post peak metamorphic fault between MC7 and the lower samples.

Group II samples are distributed over a 4 km- thick section of the Greater Himalayan sequence and P-T results agree with phase equilibrium constraints for samples from the base and top of this sub- section (MC4 and MC7). However, the middle samples (MC18, MC19, and MC5) plot in the kyanite stability field if GARB-GASP is applied, despite the fact that fibrolitic sillimanite was the only aluminum-silicate polymorph observed. Application of GARB-GMAP to the same samples yields P-T results that

overlap the kyanite-sillimanite divariant curve (Figure 4) as well as the muscovite breakdown reaction [1] (curve B in Figure 3; Thompson and Tracy, 1979; Thompson, 1982). Although there is no longer any kyanite present in the middle Group II samples, they were collected not far above sample MC4 which contains both kyanite and fibrolitic sillimanite. Agreement between phase equilibrium constraints and the results obtained from applying GARB-GMAP provides strong evidence that sillimanite was not in equilibrium with the other thermobarometric phases, and indicates that GARB-GMAP result are the best estimates for P-T conditions during D2 from the middle samples. GARB-GMAP P-T results from samples MC18, MC19, and MC5#1, and MC5#2, yield internally consistent pressures and temperatures of 750-780 MPa and 970-1010 K.

### *Group III*

Group III consisted of a single sillimanite-bearing sample (MC36) from the upper Greater Himalayan sequence. Initial application of both GARB-GASP and GARB-GMAP resulted in P-T ellipses that did not overlap and gave very different pressures but similar temperatures. The GARB-GASP solution plotted in the kyanite stability field even though sillimanite was assumed to be the stable polymorph in the simultaneous solution. The explanation for the erroneous P-T ellipse using GARB-GASP is most likely due to chemical disequilibrium between the GARB and GASP phases. Results from GARB-GMAP are plotted in figure 3 ( $630 \pm 80$  MPa at  $870 \pm 40$  K). The indicated pressure also appears to be slightly high because the ellipse sits on the kyanite side of the kyanite-sillimanite divariant curve despite the fact that sillimanite is the only aluminum silicate polymorph found at this structural level. The temperature obtained from GARB is somewhat lower than the temperature indicated from reaction textures within the sample (900K approximate # from petrogenetic grid). The temperature obtained most likely indicates final equilibration of the GARB exchange thermometer after the rock had cooled

from peak metamorphic conditions, and we consider 900K a minimum estimate of temperature during  $D_2$  at this structural level.

### **Timing constraints on metamorphism**

Geochronologic timing constraints for metamorphism and anatexis within Greater Himalayan sequence are summarized below; for more detail see Chapter 3. Metamorphic monazites from the MCT zone (sample MCT-1) have single grain U-Pb ages that span 18 to 22 Ma, indicating growth of monazite during kyanite-grade metamorphism and  $D_2$  deformation at 22 Ma, possibly continuing to 18 Ma. From the upper 3 km of the Greater Himalayan sequence, monazite ages from leucogranitic horizons within MC36 indicate migmatization at  $\leq 22$  Ma, and an earlier metamorphic or igneous event at about 35 Ma. An undeformed leucogranite dike that cuts across foliation at the top of the Greater Himalayan sequence yields both monazite and zircon ages of 18.5 Ma, and provides an upper limit to the age of  $D_2$  at high structural levels.

### **Discussion**

Thermobarometric data from the Marsyandi section appear to be reliable with a few exceptions. P-T data from Group I are the most reliable and hold up under three tests for assessing equilibrium: (1) data are consistent between samples, (2) P-T is consistent within samples when more than one thermobarometer was used, and (3) the results are supported by phase equilibrium constraints. Some of the Group II samples (MC18, MC19, and MC 5) fail the second test, GARB-GMAP results appear to be reliable in all cases. The least reliable thermobarometric data are from sample MC36. In this case, the thermobarometric data are inconsistent with the phase equilibria. However, there is good petrographic evidence that the sample reached final equilibration during reaction [1], which is a minimum temperature constraint of  $\sim 900$ K.

Thermobarometric data, combined with phase equilibrium constraints, indicate that M<sub>2</sub> was characterized by a steep to inverted geothermal gradient over a thickness in excess of 15 km within the Greater Himalayan sequence. The only obvious evidence of M<sub>1</sub> within these rocks are the inclusion-rich cores within some of the garnets. The absence of chemical zoning within the garnets indicates essentially total re-equilibration during M<sub>2</sub>. Temperatures within the lower 5 km of the Greater Himalayan sequence during final equilibration were in the kyanite stability field at granite-minimum-melt conditions. The upper 10 km were at temperatures of at least 900K, at or very close to second-sillimanite melting conditions. Geochronologic data indicate that temperatures in excess of 900K were reached throughout most of the Greater Himalayan sequence at roughly the same time (18-22 Ma).

Group I samples record higher pressures than the rest of the Greater Himalayan sequence, which is consistent with their structural position. Pressures of 1160 MPa immediately below the MCT zone indicates burial in excess of 35 km during kyanite-grade mylonitization. The structurally highest Group II sample (MC4) records a higher pressure than the samples beneath, possibly indicating a post-metamorphic fault. However, given the possibility of disequilibrium within some of the Group II samples, we are hesitant to invoke structures in the absence of compelling structural data.

The thermobarometric data from the Marsyandi transect are broadly consistent with previous studies from the central Himalaya (Hodges et al., 1988a; Hubbard, 1989; Macfarlane, 1992; Vannay and Hodges; in press), which all demonstrate that M<sub>2</sub> was characterized by a steep to inverted geothermal gradient throughout the Greater Himalayan sequence. Explanations for this unusual thermal structure are widely debated, and simple models that invoke thrusting of hot rocks over cold rocks do not adequately explain it (e.g. LeFort, 1975; England and Thompson, 1986). The possibility of other factors affecting the



thermal structure including thermal buffering (Hodges et al., 1988b), frictional heating (Molnar and England, 1990), and thermal blanketing (Jaupart and Provost, 1985), have all been discussed extensively in the literature but fall short of reproducing the pattern observed in the actual data. However, a recently developed numerical model (Huerta et al., in press) demonstrates that an inverted geotherm can be produced within an accretionary wedge of material that is enriched in radioactive elements, assuming geologically reasonable rates of accretion and erosion. Huerta et al. (in press) present a strong case for the redistribution of highly radiogenic material within the Himalayan orogen having been a critical factor in producing a steep geotherm during intercontinental subduction.

## **Conclusions**

Microfabric observations allow for two phases of metamorphism ( $M_1$  and  $M_2$ ) within the metamorphic core of the Himalaya in the Marsyandi region. However,  $M_2$  has largely obscured  $M_1$  and the thermobarometric results pertain only to  $M_2$ . Thermobarometry, petrography, and U-Pb geochronology show that  $M_2$  produced temperatures of at least 900K throughout the whole thickness of the Greater Himalayan sequence by about 22 Ma. Since all porphyroblast phases are either synchronous with or predate  $S_2$  fabric development, the age of leucogranite that cross cuts  $S_2$  foliation indicates that  $M_2$  was over by 18 Ma.

The timing of final metamorphic equilibration within the Greater Himalayan sequence is interpreted to be roughly synchronous with major displacement on the MCT and the South Tibetan detachment. Broadly coeval thrust faulting and tectonic denudation at the base and roof of the metamorphic core were probably important factors in cooling the rocks quickly enough to preserve a steep metamorphic field gradient. The Miocene thermal structure within the Marsyandi section is consistent with the predicted results from numerical modeling of an intercontinental subduction zone with similar accretion and

erosion rates as the central Himalaya (Huerta et al., in press). In this model, enough radiogenic heat is produced within the accreted wedge of continental material to produce an inverted geotherm with temperatures in excess of 900K.

## References

- Applegate, J.D.R., and K.V. Hodges. 1994. Empirical evaluation of solution models for pelitic minerals and their application to thermobarometry. *Contributions to Mineralogy and Petrology* **117**, 56-65.
- Berman, R.G. 1990. Mixing properties of Ca-Mg-Fe-Mn garnets. *American Mineralogist* **75**, 328-344.
- Chatterjee, N.D., and E. Froese. 1975. A thermodynamic study of the pseudobinary join muscovite–paragonite in the system  $\text{KAlSi}_2\text{O}_8\text{--Al}_2\text{O}_3\text{--SiO}_2\text{--H}_2\text{O}$ . *American Mineralogist* **60**, 985-993.
- Elkins, L.T., and T.L. Grove. 1990. Ternary feldspar experiments and thermodynamic models. *American Mineralogist* **75**, 544-559.
- England, P.C., and A.B. Thompson. 1986. Some thermal and tectonic models for crustal melting in continental collision zones. In *Collision Tectonics*. (Edited by M. P. Coward and A. C. Ries). Blackwell Oxford: 83-94.
- Ferry, J.M., and F.S. Spear. 1978. Experimental calibration of the partitioning of Fe and Mg between biotite and garnet. *Contrib. Mineral. Petrol.* **66**, 113-117.
- Ghent, E.D. 1976. Plagioclase-garnet- $\text{Al}_2\text{SiO}_2$ -quartz: a potential geobarometer-geothermometer. *American Mineralogist* **61**, 710-714.
- Ghent, E.D., and M.Z. Stout. 1981. Geobarometry and geothermometry of plagioclase-biotite-garnet-muscovite assemblages. *Contrib. Mineral. Petrol.* **76**, 92-97.
- Hodges, K.V., B.C. Burchfiel, L.H. Royden, Z. Chen, and Y. Liu. 1994. The metamorphic signature of contemporaneous extension and shortening in the central Himalayan orogen: Data from the Nyalam transect, southern Tibet. *Journal of Metamorphic Geology*
- Hodges, K.V., Mary S. Hubbard, and D.S. Silverberg. 1988. Metamorphic constraints on the thermal evolution of the central Himalayan Orogen. *Phil. Trans. R. Soc. Lond. A* **326**, 257-280.
- Hodges, K.V., P. LeFort, and A. Pêcher. 1988. Possible thermal buffering by crustal anatexis in collisional orogens: Thermobarometric evidence from the Nepalese Himalaya. *Geology* **16**, 707-710.
- Hodges, K.V., and L.W. McKenna. 1987. Realistic propagation of uncertainties in geologic thermobarometry. *American Mineralogist* **72**, 671-680.

- Hodges, K.V., and F.S. Spear. 1981. Geothermometry, geobarometry, garnet closure temperatures, and the  $\text{Al}_2\text{SiO}_5$  triple point, Mt. Moosilauke N.H. *EOS* **62**, 1060.
- Hubbard, M., L. Royden, and K. Hodges. 1991. Constraints on unroofing rates in the High Himalaya, Eastern Nepal. *Tectonics* **10**, 287-298.
- Hubbard, M.S. 1989. Thermobarometric constraints on the thermal history of the Main Central Thrust Zone and Tibetan Slab, eastern Nepal Himalaya. *J. Metamorphic Geol.* **7**, 19-30.
- Huerta, A. D., L. H. Royden, and K. V. Hodges. in press. The Interdependence of Deformational and Thermal Processes in Mountain Belts. *Science*
- Jaupart, C., and A. Provost. 1985. Heat focussing, granite genesis, and inverted metamorphic gradients in continental collision zones. *Earth Planet. Sci. Lett.* **73**, 385-397.
- LeFort, P. 1975. Himalaya: the collided range. Present knowledge of the continental arc. *Am. J. Sci.* **275-A**, 1-44.
- Macfarlane, A.M. 1992. The Tectonic Evolution of the Core of the Himalaya, Langtang National Park, Central Nepal. Ph.D., *Massachusetts Institute of Technology*.
- McKenna, L.W., and K.V. Hodges. 1988. Accuracy versus precision in locating reaction boundaries: Implications for the garnet-plagioclase-aluminum silicate-quartz geobarometer. *American Mineralogist* **73**, 1205-1208.
- Molnar, P., and P. England. 1990. Temperatures, heat flux, and frictional stress near major thrust faults. *J. Geophys. Res.* **95**, 4833-4856.
- Patiño-Douce, A. E., A. D. Johnston, and J. M. Rice. 1993. Octahedral excess mixing properties in biotite: A working model with applications to geobarometry and geothermometry. *American Mineralogist* **78**, 113—131.
- Pêcher, A. 1977. Geology of the Nepal Himalaya: Deformation and petrography in the Main Central thrust zone. In *Himalaya: Sciences de la Terre*. C.N.R.S. Paris: 301-318.
- Pêcher, A. 1978. Deformations et métamorphisme associées à une zone de cisaillement: Exemple du grand chevauchement central Himalayan (MCT). D.Sc., Grenoble.
- Pêcher, A. 1989. The metamorphism in the central Himalaya. *J. Metamorphic Geol.* **7**, 31-41.
- Spear, F.S., and J. Selverstone. 1983. Quantitative P-T paths from zoned minerals: theory and tectonic applications. *Contrib. Mineral. Petrol.* **83**, 348-357.

Thompson, A.B. 1982. Dehydration melting of pelitic rocks and the generation of H<sub>2</sub>O-undersaturated granitic liquids. *Am. J. Sci.* **282**, 1567-1595.

Thompson, A.B., and R.J. Tracy. 1979. Model systems for anatexis of pelitic rocks: II. Facies series melting and reactions in the system CaO-KAlO<sub>2</sub>-NaAlO<sub>2</sub>-Al<sub>2</sub>O<sub>3</sub>-SiO<sub>2</sub>-H<sub>2</sub>O. *Contributions In Mineralogy and Petrology* **70**, 429-438.



Table 1 Thermobarometers

Acronym										
GARB	$\text{Fe}_3\text{Al}_2\text{Si}_3\text{O}_{12}$ Grt	+	$\text{KMg}_3\text{AlSi}_3\text{O}_{10}(\text{OH})_2$ Bt	=	$\text{Mg}_3\text{Al}_2\text{Si}_3\text{O}_{12}$ Grt	+	$\text{KFe}_3\text{AlSi}_3\text{O}_{10}(\text{OH})_2$ Bt	Ferry and Spear (1978)		
GASP	$\text{Ca}_2\text{Al}_2\text{Si}_3\text{O}_{12}$ Grt	+	$2\text{Al}_2\text{SiO}_5$ AlSi	+	$\text{SiO}_2$	=	$3\text{CaAl}_2\text{Si}_2\text{O}_8$ Pl	Ghent (1976)		
GMAP	$\text{Fe}_3\text{Al}_2\text{Si}_3\text{O}_{12}$ Grt	+	$\text{Ca}_2\text{Al}_2\text{Si}_3\text{O}_{12}$ Grt	+	$\text{KAl}_3\text{Si}_3\text{O}_{10}(\text{OH})_2$ Ms	=	$3\text{CaAl}_2\text{Si}_2\text{O}_8$ Pl	+	$\text{KFe}_3\text{AlSi}_3\text{O}_{10}(\text{OH})_2$ Bt	Ghent and Stout (1981)

Table 2. Garnet rim analysis compositions (12 O basis)																				
Sample	MC2		MCT-1		MC3		MC4		MC18		MC19		MC5#1		MC5#2		MC7		MC36	
sio2	37.67	± 0.24	37.82	± 0.17	37.37	± 0.22	37.22	± 0.17	36.88	± 0.13	37.49	± 0.16	37.03	± 0.18	36.33	± 0.32	36.93	± 0.14	36.54	± 0.17
tio2	0.05	± 0.02	0.06	± 0.01	0.04	± 0.01	0.03	± 0.02	0.01	± 0.01	0.05	± 0.03	0.07	± 0.02	0.02	± 0.03	0.00	± 0.00	0.05	± 0.01
al2o3	21.46	± 0.20	21.16	± 0.12	20.59	± 0.11	20.80	± 0.13	21.14	± 0.24	21.24	± 0.05	20.90	± 0.13	20.53	± 0.30	20.76	± 0.06	20.77	± 0.26
cr2o3	0.07	± 0.01	0.05	± 0.01	0.10	± 0.02	0.11	± 0.02	0.09	± 0.02	0.05	± 0.05	0.09	± 0.01	0.07	± 0.05	0.09	± 0.02	0.06	± 0.01
feo	38.83	± 0.48	32.82	± 0.35	31.78	± 0.33	30.75	± 0.15	37.54	± 0.56	34.48	± 0.25	37.45	± 0.44	37.70	± 0.36	35.10	± 0.35	30.86	± 0.26
mno	0.37	± 0.11	1.85	± 0.07	1.54	± 0.26	5.44	± 0.15	3.68	± 0.10	3.98	± 0.10	2.66	± 0.10	3.44	± 0.26	2.67	± 0.10	10.61	± 0.13
mgo	4.31	± 0.31	4.77	± 0.09	4.45	± 0.30	3.54	± 0.10	2.33	± 0.11	2.33	± 0.05	2.95	± 0.23	2.37	± 0.41	2.48	± 0.12	1.71	± 0.05
cao	0.56	± 0.01	0.97	± 0.02	3.43	± 0.09	1.33	± 0.12	1.40	± 0.21	1.15	± 0.05	1.15	± 0.06	1.17	± 0.04	1.41	± 0.05	1.13	± 0.04
<b>total</b>	<b>103.31</b>	<b>± 0.17</b>	<b>99.50</b>	<b>± 0.11</b>	<b>99.29</b>	<b>± 0.13</b>	<b>99.24</b>	<b>± 0.06</b>	<b>103.07</b>	<b>± 0.17</b>	<b>100.78</b>	<b>± 16.56</b>	<b>102.30</b>	<b>± 0.54</b>	<b>101.62</b>	<b>± 0.78</b>	<b>99.44</b>	<b>± 0.11</b>	<b>101.74</b>	<b>± 0.10</b>
si	2.953		3.020		2.998		3.014													2.973
ti	0.003		0.004		0.003		0.003		0.003		3.014		2.965		2.956		3.001		0.002	
al	1.959		2.005		1.950		1.990		2.002		0.004		0.005		0.000		0.000		1.956	
cr	0.004		0.002		0.005		0.004		0.001		2.009		1.948		1.953		1.993		0.004	
fe	2.513		2.185		2.132		2.080		2.500		2.297		2.537		2.519		2.419		2.078	
mn	0.014		0.123		0.108		0.361		0.243		0.275		0.186		0.226		0.177		0.733	
mg	0.566		0.553		0.543		0.428		0.220		0.277		0.311		0.306		0.281		0.205	
ca	0.038		0.081		0.283		0.107		0.066		0.101		0.097		0.099		0.122		0.094	
<b>total</b>	<b>8.050</b>		<b>7.972</b>		<b>8.022</b>		<b>7.987</b>		<b>5.035</b>		<b>7.977</b>		<b>8.049</b>		<b>8.059</b>		<b>7.999</b>		<b>8.045</b>	



Plagioclase rim analysis compositions																			
Sample	MC2		MCT-1		MC3		MC4		MC18		MC19		MC5#1		MC5#2		MC7		MC36
sio2	67.53 ± 0.21		68.41 ± 0.89		61.23 ± 0.42		63.68 ± 0.20		64.43 ± 0.72		63.16 ± 2.12		62.68 ± 0.27		63.16 ± 0.35		61.34 ± 0.15		65.98 ± 1.55
al2o3	19.86 ± 0.16		19.87 ± 0.23		24.12 ± 0.15		22.32 ± 0.18		22.63 ± 0.19		22.11 ± 0.32		23.02 ± 0.13		23.08 ± 0.38		23.96 ± 0.20		21.31 ± 0.60
feo	0.04 ± 0.01		0.04 ± 0.02		0.10 ± 0.03		0.07 ± 0.03		0.07 ± 0.06		2.39 ± 2.18		0.34 ± 0.10		0.49 ± 0.10		0.25 ± 0.17		0.16 ± 0.05
mgo	0.00 ± 0.01		0.03 ± 0.01		0.00 ± 0.01		0.01 ± 0.01		0.00 ± 0.01		0.05 ± 0.07		0.05 ± 0.01		0.01 ± 0.02		0.00 ± 0.01		0.01 ± 0.01
cao	0.49 ± 0.03		1.03 ± 0.14		5.86 ± 0.08		3.54 ± 0.08		3.40 ± 0.17		2.97 ± 0.21		4.48 ± 0.14		4.54 ± 0.12		5.28 ± 0.06		2.27 ± 0.70
na2o	11.27 ± 0.08		10.64 ± 0.33		8.25 ± 0.12		9.44 ± 0.13		9.51 ± 0.40		8.81 ± 0.21		9.03 ± 0.11		8.68 ± 0.22		8.43 ± 0.25		9.92 ± 0.24
k2o	0.06 ± 0.01		0.05 ± 0.01		0.07 ± 0.01		0.07 ± 0.02		0.16 ± 0.04		0.37 ± 0.36		0.11 ± 0.02		0.10 ± 0.03		0.17 ± 0.03		0.23 ± 0.06
<b>total</b>	<b>99.25 ± 0.28</b>		<b>100.1 ± 0.32</b>		<b>99.63 ± 0.14</b>		<b>99.13 ± 0.08</b>		<b>100.2 ± 0.52</b>		<b>99.86 ± 0.94</b>		<b>99.7 ± 0.25</b>		<b>100.1 ± 0.15</b>		<b>99.45 ± 0.09</b>		<b>99.88 ± 0.55</b>
si	2.968		2.967		2.722		2.831		2.835		2.873		2.785		2.779		2.746		2.875
al	1.036		1.034		0.000		1.165		1.168		1.151		0.000		0.000		1.255		0.000
fe	0.002		0.001		1.270		0.002		0.001		0.014		1.203		1.222		0.014		1.130
mg	0.000		0.001		0.002		0.001		0.002		0.000		0.014		0.016		0.001		0.004
ca	0.025		0.047		0.000		0.170		0.162		0.151		0.000		0.000		0.257		0.000
Na	0.963		0.928		0.001		0.831		0.816		0.720		0.002		0.000		0.701		0.000
K	0.003		0.000		0.280		0.003		0.011		0.006		0.217		0.215		0.008		0.124
	4.997		4.978		4.275		5.003		4.995		4.914		5.005		4.985		4.981		4.986

Table 2. Biotite rim analysis compositions (11 O basis)																			
Sample	MC2	MCT-1	MC3	MC4	MC18	MC19	MC5#1	MC5#2	MC7	MC36									
sio2	36.66 ±	37.93 ±	0.17	37.35 ±	0.19	36.33 ±	0.18	34.77 ±	0.17	35.32 ±	0.36	34.62 ±	0.24	34.38 ±	0.23	34.43 ±	0.28	35.08	0.34
tio2	0.75 ±	1.19 ±	0.07	1.23 ±	0.03	1.73 ±	0.03	3.22 ±	0.08	2.02 ±	0.07	2.68 ±	0.14	2.57 ±	0.05	3.09 ±	0.03	1.33 ±	0.32
al2o3	19.07 ±	18.01 ±	0.26	19.27 ±	0.07	18.97 ±	0.13	18.36 ±	0.11	18.66 ±	0.11	19.66 ±	0.32	18.95 ±	0.21	18.72 ±	0.24	18.62 ±	0.70
feo	20.29 ±	16.69 ±	0.32	16.37 ±	0.16	17.46 ±	0.07	24.25 ±	0.34	23.78 ±	0.43	22.65 ±	0.28	22.84 ±	0.12	23.19 ±	0.40	23.65 ±	0.97
mno	0.04 ±	0.10 ±	0.03	0.07 ±	0.04	0.08 ±	0.04	0.11 ±	0.02	0.10 ±	0.07	0.07 ±	0.02	0.08 ±	0.02	0.12 ±	0.02	0.40 ±	0.13
mgo	11.50 ±	13.06 ±	0.17	12.23 ±	0.10	11.44 ±	0.06	7.08 ±	0.12	7.16 ±	0.14	7.79 ±	0.19	7.72 ±	0.03	6.49 ±	0.03	7.73 ±	0.18
cao	0.37 ±	0.00 ±	0.01	0.02 ±	0.02	0.30 ±	0.02	0.01 ±	0.01	0.02 ±	0.02	0.00 ±	0.01	0.02 ±	0.02	0.01 ±	0.01	0.02 ±	0.03
na2o	8.46 ±	0.41 ±	0.03	0.33 ±	0.03	8.46 ±	0.29	0.13 ±	0.02	0.19 ±	0.07	0.15 ±	0.04	0.15 ±	0.02	0.09 ±	0.02	0.08 ±	0.03
k2o	0.02 ±	7.57 ±	0.27	7.88 ±	0.06	0.05 ±	0.03	9.22 ±	0.06	8.66 ±	0.16	9.07 ±	0.09	8.96 ±	0.21	8.98 ±	0.10	9.29 ±	0.15
total	97.16 ±	94.97 ±	0.12	94.75 ±	0.06	94.83 ±	0.09	97.19 ±	0.10	95.92 ±	0.14	96.73 ±	0.70	95.74 ±	0.09	95.12 ±	0.14	96.21 ±	0.32
si	2.725	2.815		2.770		2.726		2.648		2.706		2.636		2.641		2.680		2.696	
ti	0.043	0.061		0.070		0.097		0.192		0.124		0.143		0.150		0.180		0.089	
al	1.683	1.599		1.690		1.690		1.648		1.693		1.760		1.721		1.728		1.725	
fe	1.239	1.021		1.025		1.090		1.559		1.530		1.457		1.485		1.476		1.490	
mn	0.002	0.004		0.002		0.005		0.007		0.003		0.004		0.005		0.010		0.018	
mg	1.263	1.429		1.358		1.289		0.822		0.820		0.892		0.886		0.753		0.858	
ca	0.000	0.001		0.002		0.000		0.002		0.004		0.000		0.004		0.002		0.000	
Na	0.055	0.063		0.045		0.043		0.016		0.018		0.019		0.022		0.015		0.014	
K	0.807	0.724		0.746		0.823		0.903		0.869		0.878		0.884		0.871		0.922	
total	6.955	6.929		6.915		6.897		7.797				7.788		7.8		7.719		7.82	

Muscovite																			
Sample	MC2		MCT-1		MC3		MC4		MC18		MC19		MC5#1		MC5#2		MC7		MC36
sio2	47.61 ± 0.20		49.81 ± 0.35		48.46 ± 0.55		48.19 ± 1.24		47.58 ± 0.35		48.85 ± 0.59		47.49 ± 0.51		47.49 ± 0.51				47.42 ± 0.47
TiO2	0.51 ± 0.03		0.25 ± 0.05		0.38 ± 0.05		0.89 ± 0.05		0.97 ± 0.05		0.60 ± 0.29		0.79 ± 0.06		0.79 ± 0.06				0.38 ± 0.04
al2o3	34.64 ± 0.20		36.72 ± 0.22		35.59 ± 0.71		34.95 ± 0.72		34.25 ± 0.14		36.05 ± 0.27		35.03 ± 0.31		35.03 ± 0.31				33.14 ± 0.28
feo	2.37 ± 0.08		1.17 ± 0.17		1.07 ± 0.16		1.46 ± 0.05		1.62 ± 0.05		1.31 ± 0.13		1.36 ± 0.07		1.36 ± 0.07				2.81 ± 0.17
MnO	0.03 ± 0.02		0.02 ± 0.03		0.03 ± 0.02		0.09 ± 0.02		0.04 ± 0.03		0.02 ± 0.02		0.04 ± 0.04		0.04 ± 0.04				0.08 ± 0.03
mgO	0.59 ± 0.04		0.24 ± 0.17		0.61 ± 0.06		0.71 ± 0.07		0.65 ± 0.03		0.43 ± 0.04		0.52 ± 0.06		0.52 ± 0.06				0.84 ± 0.01
cao	0.02 ± 0.01		0.19 ± 0.06		0.03 ± 0.02		0.03 ± 0.02		0.01 ± 0.01		0.04 ± 0.01		0.01 ± 0.01		0.01 ± 0.01				0.06 ± 0.04
na2o	2.38 ± 0.06		5.09 ± 0.35		1.04 ± 0.10		1.22 ± 0.22		0.52 ± 0.02		0.87 ± 0.11		0.41 ± 0.03		0.41 ± 0.03				0.40 ± 0.02
k2o	7.21 ± 0.10		1.26 ± 0.25		7.82 ± 0.66		8.13 ± 1.30		10.23 ± 0.10		8.77 ± 0.63		10.13 ± 0.12		10.13 ± 0.12				9.87 ± 0.31
<b>total</b>	<b>± 0.41</b>		<b>94.75 ± 0.12</b>		<b>95.03 ± 0.29</b>		<b>95.67 ± 0.54</b>		<b>95.88 ± 0.11</b>		<b>96.95 ± 0.24</b>		<b>95.77 ± 0.54</b>		<b>95.77 ± 0.54</b>				<b>94.99 ± 0.75</b>
si	3.13		3.183		3.164		3.133		2.687		3.177		3.129		3.129				3.163
al	2.689		2.765		2.744		2.693		1.676		0.056		0.036		0.036				2.621
fe	0.13		0.062		0.056		0.077		1.499		2.719		2.72		2.72				0.167
mg	0.063		0.012		0.058		0.068		0.775		0.072		0.071		0.071				0.084
ca	0.002		0.01		0.003		0		0.001		0.001		0.006		0.006				0.005
Na	0.315		0.639		0.138		0.173		0.026		0.044		0.051		0.051				0.052
K	0.601		0.114		0.667		0.732		0.9		0		0		0				0.84
<b>total</b>	<b>6.96</b>		<b>6.785</b>		<b>6.83</b>		<b>6.876</b>		<b>7.564</b>		<b>6.746</b>		<b>6.013</b>		<b>6.013</b>				<b>6.954</b>

Table 3. Rim thermobarometric data

	<u>GARB-GASP</u>		<u>GARB-GMBP</u>	
Sample	T (K)	P (MPa)	T(K)	P(MPa)
Group I				
MC2			930 (50)	1160 (100)
MCT-1	910 (30)	1130 (140)	910 (30)	1100 (110)
MC3	950 (60)	1040 (120)	950 (60)	1040 (120)
Group II				
MC4	880 (40)	720 (100)	880 (30)	710 (90)
MC18			970 (50)	780 (110)
MC19			990 (30)	780 (70)
MC5#1			990 (80)	700 (120)
MC5#2			1010 (50)	750 (60)
MC7	1050 (40)	860 (60)		
Group III				
MC36	870 (40)	630 (80)		

### **Figure Captions**

Figure 1) Geologic map of central Nepal (from Colchen et al., 1986 with minor modifications from this study) with P-T sample locations. White, gray, and black filled circles correspond to Group I, II and III samples, respectively. The major structures include the Main Central thrust (MCT), the South Tibetan detachment system (STDS), and the Thakkola graben. The inset map shows the location of the Annapurna-Manaslu region within the Himalaya.

Figure 2) Cross sections with sample locations corresponding to A-A' and B-B' on Figure 1.

Figures 3-5) Thermobarometric results obtained through simultaneous solution of GARB and GASP, and/or GARB and GMBP. The ellipses designate  $2\sigma$  uncertainties in these values based on analytical imprecision. Unlabelled curves (after Hemingway et al.) bound the aluminum silicate stability fields. Labeled curves correspond to the water-saturated granite solidus ('A': Thompson, 1982), and the nominal, water-saturated, muscovite breakdown reaction ('B': Thompson and Tracy, 1979; Thompson, 1982).



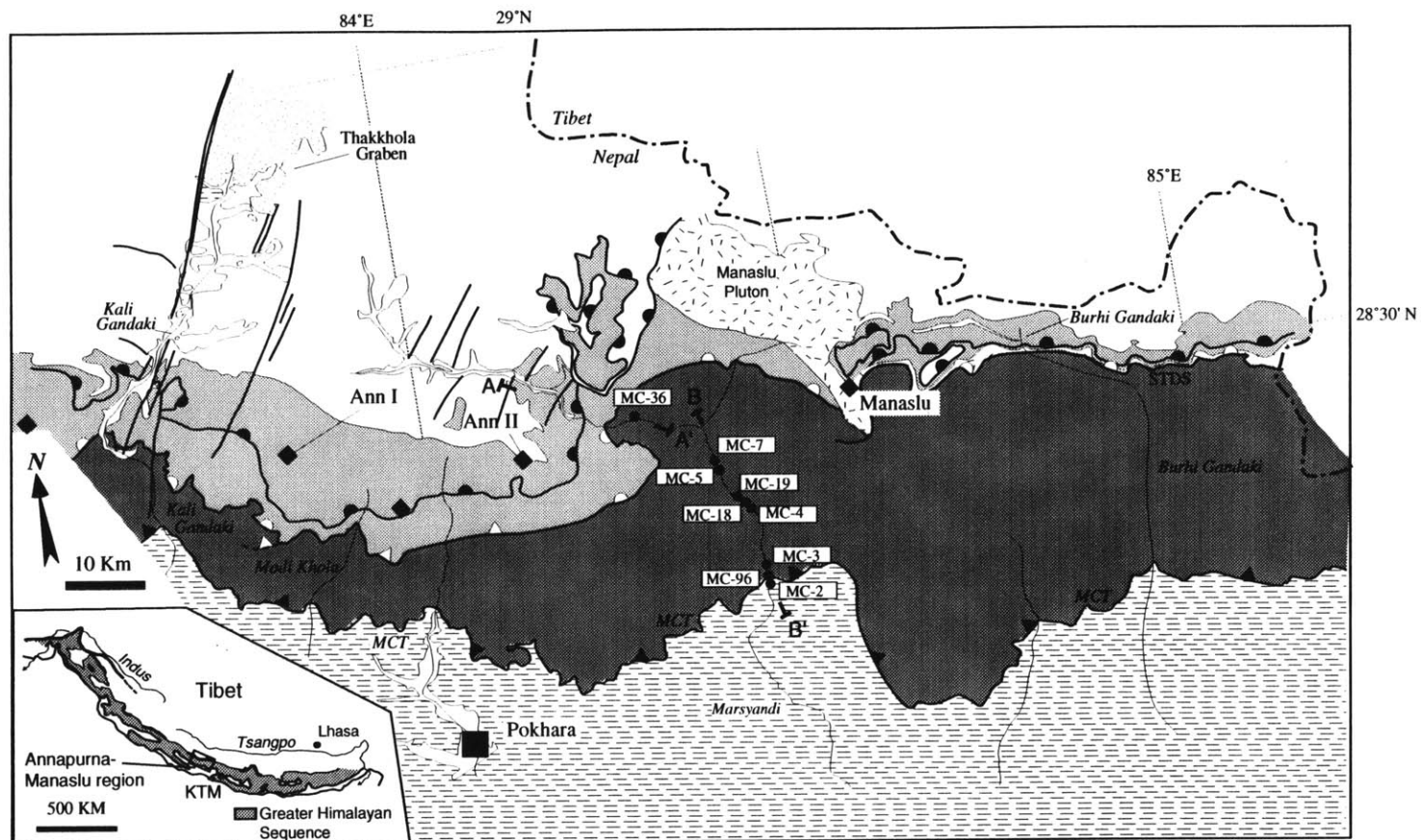


Figure 1





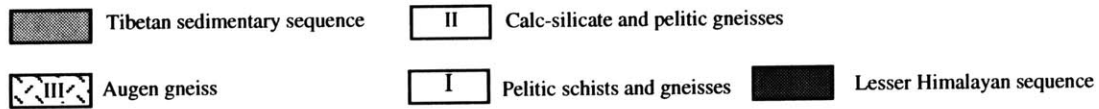
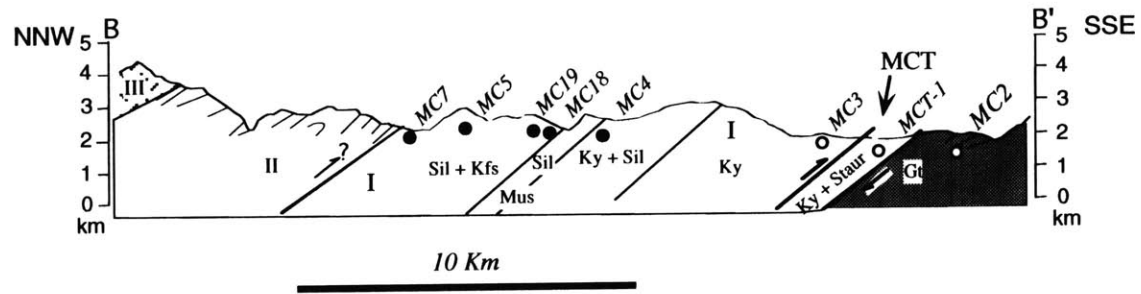
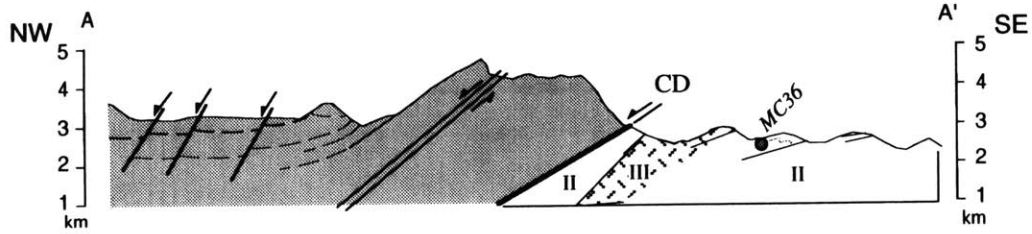


Figure 2



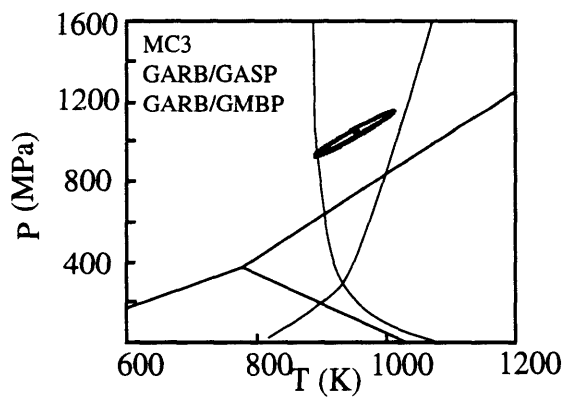
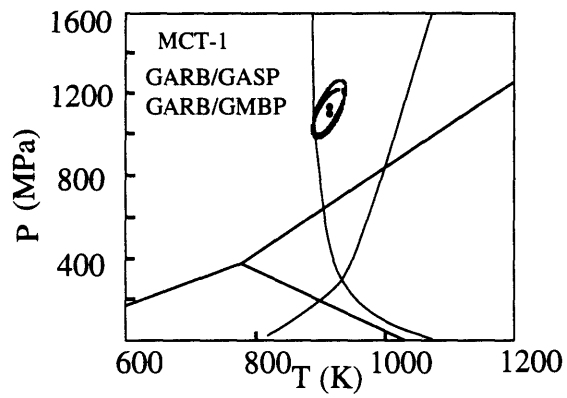
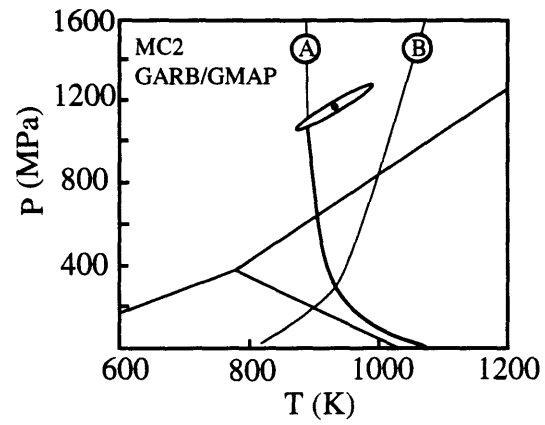


Figure 3



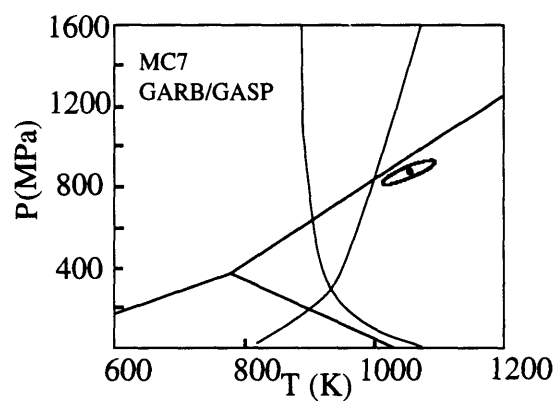
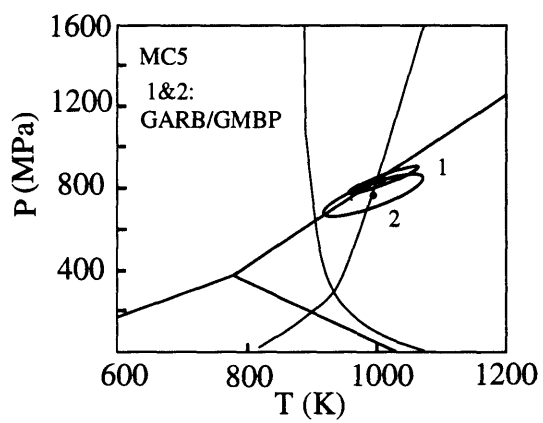
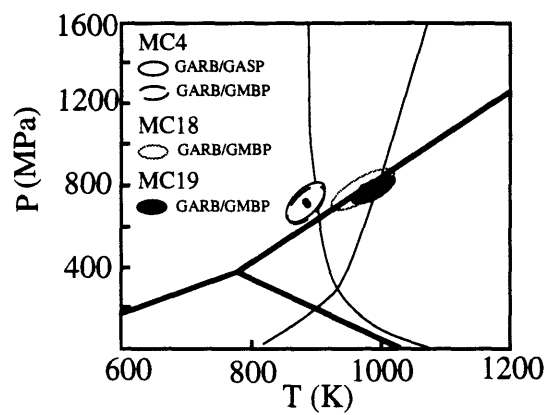


Figure 4



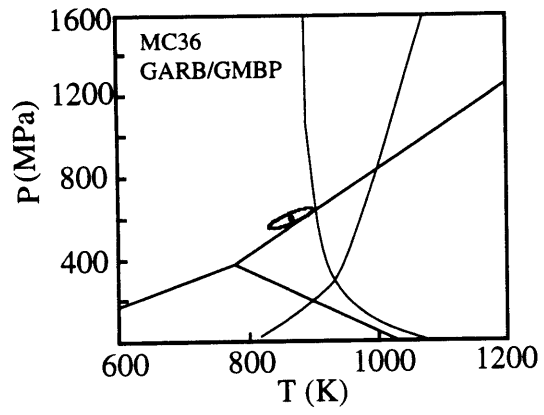


Figure 5





## Evidence for Tibetan plateau uplift before 14 Myr ago from a new minimum age for east–west extension

Margaret Coleman & Kip Hodges

Department of Earth, Atmospheric, and Planetary Sciences, 54-1116, Massachusetts Institute of Technology, Cambridge, Massachusetts 02139, USA

**IMPORTANT** changes in South Asian climate occurred in the Late Miocene epoch (~8 Myr ago)<sup>1,2</sup>, and these have been attributed by some researchers to uplift of the Tibetan plateau at about the same time<sup>3–5</sup>. Unfortunately, this link has been difficult to test because the timing of plateau uplift remains poorly constrained by independent evidence. One way to determine the minimum age of uplift is to establish the initiation age of the north-striking normal fault systems in southern Tibet that are widely regarded<sup>6–10</sup> as being related to gravitational collapse of the Tibetan plateau. Here we report an <sup>40</sup>Ar/<sup>39</sup>Ar age of ~14 Myr for hydrothermal mica from an extensional fracture belonging to such a fault system in north-central Nepal. This age implies that east–west extension began before ~14 Myr ago in at least some parts of the Tibetan plateau, suggesting that the plateau attained its high mean elevation well before Late Miocene time.

The tectonic evolution of the Himalayas and Tibet since the Palaeogene collision between India and Asia has been controlled by three classes of deformational structures. The most obvious features are east-striking, north-dipping thrust fault systems and subordinate folds related to shortening and crustal thickening. Some of these, such as the Neogene Main Central and Main Boundary thrust systems, have been traced for hundreds of kilometres parallel to the strike of the orogen (Fig. 1)<sup>11,12</sup>. The second class of structures includes east-striking, north-dipping normal faults of the South Tibetan detachment system<sup>13</sup>. Developed near the crest of the Himalayas along the southern margin of the Tibetan plateau, these Late Oligocene–Pliocene exten-

sional structures are thought to have moved in concert with contractional faults such as those of the Main Central thrust system in order to moderate high topographical and crustal-thickness gradients arising from the India–Asia convergence<sup>14,15</sup>. Active tectonics of the southern Tibetan plateau are characterized by east–west extension on a third class of structures: north-striking, east- and west-dipping normal faults and related strike-slip features (Fig. 1)<sup>6,7</sup>. Based on the results of numerical experiments on the dynamics of continental plateau uplift, there is general agreement that east–west extension in Tibet was triggered by elevation of the plateau to the point when topography-related extensional stresses exceeded compressional stresses related to continent–continent collision<sup>5,6,10</sup>.

Most estimates of the time at which east–west extension began, and thus the minimum age of the plateau attaining its high mean elevation if conventional wisdom proves correct, have been based on chronostratigraphic data for extensional basin deposits related to the second and third classes of structures near the southern margin of the plateau. The most extensively studied Neogene sedimentary sequence in this area is found in the Thakkhola and Giyong grabens (Fig. 1). Both are characterized by a lower section of fluvial and lacustrine strata separated from an upper fanlomerate section by an angular unconformity<sup>16,17</sup>. Palaeontological and palaeomagnetic data suggest that units found beneath the unconformities range in age from Late Miocene to Early Pliocene<sup>18,20</sup>. The structural setting of the basins in which these rocks were deposited is poorly understood, but the basal units found within the Thakkhola graben overlap NNE-striking extensional faults<sup>17</sup>, suggesting that east–west extension may have started before Late Miocene basin sedimentation. There is no question that units above the unconformity were deposited synchronously with the opening of north-trending grabens<sup>17,18</sup>. Palaeomagnetic investigations of these strata indicate Late Pliocene and younger ages. The lack of ambiguity associated with assigning a structural setting to these deposits prompted some researchers<sup>8,18</sup> to postulate a 5–2 Myr age for the inception of east–west extension. More recently, structural and geochronological studies along the western flank of the Yangbajian graben (Fig. 1) suggest that east–west extension in at least one part of the plateau began 11–5 Myr ago<sup>21,22</sup>.

Our new constraints on the age of this phase of extension are derived from current studies of the structural evolution of the Annapurna range of north-central Nepal, east of the Thakkhola graben (Fig. 2). The extensional faults that are overlapped by basal units of the Thakkhola Neogene sequence are part of a regionally important family of NNE-striking normal faults with minor displacements that disrupt Palaeozoic and Mesozoic bedrock stratigraphy for ~40 km to the east of the Thakkhola graben<sup>23,25</sup>; we will refer to these structures, together with the syndepositional faults found in the graben, as the Thakkhola fault system. Faults of this system are confined to the region north of the high peaks of the Himalaya, structurally above the lowermost shear zones of the South Tibetan detachment system<sup>25,26</sup>.

Our study has focused on some of the easternmost structures of the Thakkhola fault system in the northern part of the Marsyandi river valley (Fig. 2). The most significant of these are normal faults developed in essentially unmetamorphosed Palaeozoic and Mesozoic rocks. They strike N20°E–N40°E and dip 45–60° northwest, similar in orientation to bounding faults of the Thakkhola graben, although we consider them to be older and related to the earliest stages of east–west extension. Striae on exposed fault surfaces are oriented N90°E ± 10°. Kinematic indicators, including slickenside surface characteristics and orientations of extensional fractures within discrete fault zones, demonstrate that displacement was primarily hanging wall down to the WNW. These oldest and easternmost faults of the Thakkhola system cut mylonitic fabrics related to structurally high shear zones of the South Tibetan detachment system, and are

FIG 1 Generalized tectonic map of the Tibetan plateau (adapted from refs 9 and 11) showing the location of major structural features discussed in the text, and the area of Fig. 2

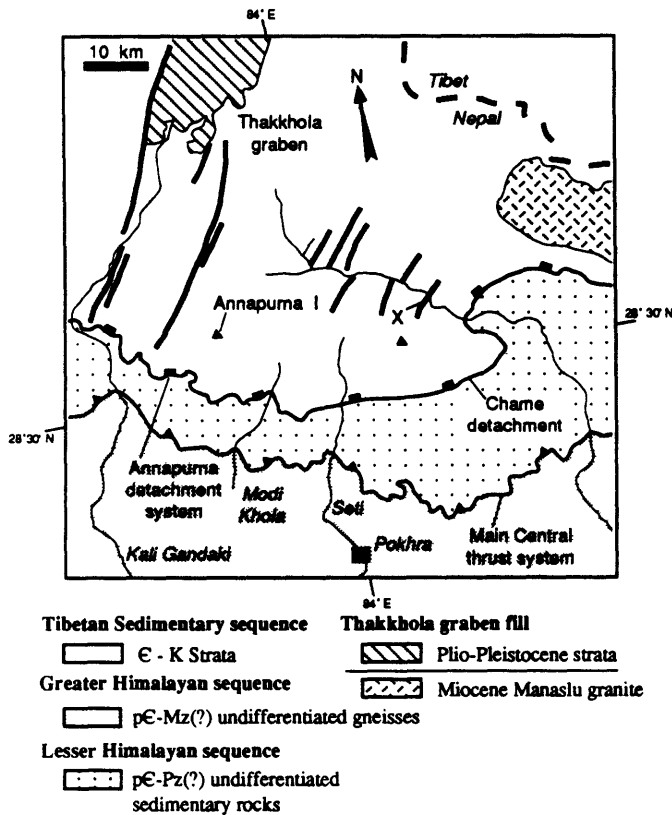
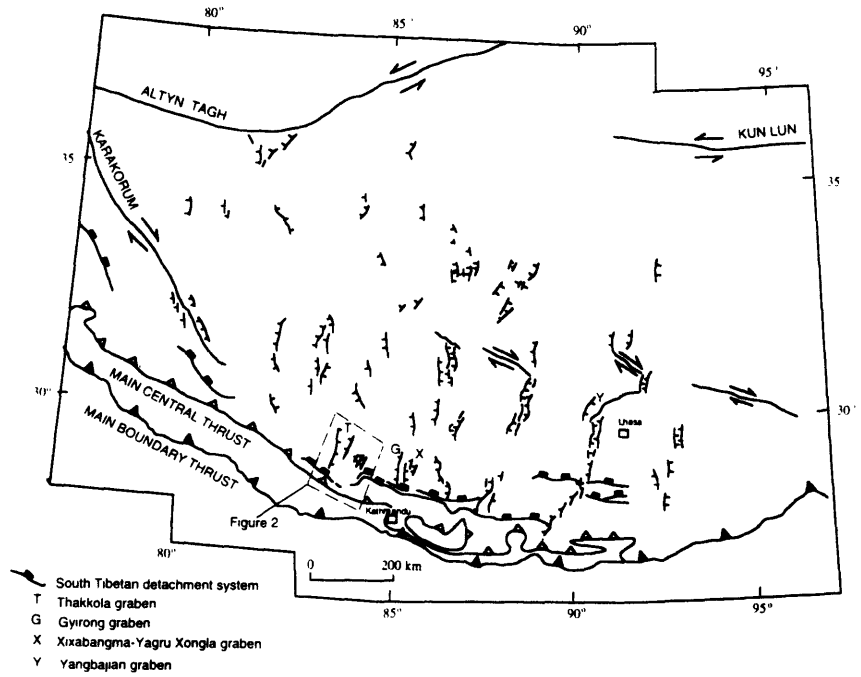


FIG 2 Simplified geological map of the Annapurna region. X marks the sample location. E, Cambrian; K, Cretaceous; pE, Precambrian; Mz, Mesozoic; Pz, Palaeozoic; Plio, Pliocene.

TABLE 1  $^{40}\text{Ar}/^{39}\text{Ar}$  data for hydrothermal muscovite, Thakkola fault system

Tube current (A)	$^{36}\text{Ar}/^{40}\text{Ar}$	$^{39}\text{Ar}/^{40}\text{Ar}$	$^{39}\text{Ar}_k$ ( $\times 10^{-14}$ mol)	Cum. $^{39}\text{Ar}_k$ (%)	$^{40}\text{Ar}^*$ (%)	Age (Myr)	
Split no. 1							
11.5	0.00322	0.00694	0.004	0.12	4.71	7.2 $\pm$ 0.3	
12.5	0.00228	0.02939	0.007	0.34	32.74	11.9 $\pm$ 0.5	
13	0.00256	0.02851	0.014	0.77	24.33	9.1 $\pm$ 0.3	
13.5	0.00122	0.05077	0.095	3.66	63.96	13.4 $\pm$ 0.5	
14	0.00081	0.05709	0.192	9.51	76.03	14.2 $\pm$ 0.5	
14.5	0.00033	0.06555	0.311	19.01	90.16	14.7 $\pm$ 0.6	
15	0.00033	0.06895	0.208	25.36	90.40	14.0 $\pm$ 0.5	
16	0.00049	0.06333	0.332	35.48	85.54	14.4 $\pm$ 0.5	
18	0.00043	0.06303	0.826	60.67	87.26	14.8 $\pm$ 0.6	
20	0.00033	0.06865	1.289	100.00	90.17	14.0 $\pm$ 0.5	
						Average	14.3 $\pm$ 0.1
Split no. 2							
14	0.00100	0.05075	0.168	6.49	70.57	14.8 $\pm$ 0.6	
16	0.00042	0.06430	0.904	41.43	87.62	14.5 $\pm$ 0.6	
18	0.00035	0.06596	1.304	91.79	89.77	14.5 $\pm$ 0.6	
20	0.00022	0.06905	0.149	97.53	93.39	14.4 $\pm$ 0.5	
22	0.00035	0.07043	0.064	100.00	89.78	13.6 $\pm$ 0.5	
						Average	14.5 $\pm$ 0.3

$^{39}\text{Ar}_k$ , the number of moles of K-derived  $^{39}\text{Ar}$  released during each heating step, and Cum.  $^{39}\text{Ar}_k$ , the cumulative percentage after each heating increment;  $^{40}\text{Ar}^*$  (%), the percentage of radiogenic  $^{40}\text{Ar}$  in the total  $^{40}\text{Ar}$  for each analysis. Average ages are means weighted by the amount of  $^{39}\text{Ar}_k$  in each increment, with uncertainties corresponding to 2 standard errors of the mean.

thus demonstrably younger<sup>25</sup>. The age of the mylonitic fabrics associated with the South Tibetan detachment system in central Nepal is constrained by cross-cutting leucogranites (such as the Manaslu pluton) to be at least 22 Myr old<sup>27, 30</sup>.

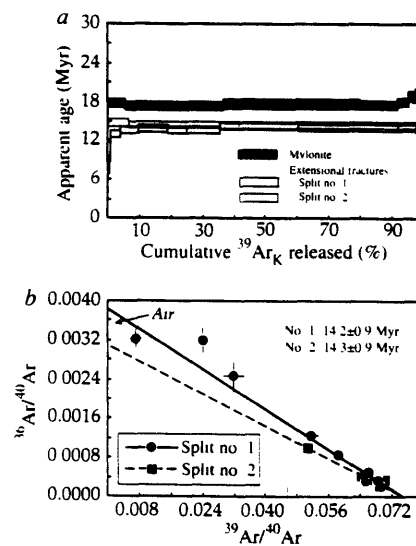
The Thakkola fault system also includes vertical extensional fractures, striking N0°E  $\pm$  10°, which are pervasive in Palaeozoic rocks of the upper Marsyandi valley. Many of these fractures contain minerals precipitated from late-stage hydrothermal fluids, apparently injected during extensional faulting. One of the more common vein materials is muscovite, which provides the opportunity to place minimum age constraints on extensional fracturing through  $^{40}\text{Ar}$ – $^{39}\text{Ar}$  dating. We applied this technique to coarse-grained muscovite ( $\text{Si}^{\text{IV}} = 3.20$  per formula unit,  $(\text{Fe}_{\text{total}} + \text{Mg}) \text{Al}^{\text{VI}} = 0.145$ , where superscript IV or VI refers to a crystallographic site with tetrahedral or octahedral coordination, respectively) from a fracture developed in a lower amphibolite facies, impure metacarbonate rock from the Annapurna Yellow Formation<sup>31</sup>. The rock itself contained disseminated, fine-grained muscovite that grew before extensional fracturing.

To ensure that our sample of hydrothermal muscovite was not contaminated by older muscovite, the rock was broken along the fracture and 10–15 single-crystal fragments of hydrothermal muscovite were hand-picked from the cleavage surface under a binocular microscope. The material was then split in two fractions that were analysed separately to test for reproducibility of the results.

The two splits exhibited easily interpretable behaviour during laser incremental heating (Table 1; Fig. 3). The first was analysed in the most detail, yielding a relatively flat age spectrum with an average age of 14.3  $\pm$  0.1 Myr. Split no. 2 had a statistically indistinguishable average age of 14.5  $\pm$  0.3 Myr. Data from both splits defined linear arrays on an inverse isotope correlation diagram<sup>12</sup>, indicating isochron ages of 14.2  $\pm$  0.9 Myr (split no. 1) and 14.3  $\pm$  0.9 Myr (split no. 2). Increments from split no. 1 show greater dispersion on the correlation diagram and provide a better constraint on the initial  $^{40}\text{Ar}$ – $^{36}\text{Ar}$  ratio of these micas, but both regression curves indicate an initial ratio within uncertainty of the present-day atmospheric value.

FIG. 3 Incremental release spectrum (a) and inverse isotope correlation (b) diagrams for hydrothermal muscovites from the Thakkola fault system and metamorphic muscovite from the surrounding mylonite (errors at  $2\sigma$ ). ('Cumulative  $\text{Ar}_k$ ' is defined in Table 1.) Uncertainties for samples shown without error bars in b are smaller than the designating symbols. Solid and dashed lines in b designate least-squares linear regression fits using the algorithm of York<sup>37</sup>.

**METHODS.** Samples were wrapped in cadmium foil and irradiated before analysis in the McMaster University research reactor in Hamilton, Ontario, Canada. Salts included in the irradiation package were used to correct for interference by reactor-induced masses. The fast-neutron fluence during irradiation was monitored using Fish Canyon sanidine (27.84 Myr); ages and age uncertainties were calculated using an estimated irradiation parameter ( $J$ ) of  $0.00059 \pm 0.00001$  ( $2\sigma$ ). Incremental heating experiments were done at the Massachusetts Institute of Technology using a 10-W argon-ion laser with the technique described by Hodges<sup>38</sup>.



To evaluate the possibility that, despite our best efforts, the analysed micas were somehow relicts from the earlier mylonitic fabric rather than neoblasts crystallized during hydrothermal activity, we also dated compositionally similar muscovite ( $Si^{IV} = 3.24$  per formula unit;  $(Fe_{total} + Mg) Al^{VI} = 0.141$ ) that defines the mylonitic foliation within the South Tibetan detachment zone in this area. Data for this mica defined a plateau age of  $17.6 \pm 0.3$  Myr (Fig. 3), an inverse isochron age of  $17.4 \pm 0.7$  Myr, and an initial ratio within uncertainty of the present-day atmosphere. The ages of the micas in the mylonite and the micas in the extensional fractures are significantly different (at a confidence level of  $>95\%$ ), demonstrating that the micas separated from the fracture grew after cooling of the surrounding mylonitic rocks to temperatures below  $\sim 625$  K (the nominal closure temperature for Ar diffusion in muscovite<sup>33</sup>) and that the  $\sim 14$ -Myr age does not reflect the long-term thermal effects of pre-22 Myr igneous activity.

We interpret the hydrothermal muscovite data as strong evidence that east-west extension began before 14 Myr ago in the area corresponding to the present-day southern margin of the Tibetan plateau. This finding supports earlier suggestions of an age of at least 13 Myr for the plateau based on the  $^{40}Ar$ – $^{39}Ar$  age of volcanic rocks that are thought to have been derived from thinned mantle lithosphere beneath Tibet<sup>14</sup>. It is also consistent with interpretations relating geochronological evidence for rapid cooling of rocks in southern Tibet to Early Miocene plateau uplift<sup>10,35</sup>.

Previous studies in southern Tibet suggested that east-west extension had not progressed to the point that sedimentary basins, such as the Thakkola graben, began to form until the Pliocene epoch; however, the existence of significantly older, north-striking normal fault systems implies that the stress field responsible for east-west extension had developed by the Middle Miocene epoch. If the onset of east-west extension marks the beginning of accelerated uplift of the plateau due to an increase in the potential energy of the Tibetan lithosphere<sup>9</sup>, then our data imply that uplift was not simultaneous with the marked change in South Asian climate at  $\sim 8$  Myr ago but began several million years earlier. Future models of Cenozoic global climate change must be reconciled with a growing body of geological evidence suggesting that the Tibetan plateau was an established geomorphologic feature at least as early as Middle Miocene time, possibly as old as Palaeogene<sup>36</sup>. □

- 26 Brown R L & Nazarchuk, J H in *Himalayan Tectonics* (eds Treloar, P J & Searle, M P.) 461–473 (Spec. Publ. 47 Geol. Soc., London, 1993)
- 27 Deniel, C, Vidal, P, Fernandez, A., LeFort, P. & Peucat, J. J. *Contr. Miner. Petro.* **96**, 78–92 (1987)
- 28 Guillot, S., Hodges, K V, LeFort, P. & Pêcher, A. *Geology* **22**, 559–562 (1994)
- 29 Parrish, R R & Hodges, K V *Geol. Soc. Am. Abstr. Progr.* **23**, A174 (1993)
- 30 Harrison, T M & McKeegan, K D *Geol. Soc. Am. Abstr. Progr.* **23**, A367 (1994)
- 31 Colchen, M., LeFort, P. & Pêcher, A. *Annapurna-Manaslu-Ganesh Himal* (Centre Natl. Rech. Sci., Paris, 1986)
- 32 Roddick, J C, Cliff, R A & Rex, D C *Earth planet. Sci. Lett.* **48**, 185–208 (1980)
- 33 McDougall, I. & Harrison, T M. *Geochronology and Thermochronology by the  $^{40}Ar/^{39}Ar$  Method* (Oxford Univ. Press, New York, 1988)
- 34 Turner, S. *Nature* **364**, 50–54 (1993)
- 35 Richter, F M, Lovera, O M, Harrison, T M & Copeland, P C. *Earth planet. Sci. Lett.* **105**, 266–278 (1991)
- 36 England, P. & Searle, M. *Tectonics* **5**, 1–14 (1986)
- 37 York, D. *Earth planet. Sci. Lett.* **5**, 320–324 (1969)
- 38 Hodges, K V, Hames, W E & Bowring, S A. *Geology* **22**, 55–58 (1994)

ACKNOWLEDGEMENTS. We thank K. Bull for first drawing our attention to the fractures containing hydrothermal muscovite, and B. N. Upreti for helpful discussions and logistical assistance. S. Kelley and M. Searle helped improve the manuscript with their comments on an earlier version. This work was supported by the US NSF.

Received 17 June 1994; accepted 9 January 1995

- 1 Quade, J., Cerling, T E & Bowman, J R. *Nature* **342**, 163–166 (1989)
- 2 Prell, W L, Murray, D W., Clemens, S C & Anderson, D M. in *Synthesis of Results from Scientific Drilling in the Indian Ocean* (ed. Duncan, R A.) 447–469 (Am. Geophys. Union, Washington DC, 1992)
- 3 Prell, W L & Kutzbach, J E. *Science* **256**, 647–652 (1992)
- 4 Raymo, M F. & Ruddiman, W F. *Nature* **359**, 117–122 (1992)
- 5 Molnar, P., England, P. & Martinod, J. *Rev. Geophys.* **31**, 357–396 (1993)
- 6 Molnar, P. & Tapponnier, P. *J. geophys. Res.* **83**, 5361–5375 (1978)
- 7 Ni, J. & York, J. E. *J. geophys. Res.* **83**, 5277–5384 (1978)
- 8 Armijo, R., Tapponnier, P., Mercier, J. & Han, T. *J. geophys. Res.* **91**, 13803–13872 (1986)
- 9 England, P. & Houseman, G. *J. geophys. Res.* **94**, 17561–17579 (1989)
- 10 Harrison, T M., Copeland, P., Kidd, W S F. & Yin, A. *Science* **255**, 1663–1670 (1992)
- 11 Gansser, A. *Geology of the Himalayas* (Wiley Interscience, London, 1964)
- 12 LeFort, P. *Am. J. Sci.* **275A**, 1–44 (1975)
- 13 Burchfiel, B C et al. *The South Tibetan Detachment System, Himalayan Orogen Extension Contemporaneous with and Parallel to Shortening in a Collisional Mountain Belt 1–41* (Geological Soc. Am. Boulder, 1992)
- 14 Burchfiel, B C & Royden, L H. *Geology* **13**, 679–682 (1985)
- 15 Hodges, K V et al. *Science* **258**, 1466–1470 (1992)
- 16 Chen, W Y. in *Geological and Ecological Studies of the Qinghai-Xizang Plateau* (ed. Liu, D S.) 343–352 (Science Press, Beijing, 1981)
- 17 Fort, M., Freytag, P. & Colchen, M. *Z. Geomorph.* **42**, 75–98 (1982)
- 18 Mercier, J.-L., Armijo, R., Tapponnier, P., Carey-Gailhardis, E. & Han, T L. *Tectonics* **6**, 275–304 (1987)
- 19 Wang, F B., Li, B Y. & Zhang, Q S. in *Geological and Ecological Studies of the Qinghai-Xizang Plateau* (ed. Liu, D S.) 231–238 (Science Press, Beijing, 1981)
- 20 Yoshida, M., Igarashi, Y., Arita, K., Hayashi, D. & Sharman, T. *J. Nepal geol. Soc.* **4**, 101–120 (1984)
- 21 Pan, Y. & Kidd, W S F. *Geology* **20**, 775–778 (1992)
- 22 Copeland, P. & Harrison, T M. *Geol. Soc. Am. Abstr. Progr.* **23**, A-175 (1993)
- 23 Bordet, P. et al. *Recherches Géologiques dans l'Himalaya du Népal, Région de la Thakkola* (Centre Natl. Rech. Sci., Paris, 1971)
- 24 Colchen, M. *C. r. hebdo. Séanc. Acad. Sci. Paris* **290**, 311–314 (1980)
- 25 Coleman, M E. *Geol. Soc. Am. Abstr. Progr.* **23**, A174–A175 (1993)

## Chapter 7

### Tectonic synthesis

#### Introduction

The Himalayan orogen provides a spectacular example of continent-continent collision. While we know the general progression of Himalayan tectonic events over the past 50 million years, many important questions about the history and dynamics of the orogen remains uncertain. This paper is a synthesis of the previous chapters and is intended to highlight important new insights gained from the combined results into three of the less well understood aspects of the Himalayan orogeny. The three topics include:

- Oligocene crustal thickening within the Indian plate, north of the Main Central Thrust zone
- The Miocene structural and thermal evolution of the metamorphic core
- The transition from north-south to east-west extension within the northern Himalaya and southern Tibetan plateau

#### Oligocene tectonic history of the central Himalaya

One of the gray areas in our present understanding of the Himalayan orogen concerns how much crustal thickening was accomplished in the central part of the range, within the Indian plate, prior to about 22 Ma. A very strong, early Miocene, syn-tectonic thermal overprint was imposed on Indian-plate rocks north of the Main Central thrust, obscuring their earlier deformational and metamorphic history (e.g. Hodges et al., 1988). Although it has been established that continental collision occurred by about 50 Ma (Patriat and Achache, 1984; Searle et al., 1987 and 1988; Dewey et al., 1988), there is limited information about the next 30 million years of orogenic evolution. Tectonic reconstructions for the central Himalaya have invoked Oligocene thrust imbrication north of the MCT and south of the Indus Tsangpo suture zone (e.g., Hodges et al., 1988) in order

to accommodate initial burial of the Greater Himalayan sequence and explain textural evidence of a polymetamorphic history (see Hodges et al. 1988, and Pecher, 1989, for a review). A growing body of evidence from the western Himalaya has improved our understanding of this event. Metamorphism in the Greater Himalayan sequence in the northwest is constrained to at least 38 Ma in one area from a hornblende cooling age (Treloar et al., 1989). Structural data suggests that Oligocene crustal thickening was at least in part accomplished by imbrication on thrust and fold nappes that pre-dated the extensional north-dipping Zaskar shear zone at the top of the Greater Himalayan sequence (Patel et al., 1993; Steck et al., 1993). In addition, recent documentation of ~35 Ma sedimentation within the foreland basin of the northwest Himalaya, indicates that there was high relief within the Indian plate north of the MCT (Najman et al., 1994). A few isolated isotopic age determinations from the Greater Himalayan sequence in the central part of the range have provided hints of pre-Miocene metamorphism (e.g., Inger and Harris, 1993; Hodges et al., 1994; Hodges et al., in press; Vannay and Hodges, in press). However, the Miocene overprint has made it difficult to correlate these ages with specific structures. In short, although there already exists evidence of Oligocene tectonic burial of Indian plate rocks between the Main Central Thrust and the Indus Tsangpo suture, no unequivocally Oligocene shortening structures had been identified prior to the work reported in this thesis.

In Chapters 2 and 4, I have shown that syn-metamorphic, southwest verging contractional structures in the Tibetan Sedimentary sequence of the Marsyandi area have a minimum age of ~30 Ma. The key evidence for Oligocene syn-tectonic metamorphism is the preservation of Oligocene foliation and south-west vergent folds in the lower Tibetan Sedimentary sequence. A minimum Oligocene age was determined for SW-verging folds by  $^{40}\text{Ar}/^{39}\text{Ar}$  analyses of syn-kinematic phlogopite. Although cooling ages within the Greater Himalayan sequence are mostly Miocene, an amphibolite gneiss from the top of

the sequence retains a hornblende cooling age of ~30 Ma (Chapter 4). This result, combined with an Oligocene U-Pb inherited component within monazite from an adjacent leucogranite (Chapter 3), provide evidence that the upper Greater Himalayan sequence was also metamorphosed to at least upper amphibolite facies prior to ~30 Ma. Oligocene hornblende cooling ages within the Greater Himalayan sequence in the Kali Gandaki valley (Hodges et al., in press; Vannay and Hodges, in press) and at Dinggye (in southern Tibet, NE of Everest; Hodges et al., 1994), contributes supporting evidence that Oligocene metamorphism of the upper Greater Himalayan sequence was a regional phenomenon and not just localized in the Marsyandi region.

Invoking an Oligocene north-dipping crustal-scale thrust fault between the Tibetan Sedimentary - Greater Himalayan sequence contact is one way to explain the metamorphism and style of folding within the Tibetan sedimentary sequence and the older cooling ages below. No viable alternative candidates for crustal-scale thrust faults higher in the Tibetan sedimentary sequence have yet been identified, although the amount of thickening accomplished by folding and imbrication within it has not been evaluated either. The proposed thrust fault is nowhere exposed at present, having been cut out by Early Miocene displacement on the Chame detachment. Pre-Miocene thrusting at this same structural level in the Annapurna region has also been suggested by Vannay and Hodges (in press), who argue that it would have been obliterated by Miocene recrystallization and displacement on the extensional Annapurna detachment. Vannay and Hodges attribute the formation of a large refolded SW-verging antiform within the lower Tibetan Sedimentary sequence to SW directed thrust emplacement at the base of the Tibetan Sedimentary sequence. It is probable that this fold is of the same generation as the >30 Ma SW-verging folds in the Tibetan Sedimentary sequence of the upper Marsyandi valley.

In summary, the Annapurna range results indicate Oligocene (pre-30 Ma) burial and amphibolite facies metamorphism of Indian plate sediments probably as a consequence of south-vergent thrust faulting. Combined with results from the northwest Himalaya (e.g. Treloar et al., 1989; Patel et al., 1993; Steck et al., 1993; Najman et al., 1994), these data make a strong case for Oligocene crustal thickening along a large portion of the orogen within the Indian plate north of the MCT.

### **Early Miocene structural and thermal history of the metamorphic core**

The combined results of U-Pb dating of migmatite from the upper and lower Greater Himalayan sequence (Chapter 3) and thermobarometry throughout the section (Chapter 5), document the existence of a steep thermal gradient during the early Miocene, similar to what has been found in other transects within the central Himalaya (Hubbard, 1989; Hodges et al., 1988). Although the Marsyandi results are not significantly different from previous findings in most regards, they provide better resolution of temporal relationships between major structures, like the MCT and the South Tibetan detachment, and metamorphism. The causal mechanism for the steep to inverted thermal structure in the Himalaya and other orogens remains controversial. Most recent thermal models suggest that the distribution of radiogenic heat (produced by in situ U, Th, and K decay) and denudation rates control the thermal structure of an active orogen ( e.g., Royden, 1993; Huerta et al., in press). Both of these parameters are themselves controlled by deformational processes, so an important part of testing the viability of such models is establishing the linkages between structural and thermal processes in real orogenic settings.

In the Marsyandi region, a 15 km thick section of the Greater Himalayan sequence reached temperatures in excess of 900K (Chapter 5) by ~22 Ma (Chapter 3). This heating event produced migmatization throughout the section and lead to the intrusion of cross-cutting leucogranites within the upper half (Chapter 3). Structural relationships (Chapter 2)



demonstrate that 22 Ma melting at the base and at the top of the section was synchronous with thrusting on the MCT and extension on the Chame detachment. The age of cross-cutting leucogranite dikes at the top of the Greater Himalayan sequence show that metamorphism and extensional faulting ceased by 18 Ma.

In the upper Marsyandi valley 22-18 Ma normal faulting on the Chame detachment juxtaposed the Tibetan sedimentary sequence with the Greater Himalayan metamorphic core (Chapters 2 and 3). Previously it was impossible to definitely determine a difference in age of metamorphism between the Tibetan Sedimentary sequence and the Greater Himalayan sequence in the Annapurna-Manaslu region. Both the upper Greater Himalayan sequence and basal Tibetan sedimentary sequence were metamorphosed at amphibolite facies (Schneider and Masch, 1993), an observation that resulted in a reluctance of some researchers working in the area to accept the possibility of a structural discontinuity between the two rock packages. It is now clear from the  $^{40}\text{Ar}/^{39}\text{Ar}$  data that the Chame detachment emplaced >30 Ma amphibolite facies rocks on ~22 Ma amphibolite facies rocks, such that the metamorphic “conformity” is pure coincidence.

Pressure-temperature constraints from the top 3 kilometers of the Greater Himalayan sequence (Chapter 5) require burial to at least 20 kilometers depth prior to Miocene unroofing. The existence of a ~22 Ma steep thermal gradient within the Greater Himalayan sequence at a temperature over 770K, indicates that the strength of the section would have been relatively low in Early Miocene time. Melt enhanced deformation (i.e. Hollister and Crawford, 1986) is a plausible mechanism for triggering normal faulting at the top of the Greater Himalayan sequence along the South Tibetan detachment system as previously suggested (Burchfiel et al., 1992), and the age constraints from the migmatite deformed by extensional shearing (Chapter 3) is consistent with this model. However, the

existence of younger, cross-cutting leucogranites suggest that tectonic denudation could also be the cause of some anatexis through decompression melting.

Deformation within and at the top of the Greater Himalayan sequence in the Marsyandi valley indicates that significant amount of thinning of the section was accomplished by lateral deformation, parallel to the strike of the orogen. West-directed extension in the Marsyandi valley on the Chame detachment (orogen-parallel) is roughly coeval with north-directed displacement (orogen-perpendicular) on the South Tibetan detachment system only 15 km away. The footwalls of both structures (and the entire section of the Greater Himalayan sequence throughout the central Himalaya) was deforming plastically at temperatures at or above  $\sim 770\text{K}$  during the early to middle Miocene. This temperature is well within the range under which rocks yield by ductile flow at geologic strain rates (Brace and Kohlstedt, 1980). The fact that the whole section was ductile, as well as the observation that the thickness of the Greater Himalayan sequence varies dramatically while the lithostratigraphy remains relatively constant, indicate a net flow of material towards the east within the Greater Himalayan sequence. In regions of crustal thickening, lateral pressure gradients caused by differential thinning (or thickening) of the overlying crust will drive lower crustal flow, provided the underlying crust is hot and weak enough (Block and Royden, 1990). Flow towards the east within the Greater Himalayan sequence could account for west-directed shear between the Greater Himalayan sequence and the relatively rigid overlying Tibetan Sedimentary sequence in the Marsyandi valley. Further field analysis is required in order to determine if there is a continuous variation in the strain or "flow" pattern between different areas that might be reflected in the footwall kinematics.

It is clear from the structural analysis of the Greater Himalayan sequence in this study and in others (e.g., Pecher, 1991) that orogen-parallel deformation (or at least

elongation) at the top of the Greater Himalayan sequence during peak metamorphism was an important element of the Miocene high-temperature deformation. Orogen-parallel deformation during convergence has been documented in other orogens including the Alps (e.g., Mancktelow 1992, Froitzheim et al. 1994, Ratschbacher et al. 1991). In these examples, there is a change from extension normal to the orogenic core zone early in the deformation to extension roughly parallel to the core later in the deformation roughly coeval with peak metamorphic conditions. This consistent pattern suggests a fundamental change in the geometry of the deformation within orogens in general. The fact that the timing of orogen-parallel deformation seems to coincide with peak metamorphism within the core zone of orogens suggests a link between the mode of deformation and the strength of the deforming wedge.

### **Middle Miocene east-west extension of southern Tibetan plateau and Northern Himalaya**

After major displacement on the Main Central thrust during the Miocene, shortening was transferred towards the foreland and taken up on the Main Boundary Thrust and successively younger faults (Molnar and Lyon-Caen, 1989). The post-early Miocene history of the hinterland (northern Himalaya and southern Tibetan plateau) was dominated by a transition from primarily north-south shortening and extension along north-dipping structures, to east-west extension on north-striking grabens and strike-slip faulting at the margins of the plateau (Molnar and Tapponier, 1978; Armijo et al., 1986). This transition has been linked to rapid uplift of the Tibetan plateau (Molnar and Tapponier, 1978; England and Houseman, 1989; Molnar et al., 1993). The timing of the onset of east-west extension was previously thought to be at around 8 Ma (Pan and Kidd, 1992; Copeland and Harrison, 1993).

Results from Chapter 6 (Coleman and Hodges, 1995) show that east-west extension north of the central Himalaya initiated at least by 14 Ma, not long after extension on the South Tibetan Detachment system. The combined results from the Marsyandi region suggest that orogen-parallel extension started at mid-crustal levels within the Himalaya during the Early Miocene. Initiation of orogen-parallel extension seems to coincide with the entire Greater Himalayan sequence reaching temperatures in excess of 500°C. It is possible to look at east-west extension in the Marsyandi region as part of a continuum which propagated from within the deforming wedge of the greater Himalayan sequence towards the north to the southern Tibetan plateau over a 5-10 Ma interval. Initiation of east-west extension has been linked to changes in rheology of the mantle lithosphere (England and Housman, 1989). Alternatively, a change in the rheology of the *middle* crust may have been accomplished by the “radioactive wedge” (i.e., Huerta et al. (in press)) reaching a critical temperature at which point material began to flow laterally, driven by a combination of gravitational forces and north-south convergence. Once the Greater Himalayan wedge started to flow, it would no longer provide a rigid back stop for the southern part of the Tibetan plateau. It is certainly plausible that this change in physical boundary condition triggered east-west extension along the southern Tibetan plateau.

## References

- Armijo, R., P. Tapponier, J. Mercier, and T. Han. 1986. Quaternary extension in Southern Tibet: Field observations and tectonic implications. *Journal of Geophysical Research* **91**, 13803-13872.
- Block, L. and Royden, L. 1990. Core complex geometries and regional scale flow in the lower crust: *Tectonics*, **9**, 557-567.
- Brace, W.F., and D.L. Kohlstedt. 1980. Limits on lithospheric stress imposed by laboratory experiments. *J. Geophys. Res.* **85**, 6248-6252.
- Burchfiel, B.C., Z. Chen, K.V. Hodges, Y. Liu, L.H. Royden, C. Deng, and J. Xu. 1992. The South Tibetan Detachment System, Himalayan Orogen: Extension Contemporaneous With and Parallel to Shortening in a Collisional Mountain Belt. Geological Society of America Special Paper 269. Boulder, CO: Geological Society of America.
- Coleman, M.E., and K.V. Hodges. 1995. Evidence for Tibetan plateau uplift before 14 Myr ago from a new minimum age for east-west extension. *Nature* **374**, 49-52.
- Copeland, P., and T.M. Harrison. 1993. The Nyainqentanghla Range, southern Tibet: Timing of the attainment of a large, high plateau and implications for the development of the Asian monsoon. *Geological Society of America Abstracts with Programs* **25**, A-175.
- Dewey, J.F., R.M. Shackleton, C. Chang, and Y. Sun. 1988. The tectonic evolution of the Tibetan Plateau. *Philosophical Transactions of the Royal Society of London, Series A* **327**, 379-413.
- England, P., and G. Houseman. 1989. Extension during continental convergence, with application to the Tibetan Plateau. *J. Geophys. Res.* **94**, 17561-17579.
- Froitzheim, N., S. M. Schmid, and P. Conti. 1994. Repeated change from crustal shortening to orogen-parallel extension in the Austroalpine units of Graubünden. *Eclogae geol. Helv.* **87**, 559-612.
- Gansser, A. 1964. *Geology of the Himalaya*. London: Wiley Interscience.
- Harrison, T.M., P. Copeland, W.S.F. Kidd, and A. Yin. 1992. Raising Tibet. *Science* **255**, 1663-1670.
- Hodges, K.V., B.C. Burchfiel, L.H. Royden, Z. Chen, and Y. Liu. 1994. The metamorphic signature of contemporaneous extension and shortening in the central Himalayan orogen: Data from the Nyalam transect, southern Tibet. *Journal of Metamorphic Geology*

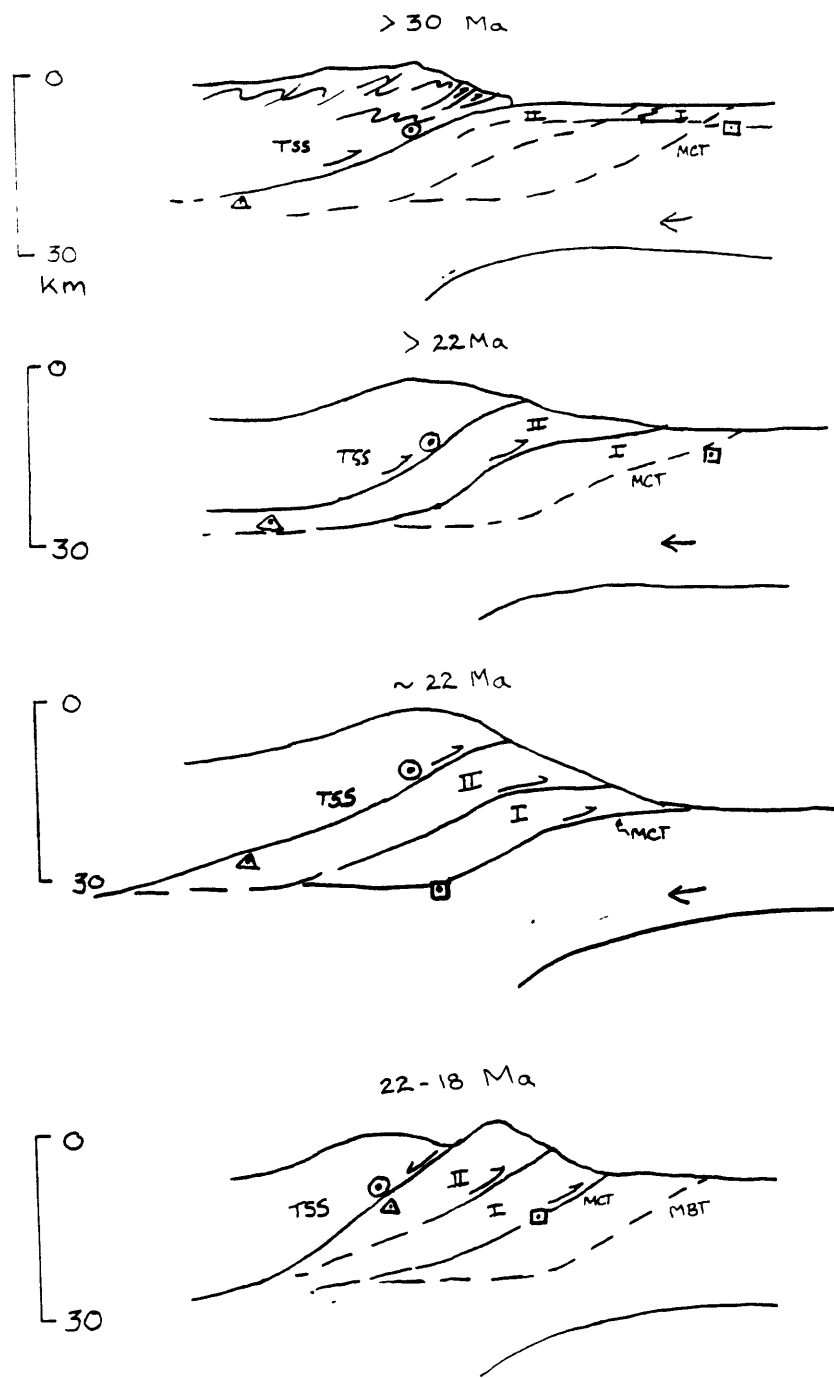
- Hodges, K.V., P. LeFort, and A. Pêcher. 1988. Possible thermal buffering by crustal anatexis in collisional orogens: Thermobarometric evidence from the Nepalese Himalaya. *Geology* **16**, 707-710.
- Hodges, K.V., and F.S. Spear. 1981. Geothermometry, geobarometry, garnet closure temperatures, and the  $\text{Al}_2\text{SiO}_5$  triple point, Mt. Moosilauke N.H. *EOS* **62**, 1060.
- Hollister, L.S., and M.L. Crawford. 1986. Melt-enhanced deformation: A major tectonic process. *Geology* **14**, 558-561.
- Hubbard, M.S. 1989. Thermobarometric constraints on the thermal history of the Main Central Thrust Zone and Tibetan Slab, eastern Nepal Himalaya. *J. Metamorphic Geol.* **7**, 19-30.
- Huerta, A. D., L. H. Royden, and K. V. Hodges. in press. The Interdependence of Deformational and Thermal Processes in Mountain Belts. *Science*
- Inger, S., and Harris, N. 1993. Geochemical constraints on leucogranite magmatism in the Langtang valley, Nepal Himalaya: *Journal of Petrology*, **34**, 345-368.
- Mancktelow, N.S., 1992, Neogene lateral extension during convergence in the Central Alps: Evidence from interrelated faulting and backfolding around the Simplon pass (Switzerland): *Tectonophysics* , v. 215, p. 295-317.
- Molnar, P. 1984. Structure and tectonics of the Himalaya: constraints and implications of geophysical data. *Ann. Rev. Earth Planet. Sci.* **12**, 489-518.
- Molnar, P., and P. Tapponnier. 1978. Active tectonics of Tibet. *J. Geophys. Res.* **83**, 5361-5375.
- Molnar, P., England, P. and Martinod, J. 1993. Mantle dynamics, uplift of the Tibetan Plateau, and the Indian monsoon. *Reviews of Geophysics*, No. 4, 357-396.
- Najman, Y.M.R., Enkin, R.J., Johnson, M.R.W., Robertson, A.H.F., and Baker, J. 1994. Paleomagnetic dating of the earliest continental Himalayan foredeep sediments: Implications for Himalayan evolution. *Earth and Planetary Science Letters*, **128**, 713-718.
- Patel, R.C., Singh, S., Asokan, A., Manickavasagam, R.M., and Jain, A.K. 1993. Extensional tectonics in the Himalayan orogen, Zaskar, NW India. In: Himalayan Tectonics (eds. Treloar, P.J., and Searle, M.P.P, *Geological Society Special Publication*, **74**, 445-459.
- Patriat, P., and J. Achache. 1984. India-Eurasia collision chronology and its implications for crustal shortening and driving mechanisms of plates. *Nature* **311**, 615-621.
- Pêcher, A. 1989. The metamorphism in the central Himalaya. *J. Metamorphic Geol.* **7**, 31-41.

- Pêcher, A. 1991. The contact between the Higher Himalayan crystallines and the Tibetan sedimentary series: Miocene large-scale dextral shearing. *Tectonics* **10**, 587-599.
- Ratschbacher, L., Frisch, W., and Linzer, H.G. 1991. Lateral extrusion in the Eastern Alps, part II; structural analysis: *Tectonics*, **10**, 257-271.
- Royden, L.H. 1993. The steady-state thermal structure of eroding orogenic belts and accretionary prisms. *Journal of Geophysical Research*
- Schneider, C. and Masch, L. 1993. The metamorphism of the Tibetan Series from the Manang area, Marsyandi Valley, Central Nepal, in P.J. Treloar and M.P. Searle, eds., *Himalayan Tectonics*, the *Geological Society*, London, Special Publication No. 47, p. 357-374.
- Searle, M.P., D.J.W. Cooper, and A.J. Rex. 1988. Collision tectonics of the Ladakh-Zaskar Himalaya. In *Tectonic Evolution of the Himalaya and Tibet*. (Edited by R. M. Shackleton, J. F. Dewey and B. F. Windley). The Royal Society London: 117-149.
- Searle, M.P., Windley, B.F., Coward, M.P., Cooper, D.J.W., Rex, A.J., Rex, D.C., Li Tingdong, Xiao Xuchang, Jan, M.Q., Thakur, V.C., and Kumar, S. 1987. The closing of Tethys and the tectonics of the Himalaya. *Geological Society of America Bulletin*, **98**, 678-701.
- Steck, A., Spring, L., Vannay, J.C., Masson, H., Bucher, H., Stutz, E., Marchant, R., and Tietche, J.C. 1993. Geological transect across the Northwestern Himalaya in eastern Ladakh and Lahul (A model for the continental collision of India and Asia). *Eclogae Geologicae Helveticae*, **86**(1), 219-263.
- Treloar, P.J., R.D. Broughton, M.P. Williams, M.P. Coward, and B.F. Windley. 1989. Deformation, metamorphism and imbrication of the Indian plate, south of the Main Mantle Thrust, north Pakistan. *J. metamorphic Geol.* **7**, 111-125.

**Figure caption**

Figure 1) Schematic tectonic reconstructions of the central Himalayas from >30 Ma to 18 Ma. The relative positions of samples MCT-1, MC-36, and MC-93 (Chapters 3 and 4) are indicated by the square, triangle and circle, respectively. The map units include the Tibetan Sedimentary sequence (TSS), Formation II (II) , and Formation I (I).



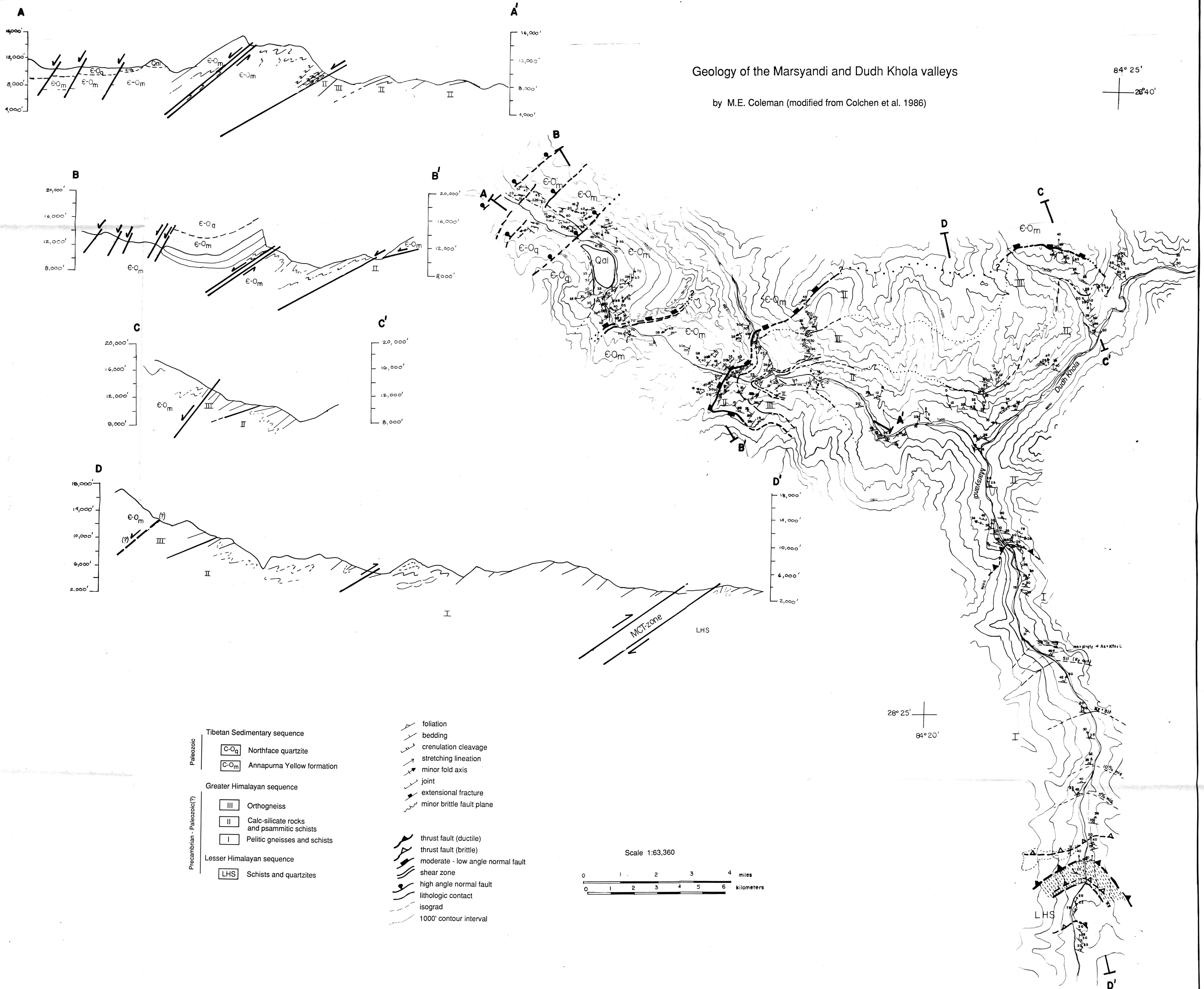


□ MCT-1    △ MC-36    ○ MC-93

# Geology of the Marsyandi and Dudh Khola valleys

by M.E. Coleman (modified from Colchen et al. 1986)

84° 25'  
28° 40'



- Tibetan Sedimentary sequence**
- C-O<sub>q</sub> Northface quartzite
  - C-O<sub>m</sub> Annapurna Yellow formation
- Greater Himalayan sequence**
- III Orthogneiss
  - II Calc-silicate rocks and psammitic schists
  - I Pelitic gneisses and schists
- Lesser Himalayan sequence**
- LHS Schists and quartzites

- foliation
- bedding
- crenulation cleavage
- stretching lineation
- minor fold axis
- joint
- extensional fracture
- minor brittle fault plane
- thrust fault (ductile)
- thrust fault (brittle)
- moderate - low angle normal fault
- shear zone
- high angle normal fault
- lithologic contact
- isograd
- 1000' contour interval

Scale 1:63,360

0 1 2 3 4 miles  
0 1 2 3 4 5 6 kilometers

28° 25'  
84° 20'